INFORMATION TO USERS

This manuscript has been reproduced from the microfilm master. UMI films the text directly from the original or copy submitted. Thus, some thesis and dissertation copies are in typewriter face, while others may be from any type of computer printer.

The quality of this reproduction is dependent upon the quality of the copy submitted. Broken or indistinct print, colored or poor quality illustrations and photographs, print bleedthrough, substandard margins, and improper alignment can adversely affect reproduction.

In the unlikely event that the author did not send UMI a complete manuscript and there are missing pages, these will be noted. Also, if unauthorized copyright material had to be removed, a note will indicate the deletion.

Oversize materials (e.g., maps, drawings, charts) are reproduced by sectioning the original, beginning at the upper left-hand corner and continuing from left to right in equal sections with small overlaps. Each original is also photographed in one exposure and is included in reduced form at the back of the book.

Photographs included in the original manuscript have been reproduced xerographically in this copy. Higher quality 6" x 9" black and white photographic prints are available for any photographs or illustrations appearing in this copy for an additional charge. Contact UMI directly to order.

UMI

A Bell & Howell Information Company
300 North Zeeb Road, Ann Arbor MI 48106-1346 USA
313/761-4700 800/521-0600

Monte Carlo Simulations of the CO_2/NaCl(001) and CH_3Br/LiF(001) Systems

Wei Hu

A Thesis

in

The Department

of

Physics

Presented in Partial Fulfillment of the Requirements
for the Degree of Master of Science at
Concordia University
Montréal, Québec, Canada

March 1997

CONCORDIA UNIVERSITY
School of Graduate Studies

This is to certify that the thesis prepared

by: **Wei Hu**

Entitled: **Monte Carlo Simulations of the CO_2/NaCl(001) and CH_3Br/LiF(001) Systems**

and submitted in partial fulfillment of the requirements for the degree of

Master of Science

Complies with the regulation of this University and meets the accepted standards with respect to originality and quality.

Signed by the final examining committee:

_____Chair

_____Examiner

_____Examiner

_____Supervisor

Approved by_____
Chair of the Department or Graduate Program Director

_____19 _____
Dean of Faculty

ABSTRACT

Monte Carlo Simulation of the CO_2/NaCl(001) and CH_3Br/LiF(001) Systems

Wei Hu

Metropolis Monte Carlo simulations were used to examine the stable structures, phase coexistence and mechanism of nucleation and growth of films of CO_2 molecules adsorbed on the (001) surface of NaCl. This was done for submonolayer, monolayer, and multilayer coverages.

The results show that the monolayer has two stable structures, a (2×1) herringbone structure and a (1×1) structure while the bilayer system has three stable structures: the (2×1), the (1×1) and the c(2×2). The trilayer system adopts a c(2×2) structure owing to the instability of the (2×1) structure. Multilayers most likely grow in the Stranski-Krastanov fashion whereby multilayer islands on top of a monolayer adopt a bulk-like crystalline structure {c(2×2)}.

At low coverages the CO_2 molecules behave like a 2D gas which aggregates into low density islands but finds it hard to nucleate the denser 2D solid phase directly, even in the presence of a surface step. This suggests that the adsorption of CO_2 molecules on the low density islands nucleates the 2D solid phase. The 2D gas-solid phase

coexistence was found to obey the (2D) van der Waals equation of state. The critical coverage Θ_c and temperature T_c were found to be 0.162 and 142.9K respectively, close to the theoretical values of Θ_c =1/6 and T_c=151.2K .

For the CH_3Br/LiF(001) system, submonolayer and monolayer coverages were examined. The results show that for low coverages the molecules are tilted by 60° from surface normal while at monolayer coverage a stable (2×1) herringbone structure was found with a molecular tilt of 39.2° in agreement with experiment. An alternative incommensurate monolayer structure was found where the molecules are antiferroelectrically ordered perpendicular to the surface.

ACKNOWLEDGMENTS

I would like to take this opportunity to thank my research supervisor, Dr. David Jack, for his precious guidance and encouragement throughout the course of research and in the preparation of this thesis. I have greatly benefited from his comments and constructive criticisms. My great thank are also extended to the members of my Research Committee, Dr. N. Eddy and Dr. P. Vasilopoulos, for their helpful suggestions towards the completion of this thesis. I am also grateful to Thanh Vu, Araz Jakalian and Ali for being helpful to my knowledge and achievement.

To my wife

and my parents

Table of Contents

List of Figures

List of Tables

1.0 Introduction:

The physisorption of small molecules on alkali halide single crystal surface, is one of the elementary fields of surface science. It has provided much information on the fundamental physical interactions between molecules and the surface[1], surface diffusion[2], adlayer growth[3], two-dimensional phase transitions [4][5][6] and the role of many-body interactions in condensed phase system. Owing to its specified properties, the CO_2/NaCl(001) system has been an ideal system for surface science studies and is of interest from both the experimental and the theoretical point of view. Before discussion of this system it is worthwhile reviewing some of the general ideas in surface science. The CH_3Br/LiF(001) system is also an ideal system to study the fundamental photochemical processes occurring at surfaces, work done on this system will be discussed later in chapter 5.

1.1 Adsorption and types

Adsorption is a process in which atoms or molecules of one material become attached to the surface of another material. It is also a process that satisfy the attraction forces which exist at a surface. These forces at the surface are only extensions of the forces within the bulk. At the surface, the average number of atomic or molecular neighbors is only half as great as under the surface. Thus there is an unbalance of forces at the surface, and a marked attraction of the surface toward atoms and molecules in its

environment. This results in the adsorption of atoms or molecules of another species at the surface[7].

Generally, there are two kinds of adsorption, physical adsorption (physisorption) and chemical adsorption (chemisorption), which are distinguished by respectively having essentially physical forces (van der Waals and electrostatic interactions) holding the adsorbate to the substrate or having chemical bonds serve the role.

In physisorption, the binding energy is typically less than 50kJ/mol. For example, the adsorption of CO_2 (32.4kJ/mol[4]) and CO (14kJ/mol[8]) molecules on alkali halide surface all fall into the physisorption category. There is usually no significant change in the molecule or the surface. Chemisorption occurs when electrons are shared between the adsorbate and substrate to form a chemical bond. The adsorbed molecules are held to the surface by covalent forces of the same type as those occurring between bound atoms in molecules. Binding energies are typically from 100 to 500kJ/mol. *e.g.* CO_2 on W(100), E_{bind}=456kJ/mol[9]. The surface bond energies are sometimes so strong as to dissociated the adsorbed molecule. For example, when H_2 adsorbs on the W(100) surface the H-H bond is broken, and the hydrogen is chemisorbed as atoms. This can also lead to a reconstruction of the solid surface. Oftentimes there is a net transfer of electrons either into or out of the solid surface and thus a change in the electronic structure (energy levels) of both molecule and surface. In either event there is significant physical change in the chemisorbed molecule and surface.

1.2 2D phases and phase transitions

For physisorption, the atoms and molecules adsorb at different surface sites on a solid. The activation-energy values for transport along the surface from one favored site to another, i.e. the surface diffusion of atoms or molecules, is much lower than those for transfer in the bulk, e.g. they are frequently one half or less of the activation energies for bulk diffusion or heats of desorption into the gas phase. As a result, a great deal of movement of molecules occurs along the surface from one site to another by surface diffusion during their residence time. For simplicity, we may assume equilibrium among molecules in the various surface sites in most circumstances, and the adsorbed layer may be viewed as a two-dimensional phase, instead of a three dimensional phase, that is well-protected from exchange with the gas or the bulk of the condensed phase by large potential-energy barriers[10].

The surface of crystalline material presents itself to exterior gas molecules as a regular two-dimensional array of adsorption sites. The degree to which the adsorbate molecules will associate with these sites depends on the competition between the substrate potential and the interactions among the gas molecules. Experimental results have shown that the monolayer at appropriate coverages and under suitable thermodynamic conditions may form condensed phases characterized by superstructures with the substrate. These phases may undergo phase transitions induced by changes in temperature or coverage[11].

1.3 Previous work on CO_2/NaCl(001)

The CO_2/NaCl(001) system is worth studying because of the following characteristic properties:

1) Crystals of CO_2 and NaCl have similar cubic crystalline structure with lattice constants which differ by only 1.3% (d_{CO_2}=5.575Å, and d_{NaCl}=5.646Å), it is therefore easy for CO_2 molecules to nucleate and subsequently grow epitaxially on NaCl substrate.

2) The NaCl(001) surface is stable, so there is no surface reconstruction.

3) The interaction potential between CO_2 molecules is of a similar order as those with the surface. This is one of the conditions for 2D phase transition[12].

4) The interactions between CO_2 and NaCl(001) are electrostatic and van der Waals in nature, and are essentially additive two-body interactions. These interactions are weak, they do not perturb the molecular structure of the individual CO_2 molecules. These CO_2 adsorbates may be viewed as two-dimensional molecular crystals[13].

The above features make the CO_2/NaCl(001) system an ideal system for studying the structure and dynamics of adsorbates and their phase transitions. Much experimental and theoretical work has been done on this system.

In their experimental work, Kozirovski and Folman first reported the infrared spectrum of carbon dioxide on a sodium chloride film in 1966[14]. By analyzing the infrared spectrum, they found that there is only one kind of adsorption site, and that carbon dioxide has a non-perpendicular orientation with respect to the surface.

Later, the Ewing group (1987-1992) also used infrared spectroscopy to study the monolayer structure of carbon dioxide on a sodium chloride surface. They found that there is only one kind of adsorption site on NaCl(001) surface, and that there are two tilted molecules per layer unit cell with the CO_2 molecular axis tilted 68° from the surface normal. They proposed that this 2×1 structure formed a herringbone pattern[15].

The Heidberg group (1978-1993) did Fourier Transform Infrared Spectroscopy using different isotope of carbon dioxide on sodium chloride surface. They found that:

(1) For a monolayer, the film forms a 2D solid phase with a (2×1) structure. In each unit cell, there are two molecules arranged in a herringbone pattern and related via a glide plane. The CO_2 molecules are tilted by 56°± 5° from the surface normal, and the angle between two molecule axes is 80°± 5°. The isosteric heats of adsorption of the 2D solid is 35.6±1.3 kJ/mol (8.510 kcal/mol)[4];

(2) For submonolayer coverage, the 2D gas phase exists with the CO_2 molecules lying flat on the surface and the isosteric heats of adsorption is 32.4±1.1 kJ/mol (7.744 kcal/mol)[4];

(3) Between 87K and 98K, a coverage dependent first order phase transition happens between 2D gas phase and 2D solid phase with increasing coverage[3][4][16].

Scoles' Group (1993) used low-energy-helium diffraction (LEHD) and found: at low temperatures (73K~92K), CO_2 physisorbs on NaCl(001) to form two distinct phases at low and high coverage. The low-coverage CO_2 layer has a $p(2\times1)$ unit mesh with two domains perpendicular to each other, and there are at most two molecules per unit mesh. At high coverage (monolayer), the structure has a $(2\sqrt{2}\times2\sqrt{2})R45°$ unit mesh with at most eight CO_2 molecules per unit mesh. These two phase structures are commensurate with the underlying NaCl(001) substrate[17].

Toennies' Group (1991-1995) used helium atom scattering (HAS) to study the structure and dynamics of CO_2 on NaCl(001), they found that: (1) at 80-83.5K, a monolayer has a (2×1) structure which is commensurate with the substrate. (2) Upon condensation over a monolayer, additional CO_2 molecules are deposited, the resulting multilayers slowly adopted $c(2\times2)$ symmetry at the expense of the $p(2\times1)$ phase, and in some range of exposures, these two structures coexisted. They proposed that coexisting $c(2\times2)$ and $p(2\times1)$ structures would yield a (2×2) diffraction pattern which would account for the

diffraction pattern of Scoles' experimental results equally well as the proposed the $(2\sqrt{2}\times 2\sqrt{2})R45°$ structure[3].

In order to confirm the Heidberg's group findings about 2D phase transition, solve the discrepancy between Scoles' group and other groups about the monolayer structure, and to understand the mechanism of CO_2 molecules nucleating and growing on the substrate as well as adsorbed layers, we have performed Monte Carlo calculations of submonolayer, monolayer and multilayer structures of CO_2/NaCl(001). In particular we have determined the possible stable structures as well as their energies, symmetries, and molecular orientations. In order to understand why the submonolayer and monolayer might prefer the (2×1) structure, we also set up a simple defect model. In order to describe the behavior of CO_2 molecules adsorbed on the NaCl(001) surface at low coverage, we get the two-dimensional van der Waals equation and draw the 2D gas and solid phase coexistence curve.

1.4 Coordinate system and phases for CO_2/NaCl(001)

In the CO_2/NaCl(001) system, if a molecule sits above the center of the connection line between two adjacent Na^+ ions with the molecular axis parallel to the surface, we consider these molecules to be in the **2D gas phase** (see Fig. 1.3.1). If molecules tilt by 55° with respect to the surface normal and align along the Na^+-Cl^- axis, they are in the **2D solid phase.**

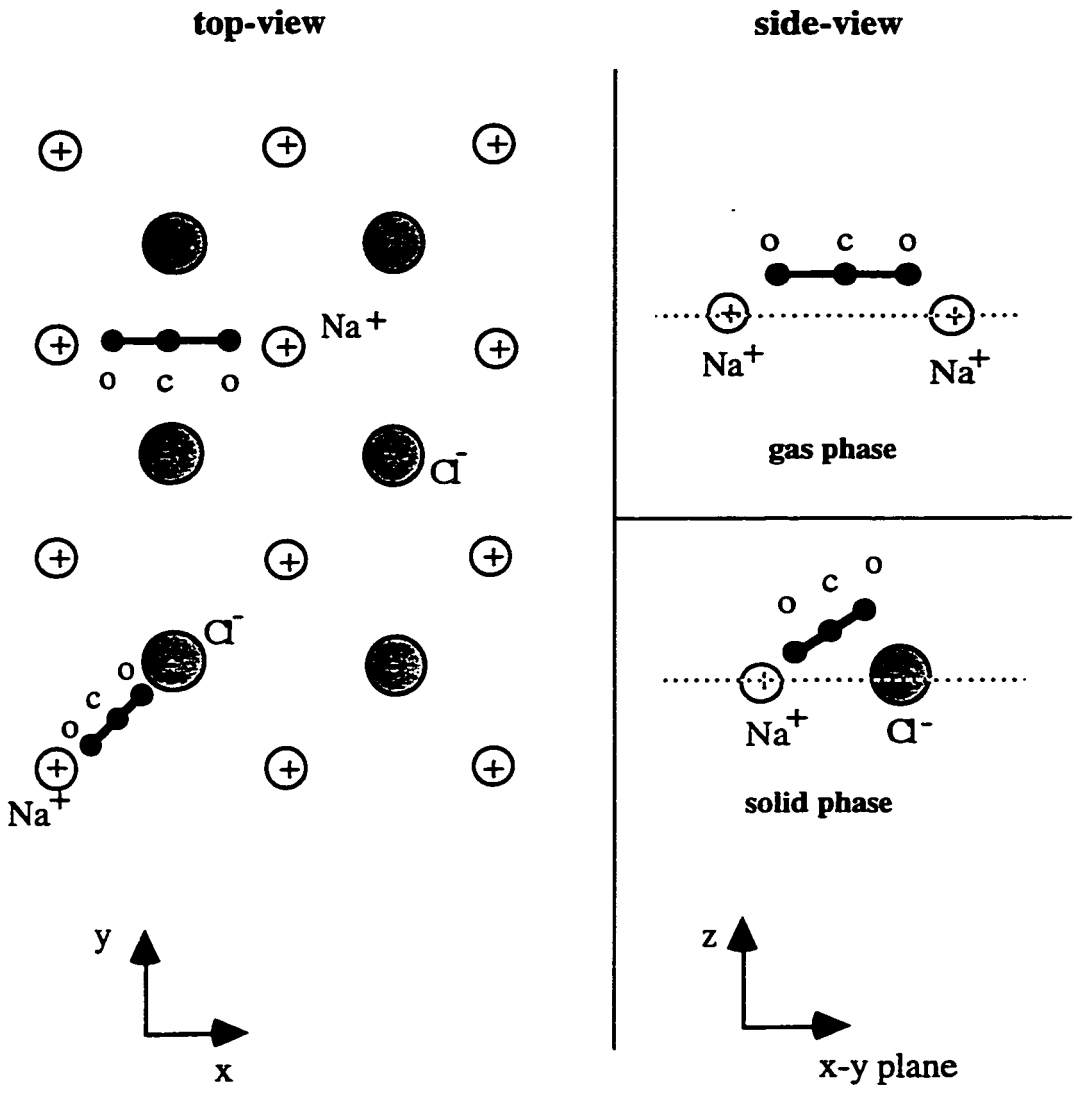

Figure 1.3.1 Orientation of CO_2 molecules on the NaCl(001) surface in the 2D gas and solid phases

2.0 Model of CO_2/NaCl(001):

To carry out Monte Carlo simulations of the CO_2/NaCl(001) system, the first step is to develop functions which will calculate the total potential of this system. If we know the total potential energy, we can determine the structure, the binding energies and other information on this system. In this work, we assume that all the many-body interaction are negligible and the physical forces are individual, so that the total interaction potential can be taken as the sum of pairwise potentials[18]. The total potential can be separated into two parts, the intermolecular potential and the surface potential. All these potentials are developed in a manner similar to those used by Polanyi's group[19][20]. The various atom-atom, atom-ion potentials assume the two body approximation with the repulsion and dispersion interactions described by either a Buckingham or Tang-Toennies potential and the electrostatic interactions handled through distributed multipoles (point charges and dipoles).

2.1 Molecule-molecule interaction potential

The interaction potential between two molecules separated by distance **r**, may be considered to be the pairwise sum of the electrostatic, repulsion, and dispersion contributions. During the calculation, the CO_2 molecules are represented by one C atom and two O atoms which interact independently with the atoms of other molecules. That is, the molecule-molecule potential is the sum of the atom-atom potentials.

2.1.1 Electrostatic model

Owing to two symmetric polar bonds, the CO_2 molecule does not have a permanent dipole moment or octopole moment but does have permanent quadrupole and hexadecapole moments. In previous work on the CO_2/NaCl system, the electrostatic model of CO_2 consists of a "3 charge model"[21], which has partial charges on the C atom (2q) and one on each of the O atoms (-q). We feel that a more sophisticated model is needed and instead use a model which assigns partial charges to the three atomic sites and point dipoles $\vec{\mu}$ to each of the O atoms ("3 charge - 2 dipole model"[22]). The dipoles represent the polarity of the C=O bonds (Fig. 2.1.1). The length of the C=O bonds has a value of 1.163Å[23] in the gas phase. The values of the point charges q_i and point dipoles $\vec{\mu}_i$ can be calculated according to the permanent quadrupole moment Θ, which has an experimental value of -4.3D-Å[24], plus an estimate of the hexadecapole moment -1.6795DÅ^3[25]. The calculated values are listed in table 2.1.1.

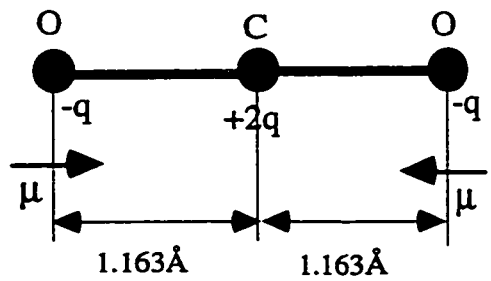

Figure 2.1.1 "3 charge - 2 dipole" model

For simplicity, we assume that the electrostatic potential energy between two CO_2 molecules includes only the Coulomb potential, and ignores any induction energy. The Coulomb potential describes the interaction between the distributed point charges q and the point dipoles $\vec{\mu}$ on the atoms of one CO_2 molecule with those of another CO_2 molecule. We can write the electrostatic potential between two "gas" molecules as follows

$$V_{el}^{gg}(\vec{r}_{ii'}^{nn'}) = \frac{1}{2}\sum_{i=1}^{3}\sum_{i'=1}^{3} (\phi_i^n(\vec{r}_{ii'}^{nn'})q_{i'}^{n'} + \phi_{i'}^{n'}(\vec{r}_{i'i}^{n'n})q_i^n + \vec{E}_i^n(\vec{r}_{ii'}^{nn'}).\vec{\mu}_{i'}^{n'} + \vec{E}_{i'}^{n'}(\vec{r}_{i'i}^{n'n}).\vec{\mu}_i^n \ldots) \qquad (2.2.1)$$

where the $\phi_i^n(\vec{r}_{ii'}^{nn'})$ and $\vec{E}_i^n(\vec{r}_{ii'}^{nn'})$ are the electrostatic potential and electric field which the **i**th atom of the **n**th molecule produces in the position of the **i**'th atom of the **n**'th molecule.

Table 2.1.1

Point charges and point dipoles on CO_2 molecule

(From ref.[22])

	point-charge(e)	point-dipole(e·Å)	Polarizability(Å^3)
C atom	1.1326	0	1.1046
O atom	-0.5663	0.1592	0.7626

2.1.2 Dispersion and repulsion interactions

Dispersion potential consists of a series of terms which arise from the induced dipole-induced dipole, induced dipole-induced quadrupole and the induced quadrupole-induced quadrupole interactions. The repulsion potential is due to pauli exclusion. In the CO_2/NaCl system, we chose the Buckingham formula to represent these two term. We have

$$V_{atom}^{gg}(r_{ii'}^{nn'}) = (B_i + B_{i'}) \exp[(A_i + A_{i'} - r_{ii'}^{nn'}) / (B_i + B_{i'})] - \sum_{m=3}^{\infty} \frac{C_{2m}^{ii'}}{(r_{ii'}^{nn'})^{2m}} \quad (2.1.2)$$

where $r_{ii'}^{nn'} = |\vec{r}_i^{\,n} - \vec{r}_{i'}^{\,n'}|$ is the distance between the **i**th atom on the **n**th molecules (**n, i**) and the **i'**th atom on the **n'**th molecule (**n', i'**); A_i, $A_{i'}$ are repulsion radii, and B_i , $B_{i'}$ are softness parameters. The coefficients $C_6^{ii'}$, $C_8^{ii'}$ and $C_{10}^{ii'}$ are dispersion constants denoting the strength of the mutually induced dipole-dipole, dipole-quadrupole and quadrupole-quadrupole plus dipole-octopole interactions, respectively.

So for molecule-molecule interaction, we have

$$V_{DR}^{gg} = \sum_{i\,i'=1}^{3} V_{atom}^{gg}(r_{ii'}^{nn'}) \quad (2.1.3)$$

Therefore, the total CO_2-CO_2 molecules interaction potential is

$$V_{mm} = \sum_{\substack{n\,n'=1 \\ n \neq n'}}^{N} (V_{DR}^{gg} + V_{el}^{gg}) \qquad (2.1.4)$$

For the CO_2-CO_2 molecules interaction, the parameters we used in the simulations are listed in Table 2.1.2.

All of the parameters have been calculated previously[22] from WMIN, which is a computer program to model molecules and crystals in term of potential energy functions. In our case the energy of a crystal of CO_2 was minimized through the variation of the repulsion parameters (radii and softness parameters) and the partitioning of the dispersion interactions; the values of the A_i and B_i which minimize the energy are the values subsequently used in our calculations of the repulsion parameters.

Table 2.1.2

Repulsion parameters for CO_2-CO_2 interaction

Parameter Name	Value
A_C (radius)Å	1.618528
A_O (radius)Å	1.552825
B_C (softness)Å	0.101357
B_O (softness)Å	0.095644
PL_6C^*(kcal)$^{1/2}$.Å^3	20.94682
PL_6O^*(kcal)$^{1/2}$.Å^3	15.83318

*) $(PL_6C)^2 = C_6(C\text{-}C)$

$(PL_6O)^2 = C_6(O\text{-}O)$

$(PL_6C^*PL_6O) = C_6(C\text{-}O)$

2.2 Molecule-surface (gas-solid) interaction

As we mentioned in the introduction, the CO_2 molecule physisorbs on the NaCl(001) surface. With no true chemical bond between molecule and surface, the interaction between them is weak and hence does not perturb the structure of the NaCl(001) surface. It is reasonable to suppose that the structure does not 'relax' at the surface, i.e. the surface is stable and has the same lattice constant as the bulk structure. For simplicity, the surface may be treated as an array of ions, which is periodic in two dimensions and regular in the z direction. The interaction potential of a gas atom with the surface is given by the sum of the interaction of the gas atom with all of the atoms (or ions,...) of the solid. So, if z is the perpendicular distance of the gas atom from the surface (Fig. 2.2.1), the total interaction potential (assuming pairwise additivity) is given by

$$V^{gs}(\vec{r}_{i'}) = \sum_i V^{gs}_{atom}(\vec{r}_{i'} - \vec{R}_i) = \sum_i V^{gs}_{atom}(\vec{r}_{ii'}) \qquad (2.2.1)$$

Where $\vec{R}_i$ is the lattice vector of solid, $V^{gs}_{atom}(\vec{r}_{ii'})$ is the interaction potential between the gas atom(i') and the ith ion in the solid separated by a distance $r_{ii'}$.

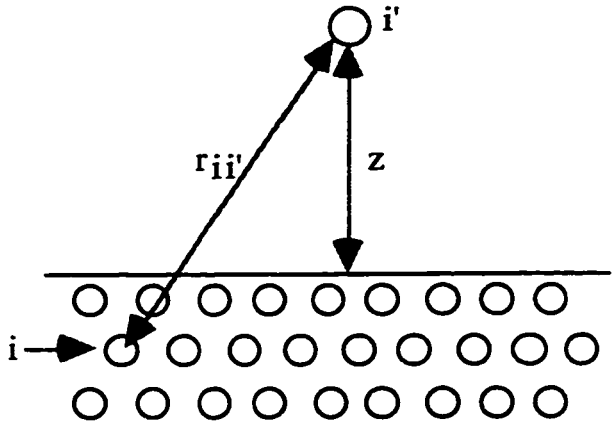

Figure 2.2.1 Coordinates for gas-surface interactions (adapted from ref.[26])

2.2.1 Electrostatic interaction

The electrostatic potential energy between a CO_2 molecule and NaCl substrate includes the Coulomb potential and the induction energy. The Coulomb potential describes the interaction of the electrostatic potential $\Phi(\vec{r}_i)$ and electric field $\vec{E}(\vec{r}_i)$ of NaCl(001) surface with the distributed charges q and dipoles $\vec{\mu}$ located on the three atomic sites of the CO_2 molecule. So the Coulomb interaction potential of a single CO_2 molecule on the NaCl(001) surface is written as below:

$$V_C^{gs} = \sum_{i=1}^{3} [\Phi(\vec{r}_i)q_i + \vec{E}(\vec{r}_i) \cdot \vec{\mu}(\vec{r}_i)] \qquad (2.2.2)$$

We set up the coordinate system so that the position vector $\vec{r}$=(x,y,z) has its origin on the surface at an Cl^- site with the z axis perpendicular to the surface (Fig. 2.2.2), and the x and y axes in the surface plane pointing toward adjacent Cl^- sites along the <1$\bar{1}$0> and <110> directions of the NaCl unit cell. The electrostatic potential $\Phi(\vec{r}_i)$ above the NaCl(001) surface may then be written[27][19][20] as

$$\Phi(\vec{r}) = -\frac{4e}{a}\left[\frac{\exp\left(-\frac{2\pi z}{a}\right)}{1+\exp\left(-\sqrt{2}\pi\right)}\right]\left[\cos\left(\frac{2\pi x}{a}\right)+\cos\left(\frac{2\pi y}{a}\right)\right] \tag{2.2.3}$$

where **a** is a constant of surface mesh and **e** is the electronic charge on an individual ion. The **a** has a relation with the lattice constant **c** of the NaCl crystal, **c**=$\sqrt{2}$ **a**.

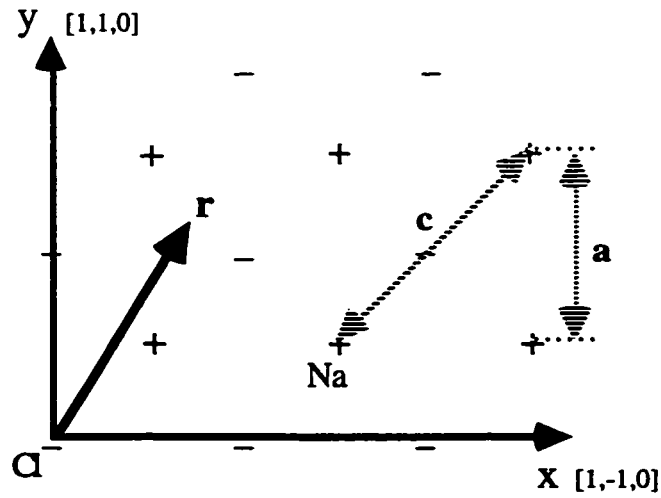

Figure 2.2.2 Top view of the coordinate system on NaCl(001) surface

The electric field is given by

$$\vec{E}(\vec{r}) = -\vec{\nabla}\Phi(\vec{r}) \tag{2.2.4}$$

An induction potential arises from the interaction between the NaCl electric field and the induced dipole moment of a CO_2 molecule placed in the electric field; i.e.

$$V_{Ind}^{gs} = -\sum_{i=1}^{3}\int_0^E \vec{\mu}_{ind}\cdot d\vec{E} = -\frac{1}{2}\sum_{i=1}^{3}\alpha_i E^2(r_i) \tag{2.2.5}$$

where α is the polarizability of the molecule.

So, the electrostatic potential of a single CO_2 molecule on the NaCl(001) surface is written as below:

$$V_{el}^{gs} = V_C^{gs} + V_{Ind}^{gs} \tag{2.2.6}$$

The values of point charge, point dipole and polarizability of CO_2 molecule are listed in table 2.1.1 and are the same as those used for the molecule-molecule interactions. Note that the molecular polarizability is distributed over the atoms.

2.2.2 Dispersion and repulsion interactions

The potential $V_{atom}^{gs}(r_{ii'})$ for gas atoms interacting with substrate ions includes two parts, the repulsion and dispersion interaction. Here we chose the Tang-Toennies form[28],

$$V_{atom}^{gs}(r_{ii'}) = A_{ii'} \exp(-\alpha_{ii'} r_{ii'}) - \sum_{n=3}^{\infty} (f_{2n}(r_{ii'}) \frac{C_{2n}^{ii'}}{(r_{ii'})^{2n}}) \qquad (2.2.7)$$

where the Born-Mayer parameters $\alpha_{ii'}$ (decay constant) and $A_{ii'}$ characterize the range and strength of the potential respectively, and

$$f_{2n}(r) = 1 - \sum_{k=0}^{2n} (\frac{(\alpha r)^k}{k!}) \exp(-\alpha r) \qquad (2.2.8)$$

is a phenomenological damping function which is characterized by the decay constant of the repulsion term. The damping function removes the singularities at r=0.

By putting the term (2.2.7) into (2.2.1) we can get the potential of one adsorbed atom interacting with the substrate by summing the appropriate pair potential over all lattice ions. However, this becomes very inefficient. If the surface potential must be calculated for each new position and orientation of the molecule, we can instead use the periodicity of the NaCl lattice and replace the direct summation by a two-dimensional Fourier series of the periodic potential $V_{atom}^{gs}(r_{ii'})$ [19][20]. We then have

$$V^{gs}(x,y,z) = \sum_{n,m}^{\infty} V_{atom}^{n,m}(z) \cos\left(\frac{2\pi n}{a}x\right) \cos\left(\frac{2\pi m}{a}y\right) \qquad (2.2.9)$$

where n, m=0,1,2,... defines an infinite series. Usually equation (2.2.9) is truncated at the n+m=2 level. One must then evaluate the Fourier coefficients, $V_{atom}^{n,m}(z)$. Note that the Fourier series contains the same periodicity as the surface lattice.

The potential of one CO_2 molecule adsorbed on the NaCl(001) surface is equal to

$$V_{DR}^{gs} = V^{gs}(C - Surface) + V^{gs}(O_1 - Surface) + V^{gs}(O_2 - Surface) \quad (2.2.1)$$

2.2.3 Model of defect on the surface

Here we just consider step defects where the step is a small area which consists of a layer of Na^+ and Cl^- ions distance d_{NaCl} above the infinitive NaCl(001) surface (Fig. 2.2.3).

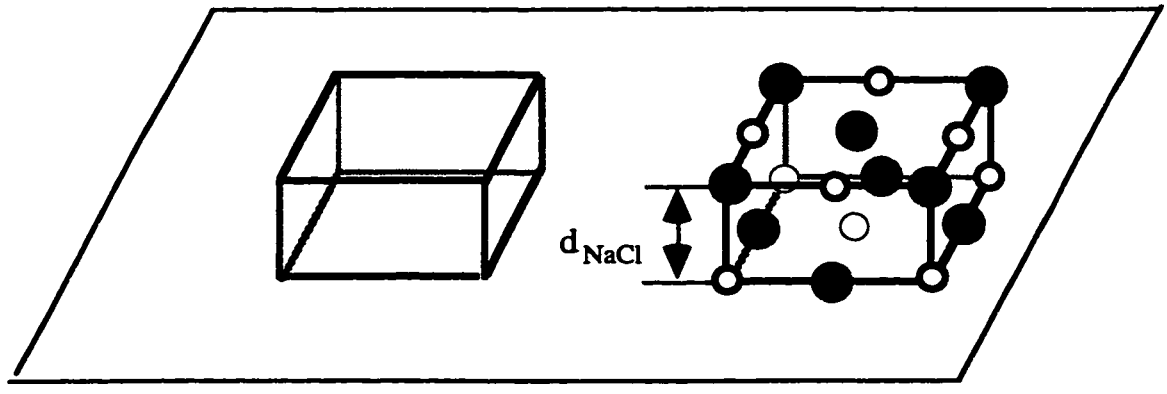

Figure 2.2.3 Step defect on surface

The total surface potential now includes two parts:

$$V_{total} = V_{infinitive\text{-}surface} + V_{defect} \tag{2.2.11}$$

where the $V_{infinitive\text{-}surface}$ is the infinite surface potential described earlier, and is calculated in the same way as in section 2.2.2; and V_{defect} is the defect potential. We calculate the latter by explicitly summing the interaction between the adsorbed molecules and defect ions. The parameters for calculating the defect potential are listed in Table 2.2.1 and Table 2.2.2.

Table 2.2.1

Repulsion parameters for CO_2-NaCl surface potential

(From ref.[22])

parameters number	value
$\alpha(C\text{-}Na^+)$ $Å^{-1}$	4.38145
$\alpha(C\text{-}Cl^-)$ $Å^{-1}$	2.91045
$\alpha(O\text{-}Na^+)$ $Å^{-1}$	4.77532
$\alpha(O\text{-}Cl^-)$ $Å^{-1}$	3.07915
$A(C\text{-}Na^+)$ K	4.18524×10^7
$A(C\text{-}Cl^-)$ K	1.26044×10^7
$A(O\text{-}Na^+)$ K	8.85913×10^7
$A(O\text{-}Cl^-)$ K	1.86054×10^7

Table 2.2.2

Dispersion constants for atom-ion interactions

(From ref.[22])

parameters number	value
C_6(C-Na^+) K-Å^6	4.5806×10^4
C_6(C-Cl^-) K-Å^6	5.2950×10^5
C_6(O-Na^+) K-Å^6	3.1597×10^4
C_6(O-Cl^-) K-Å^6	3.6526×10^5
C_8(C-Na^+) K-Å^8	3.4557×10^5
C_8(C-Cl^-) K-Å^8	6.5658×10^6
C_8(O-Na^+) K-Å^8	2.3838×10^5
C_8(O-Cl^-) K-Å^8	4.5292×10^6
C_{10}(C-Na^+) K-Å^{10}	2.6071×10^6
C_{10}(C-Cl^-) K-Å^{10}	8.1418×10^7
C_{10}(O-Na^+) K-Å^{10}	1.7984×10^6
C_{10}(O-Cl^-) K-Å^{10}	5.6163×10^7

3.0 Metropolis Monte Carlo Method

The "Monte Carlo Method" is a statistical method for analyzing systems in equilibrium or quasi-equilibrium. It has its name from the extensive use of "random numbers" to numerically generate probability distributions in order to simulate statistical fluctuations. This method can be used to obtain information on model systems, such as the spin-Ising model, X-Y and Heisenberg models for phase transitions.... To use this method for interacting molecules we must know the system's Hamiltonian. We can then generate many configurations of the system with a probability according to their Boltzmann statistical weight at thermal equilibrium. Hence we can get the thermal averages of some observables which are readily obtained from arithmetic averages of these quantities which are in the generated configurations. Given enough statistical effort, these averages can be made as accurate as desired, at least in principle[29].

Generally, in our work, the surface is not allowed to move and thus provides a constant potential in which the adsorbed molecules "move". The admolecules are considered to be rigid which is a reasonable assumption in light of the strong force constants of CO_2 and CH_3Br molecules. In our simulations work, a large number of possible configurations at a non-zero temperature should be sampled. The total number of molecules in the system needs to be fixed and we are primarily concerned with the structure of the adlayer as well as energies, so the Metropolis Monte Carlo method

(canonical ensemble Q(N, V, T)) is chosen for statistical work. The partition function of the canonical ensemble is

$$Q_{NVT} = \sum_{\Gamma} \exp\left(-H(\Gamma)/k_B T\right) \qquad (3.0.1)$$

where $H(\Gamma)$ is the Hamiltonian of a system, $\Gamma=\{\vec{x}_i\}$ is the space which is spanned by all possible microstates (configurations) of a system, and $\vec{x}_i$ contains the values of all possible degrees of freedom for each particle of the system, e.g. position (x, y, z), orientation (φ, θ, ψ), where φ is an azimuthal angle between the x axis and the projection of the molecular axis onto the plane of the surface, θ is the tilt angle with respect to the surface normal and ψ is rotation angle around the molecular axis). In our system, canonical ensemble means that the position and orientation of adsorbed molecules can be changed while the number of molecules, as well as the volume and temperature of this system are kept constant.

The general steps of Metropolis Monte Carlo simulation are listed in Figure 3.0.1. A configuration of a system is given and the total energy, E_{old}, is calculated, then a randomly chosen molecule temporarily moves to a new position by choosing a random translation (changing x or y or z) or rotation (changing φ or θ or ψ). Based on the new temporary configuration, the new energy E_{new} and the energy difference $\Delta E=E_{new}-E_{old}$ are calculated. If ΔE is zero or has negative value, then the move is accepted; if the ΔE is positive, then an acceptance probability $P=\exp(-\Delta E/k_B T)$ is calculated and compared with a random number ξ which is generated by computer.

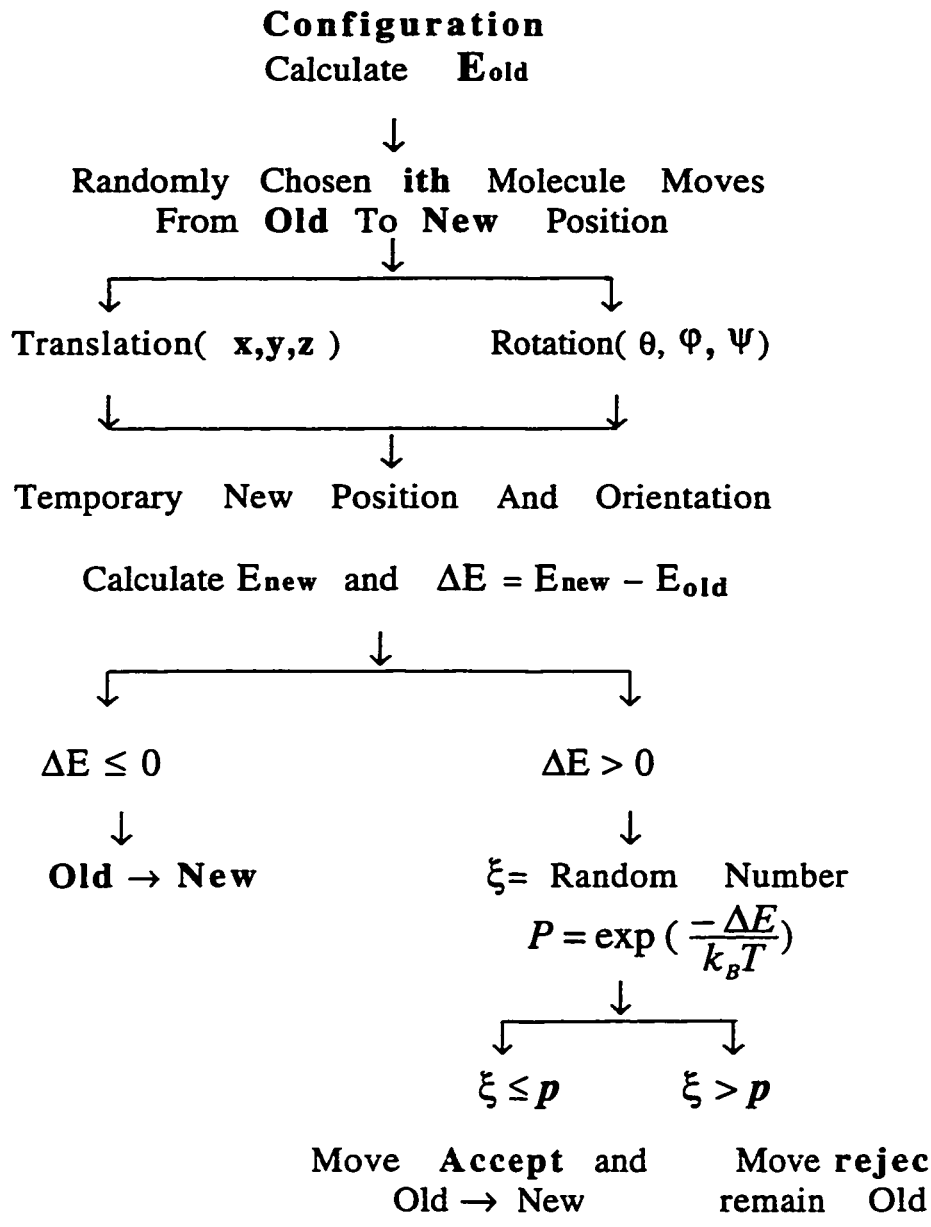

Figure 3.0.1 The flowchart of a Metropolis Monte Carlo simulation (canonical ensemble Q(N,V,T))

If ξ is small or equal to P then the move is accepted; if ξ is larger than P then the move is rejected (Fig. 3.0.2). This process is repeated for each of the other molecules. After all of the molecules are chosen one cycle is finished. One of the advantages of accepting a move with a positive ΔE is to prevent the system from getting stuck in a local minimum of the energy.

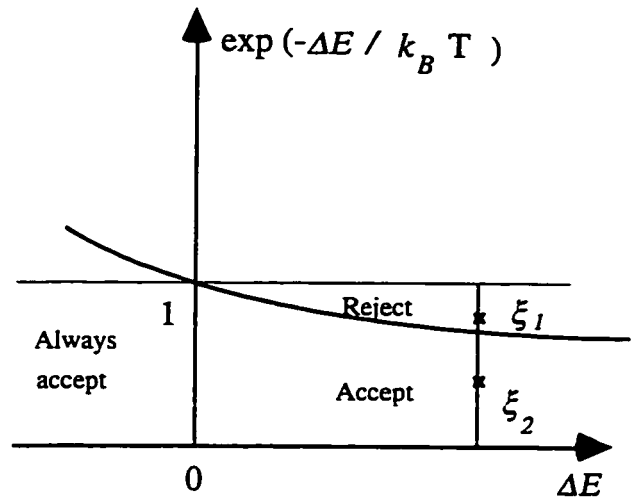

Figure 3.0.2 Acceptance criteria for "uphill" moves in the MC Simulation
(From ref.[29])

4.0 Simulation Results for CO_2/NaCl(001) System

To simulate the behavior of CO_2 molecules in the submonolayer and monolayer regime, molecules are either randomly or orderly placed on the NaCl(001) surface (both with or without a defect) and allowed to interact amongst themselves and with the surface. Through the imposition of periodic boundary conditions the molecules are confined to a certain surface area (typically 40Å×40Å). They are also subject to a cutoff radius of 13.5Å for the CO_2-CO_2 interaction. The simulations are run for large number of cycles with the first quarter of the cycles thrown away, we collect statistics only for the remaining cycles. One cycle consists of each molecule attempting a random translation (sometimes including jump) or rotation. To do work on multilayers, additional layers of molecules are placed over top of the bottom layer.

The coordinate system used to describe the position of the molecules on the NaCl(001) surface is same as that shown in Fig. 2.2.1. For the orientation of the molecules with respect to the surface, we define a polar angle theta θ (tilt with respect to the surface normal) and an azimuthal angle phi φ (angle between the x axis and the projection of the molecular axis onto the plane of the surface) which are shown in Fig. 4.0.1.

The several "crystallographic" surface meshes of the CO_2 monolayer pertinent to this work are shown in Fig. 4.0.2. For the $p(1\times1)$ structure, the periodicity of the adsorbed molecules is

identical to that of the surface mesh of sodium ion (assuming a bulk structure), and can be represented by the black dot placed exactly overtop of sodium ion sites. For the $c(2\times2)$ structure, the unit cell of the adsorbed molecules is twice as large as the underlying surface unit cell of the substrate; while the $p(2\times1)$ structure has a unit cell which is twice as long as the surface unit cell along one major crystallographic axis and has the same length along the other. The $(2\sqrt{2}\times2\sqrt{2})R45°$ structure, the unit cell of adsorbed molecules is two root two times as long as the surface unit cell and the axes are rotated 45° with respect to the substrate axes. With respect to a bulk unit cell it has a (2×2) structure.

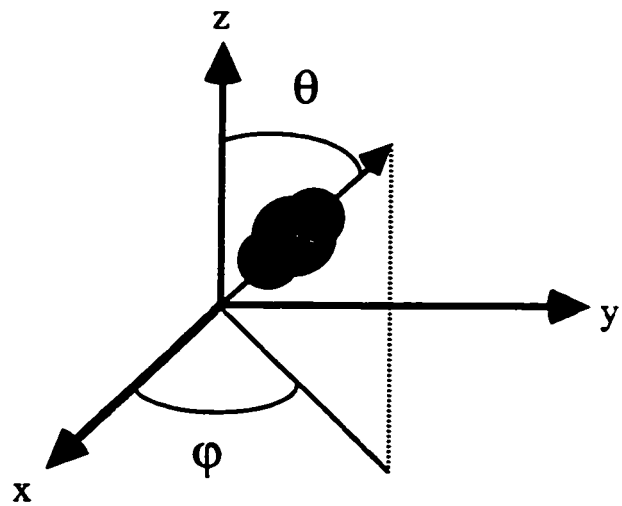

Figure 4.0.1 Angular coordinate system with respect to the xyz coordinate system

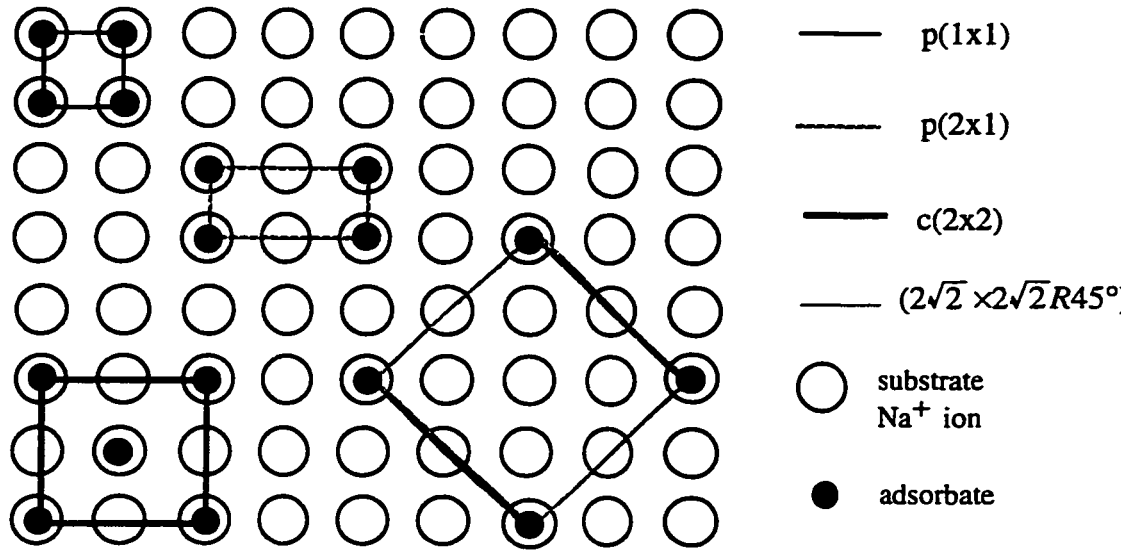

Figure 4.0.2 Several structures in the CO_2/NaCl(001) system

4.1 Monolayer system

In the previous work, two kinds of structures about monolayer have been reported, the $(2\sqrt{2}\times 2\sqrt{2})R45°$ structure, which Scoles *et al.*[17] supposed using Low Energy Helium Atom Diffraction, and the $p(2\times 1)$ structure[4]. In order to confirm which structure is energetically favored, Monte Carlo simulations are started from several kinds of monolayer structures at temperature 55K and run them at least 20 kcycles with the first quarter of the cycles discarded. The average energy of these different structures is calculated and their stability is studied. The reason we choose a temperature of 55K is that the experimental work has been performed near that temperature. Previous work[22] on the (2×1) structure indicates that it is thermally stable. Although the molecules have been allowed to adjust their positions and orientations from an initial (2×1) structure (T=0) (Fig. 4.1.1), the final configuration at T=55K (Fig. 4.1.2) is almost same as the initial one. If we start from the $c(2\times 2)$ configuration, which is the structure of CO_2 crystal, the final structure is (1×1) with lowest energy (Table 4.1.1). This structure has not been reported in experiment yet. If we start from an initial structure with all the CO_2 molecules pointing straight up, the final configuration consists of two major kinds of parts: a (2×1) and a (1×1) (Fig. 4.1.3) with slightly higher energy than either the (2×1) or the (1×1). For the $(2\sqrt{2}\times 2\sqrt{2})R45°$ structure (Fig. 4.1.4), it has broken into a disorder structure in which the (2×1) and (1×1) structures are coexist (Fig. 4.1.5).

The orientation of CO_2 molecules on the surface in term of their azimuthal angle θ and polar angle φ are tested. The φ distribution for (2×1) and (1×1) structures is shown in Figure 4.1.6. The maxim of φ distribution for $p(2\times1)$ structure at temperature 55K are found at -44° and 44°, and hence the angle between the projected molecular axes of two neighboring molecules is 88°, which is in good agreement with experimental value of 80° ± 5°; for (1×1) structure, the maximum is just found at 45°. The θ distribution is shown in Figure 4.1.7, for both (2×1) and (1×1) structures, the maxim of θ distribution are found around 59° at temperature 55K, which again in good agreement with experimental value 56°±5°[4].

Generally, for the monolayer systems, we found two kinds of stable structures, which the (2×1) structure is confirmed by the experimental results but the (1×1) structure with lower energy has not been found by the experiments.

Table 4.1.1 Energies for several structures of monolayer of CO_2 on NaCl(001) (55K)

<E>/CO_2 (kcal/mol)	(2×1)	(1×1)	(2×1) & (1×1)
CO_2-CO_2(V*)	-1.734	-1.660	-1.638
CO_2-CO_2(el**)	-0.914	-0.960	-0.707
CO_2-NaCl(V)	-1.344	-1.376	-1.387
CO_2-NaCl(el)	-4.083	-4.141	-4.137
Total Energy	-8.195	-8.242	-7.864

* Repulsion and dispersion ** Electrostatic

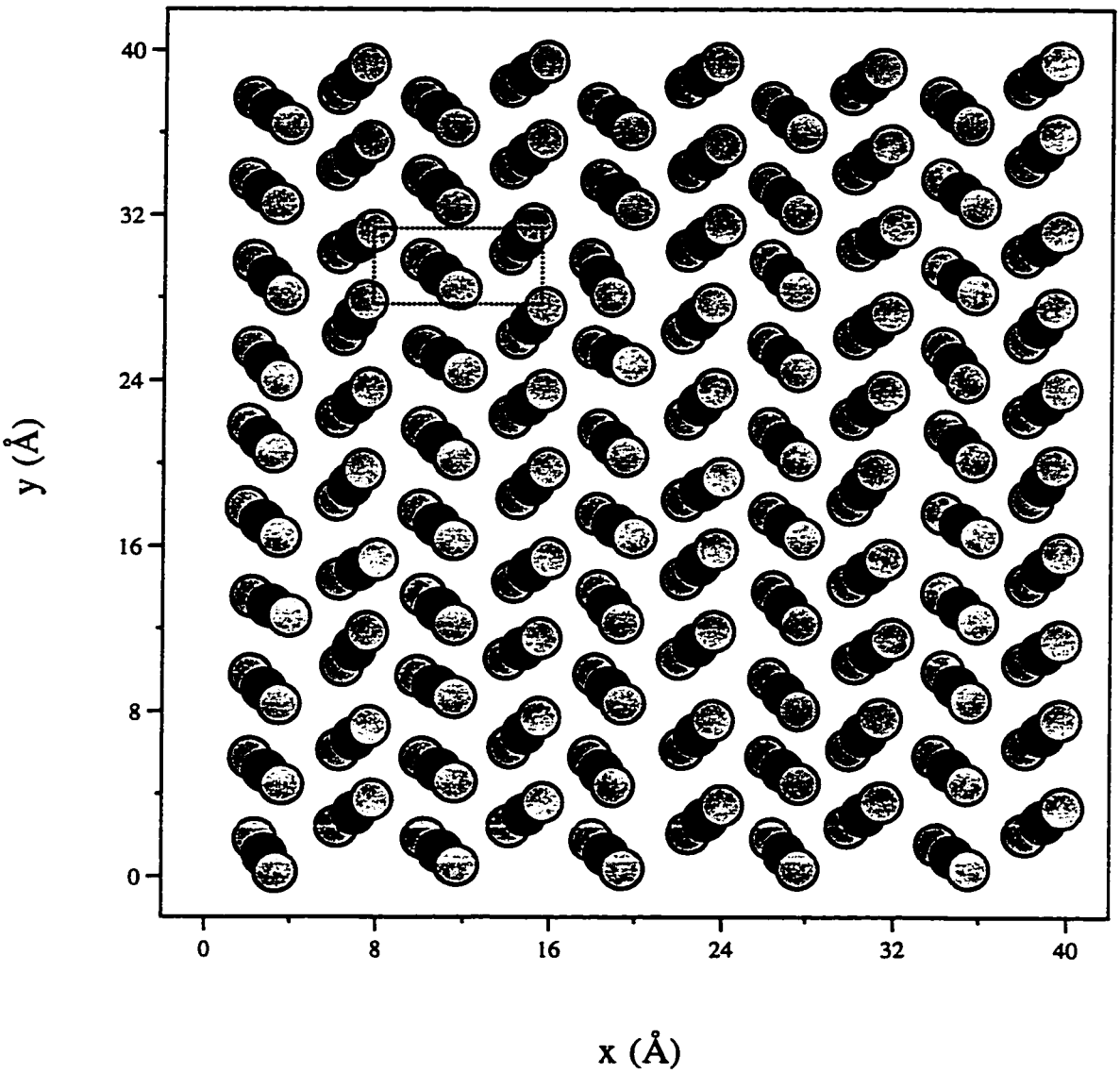

Figure 4.1.1 The $p(2\times1)$ structure and unit cell of monolayer CO_2/NaCl(001) at 55K

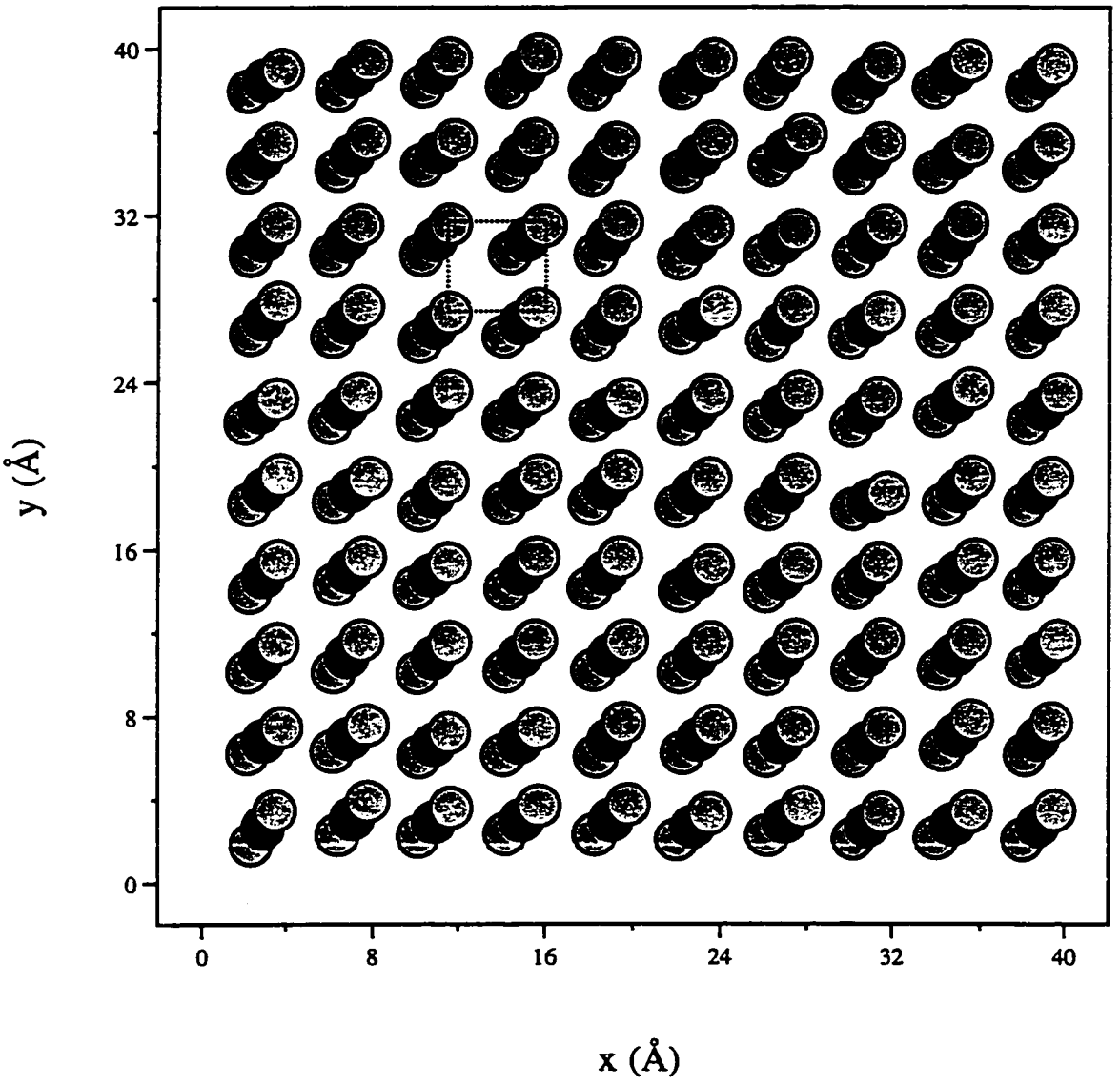

Figure 4.1.2 The $p(1\times1)$ structure and unit cell of monolayer CO_2/NaCl(001) at 55K

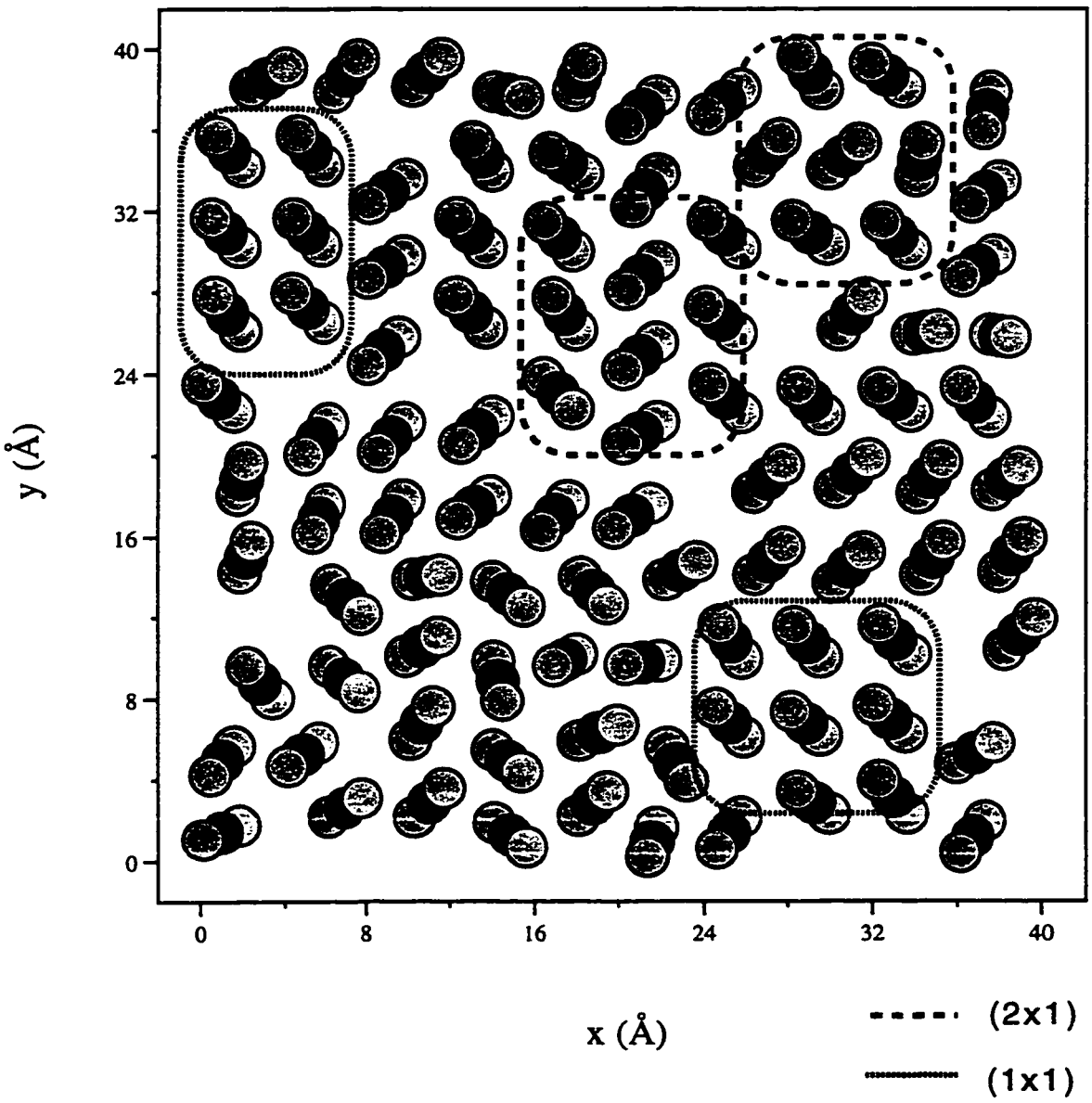

Figure 4.1.3 Final configuration of initial straight up structure of monolayer CO_2/NaCl(001) at 55K

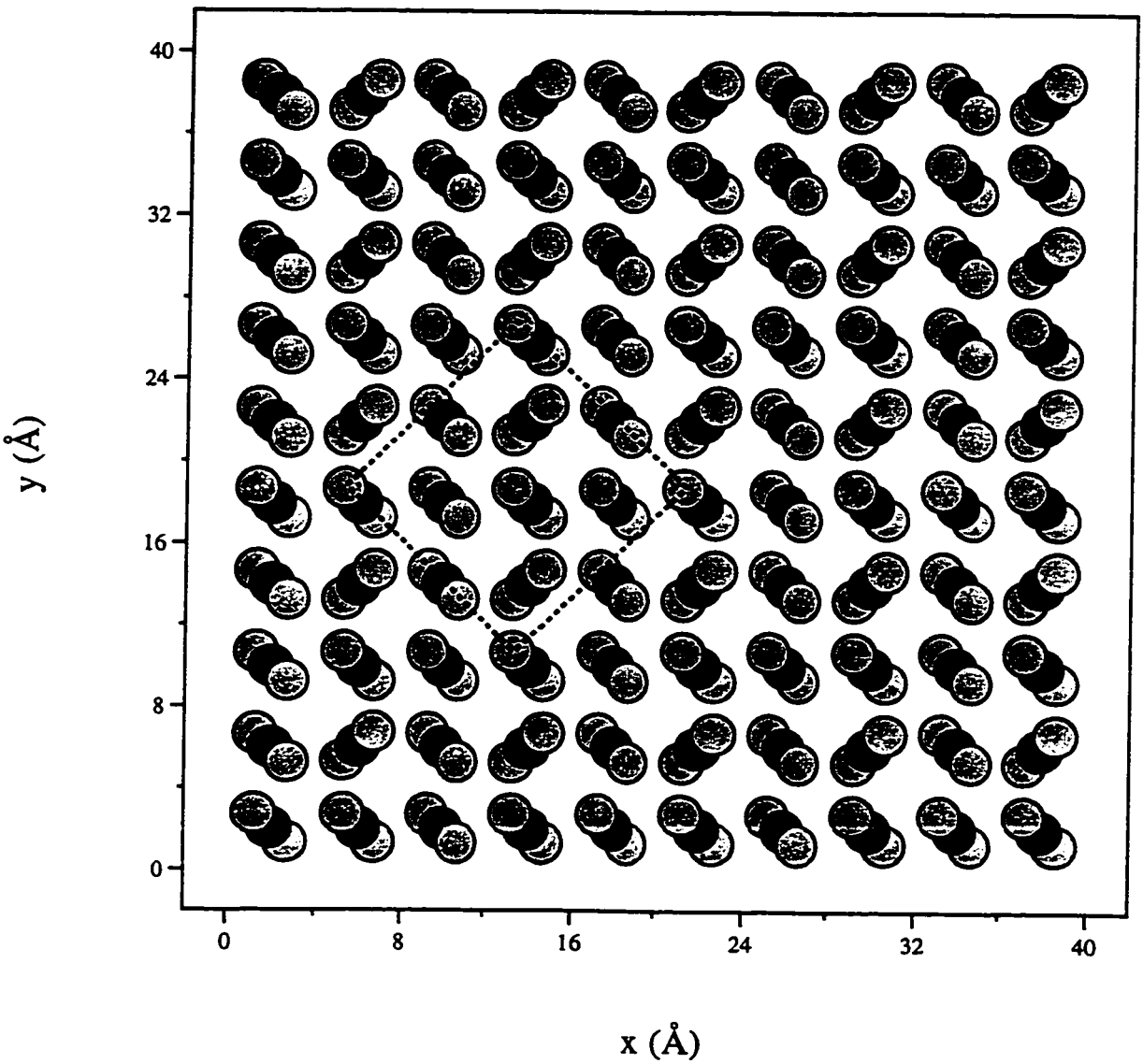

Figure 4.1.4 Initial configuration and unit cell of the $(2\sqrt{2}\times2\sqrt{2})$ structure of monolayer $CO_2/NaCl(001)$

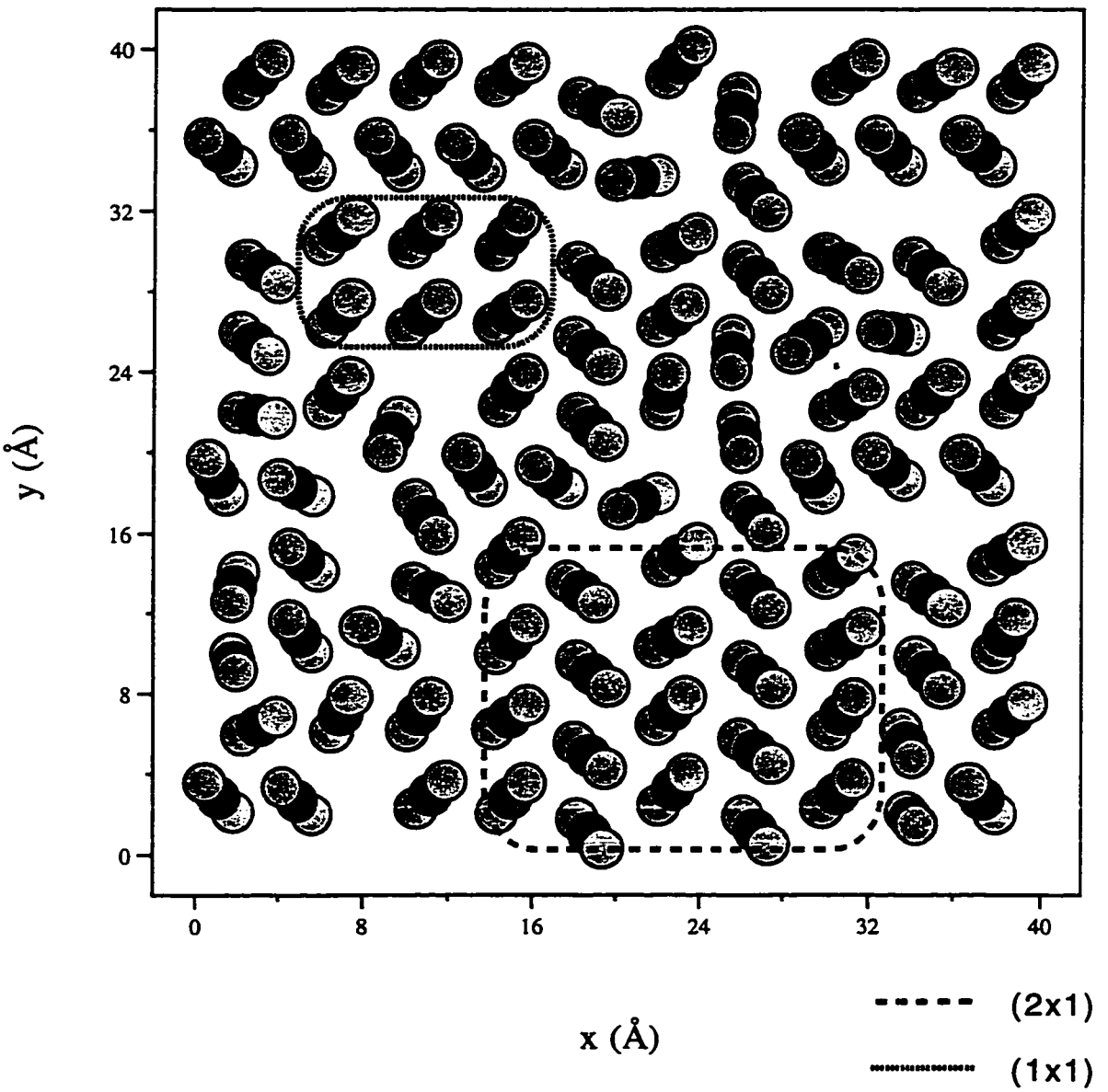

Figure 4.1.5 Final structure of "(2√2×2√2)" monolayer CO_2/NaCl(001) at 55K

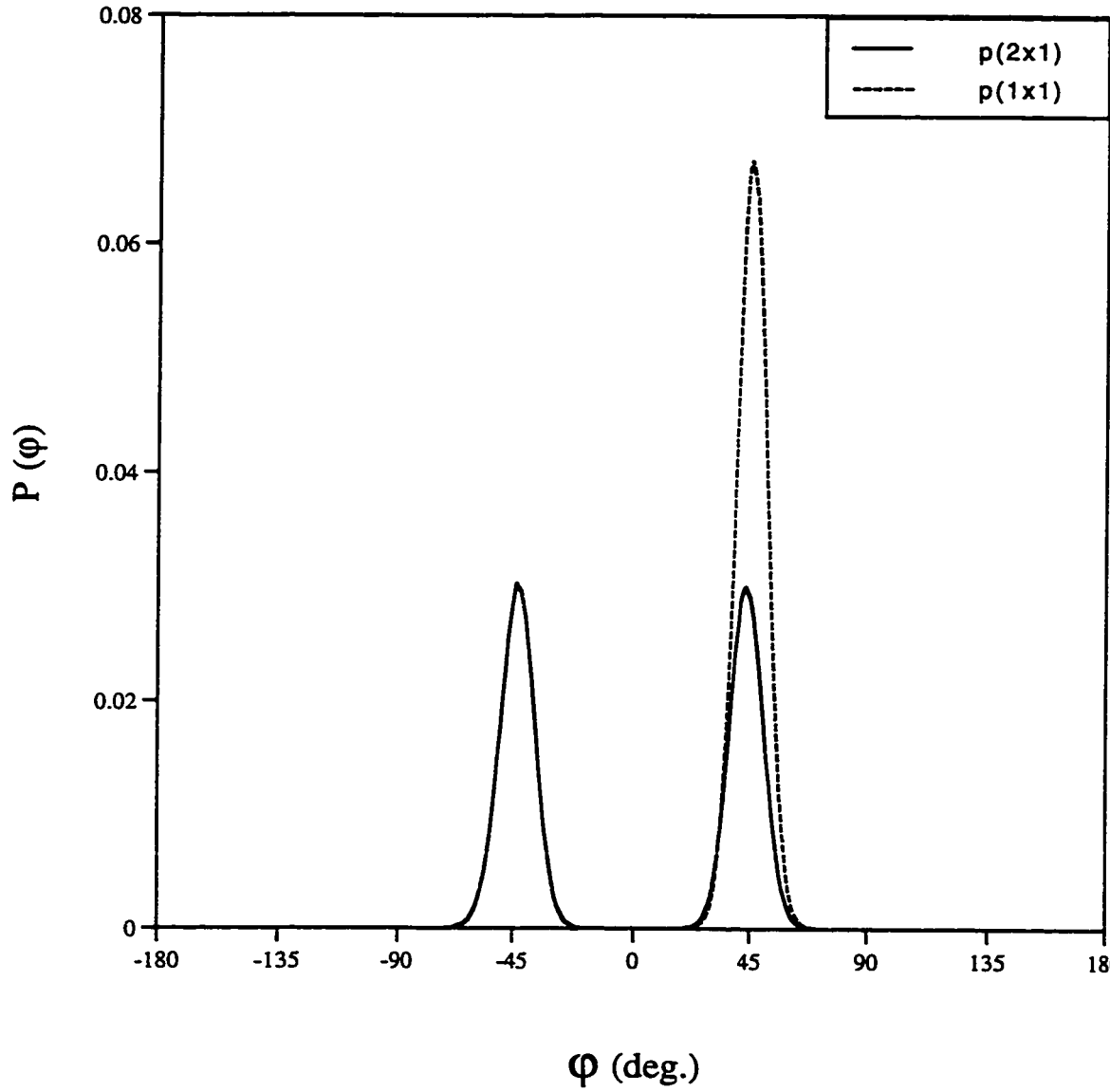

Figure 4.1.6 Phi distribution of $p(2\times1)$ and $p(1\times1)$ structures of a monolayer at 55K

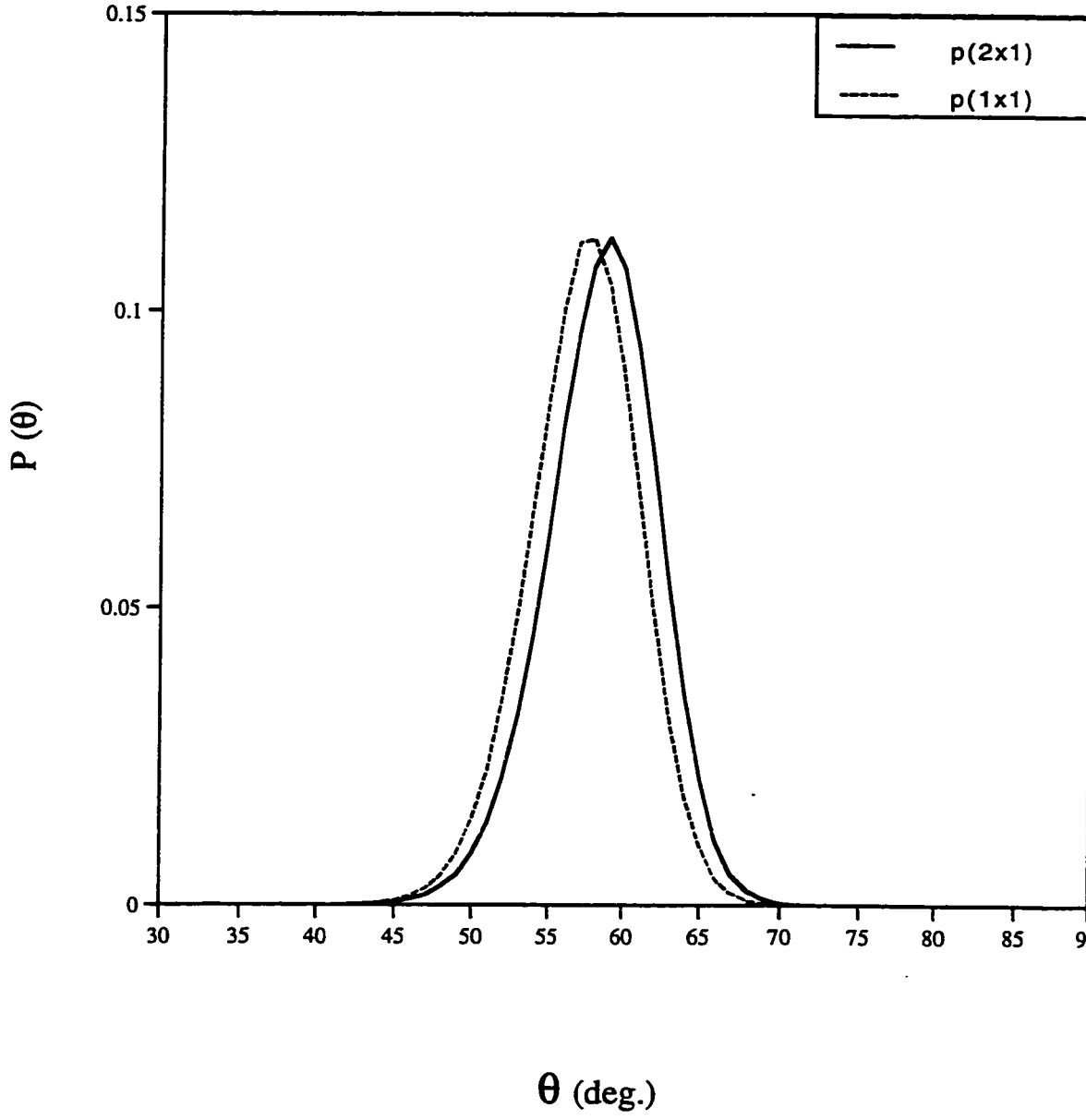

Figure 4.1.7 Theta distribution of $p(2\times1)$ and $p(1\times1)$ structures of a monolayer at 55K

4.2 Bilayer system

To test whether multilayers adopt the $p(2\times1)$ or $c(2\times2)$ structure, Monte Carlo simulations were started from three kinds of bilayer systems with symmetries consistent with either the $p(2\times1)$, $p(1\times1)$ or $c(2\times2)$ structure at T=55K. The average energy of these different structures is calculated and structure stability is also studied.

For (2×1)/(2×1) (top/bottom) structure, the final configuration (Fig. 4.2.1) is almost same as the initial configuration. This indicates that the (2×1) bilayer is thermally stable. The maximum of the φ distribution are found around -44° and 44° for the bottom layer but change to -137° and 137° for the top layer as shown in Fig. 4.2.2. It means that molecules in the top layer are "brushed" the other way from the bottom layer. The maximum of the θ distribution is found at 60° for both bottom layer and top layer (Fig. 4.2.3). The distributions for the bottom layer are both sharper than the top layer due to the restraints on the molecular motions in the bottom layer imposed by the top layer.

For (1×1)/(1×1) structure, the final configuration (Fig. 4.2.4) is also similar to the initial structure, so that this structure is also stable. The maximum of the φ distribution is found at around 46° for bottom layer and -47° for top layer (Fig. 4.2.5). It shows that molecular orientations have rotated by 90° from bottom layer to top layer. The maximum of the θ distribution is around 57° for both

layer (Fig. 4.2.6) but the bottom layer is sharper than the top layer as in the (2×1)/(2×1) case.

For the (2×2)/(2×2) structure, the bottom layer is distorted but still has $c(2\times2)$ symmetry, while the top layer maintains a (2×2) structure closer to the initial configuration (Fig. 4.2.7). Although the tilt angle remains the same (θ=57°) for both layers, there is a significant difference in azimuthal orientation between the layers. The φ distribution appears as the double peaks centered at φ=45° for the bottom layer while the top layer has more widely spaced double peaks centered at φ=-135°.

The thermally averaged potential energy per molecule for the three different structures are compared in Table 4.4.1. All of them are close to the cohesive energy (28.6kJ/mol) of a bulk crystal of CO_2, but the $c(2\times2)$ bilayer structure is slightly more favorable than the (2×1) and (1×1) bilayer structures. In experimental work, the (1×1) structure might not arise because of steric considerations during the formation of the 2D solid phase. From energetic considerations the (2×1) and (2×2) structure could presumable coexist with grains of the (2×2) phase slowly growing at the expense of the (2×1) structure.

Table 4.2.1 Energy of several structures of a bilayer of CO_2/NaCl(001) (55K)

	Different structures (T: top layer B: bottom layer)		
<E>/CO_2 kcal/mol	T: (2×1) B: (2×1)	T: (1×1) B: (1×1)	T: (2×2) B: (2×2)
CO_2-CO_2(V*)	-2.614	-2.858	-2.614
CO_2-CO_2(el**)	-1.232	-1.118	-1.275
CO_2-NaCl(V)	-0.798	-0.822	-0.807
CO_2-NaCl(el)	-2.227	-2.191	-2.229
Total Energy	-6.850	-6.928	-6.970

* Repulsion and dispersion

** Electrostatic

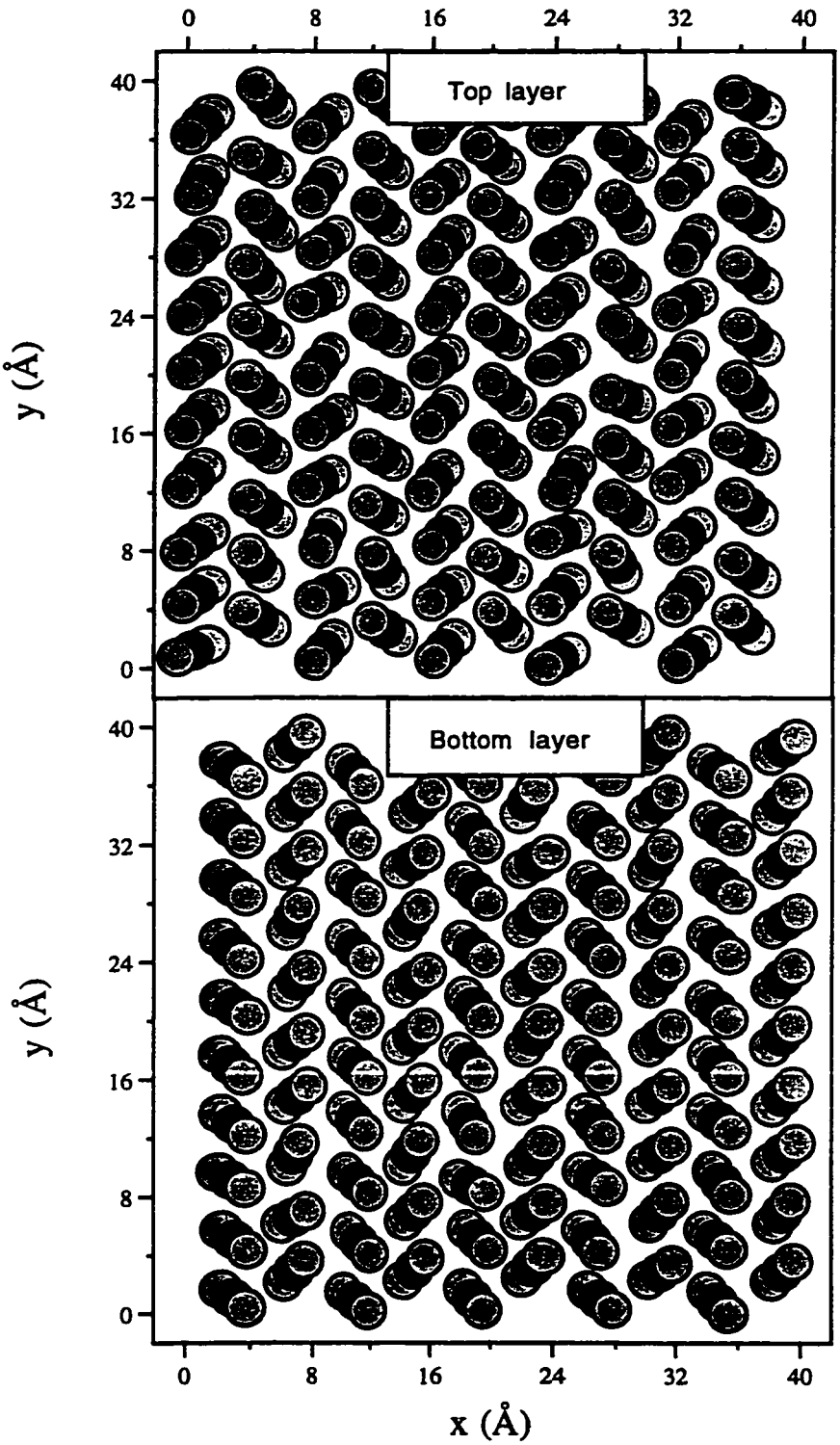

Figure 4.2.1 A bilayer {Top: $p(2\times1)$; Bottom: $p(2\times1)$} structure of CO_2/NaCl(001) at 55K

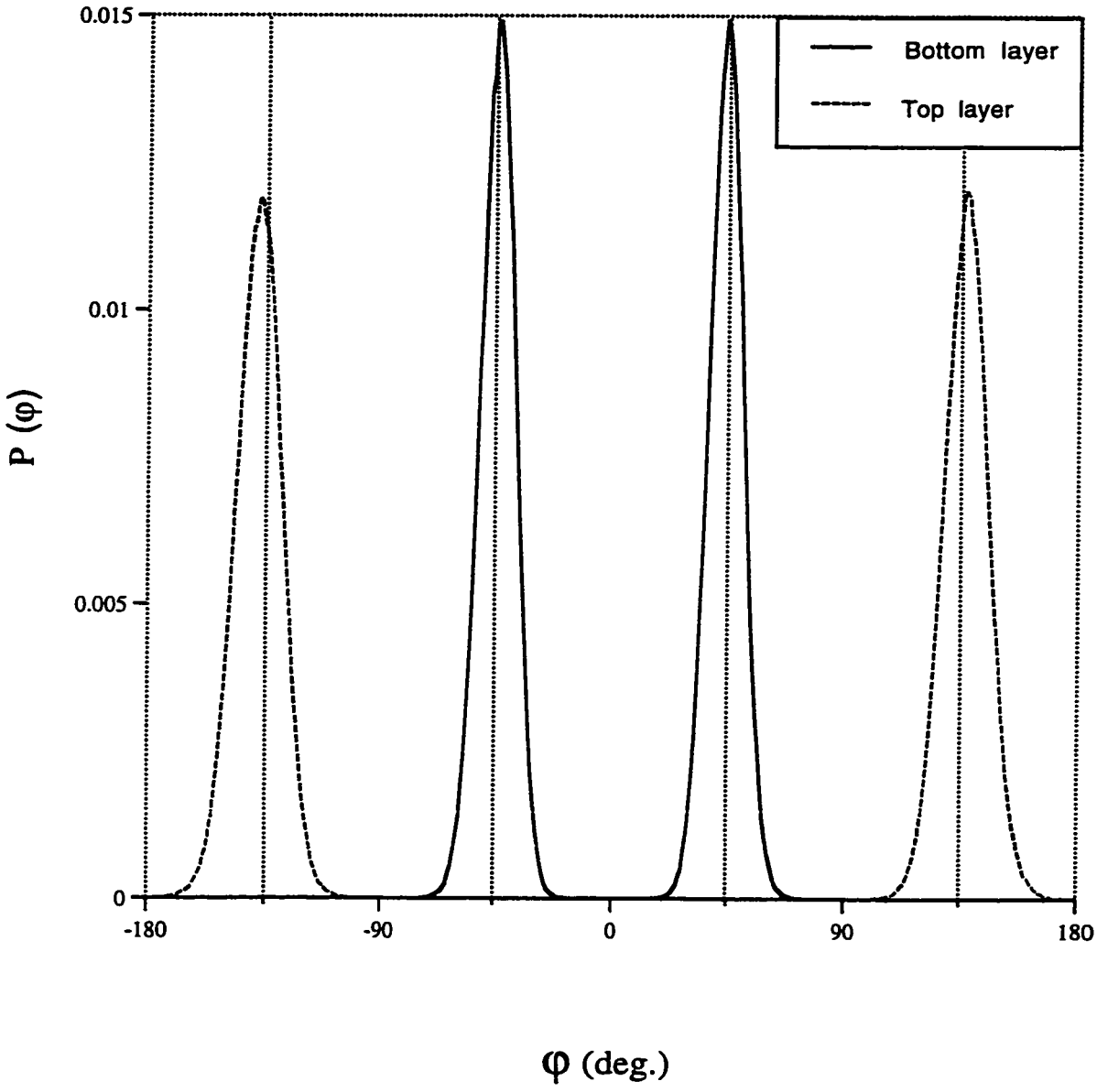

Figure 4.2.2 Phi distribution of a bilayer system at 55K {Top: $p(2\times1)$; Bottom: $p(2\times1)$}

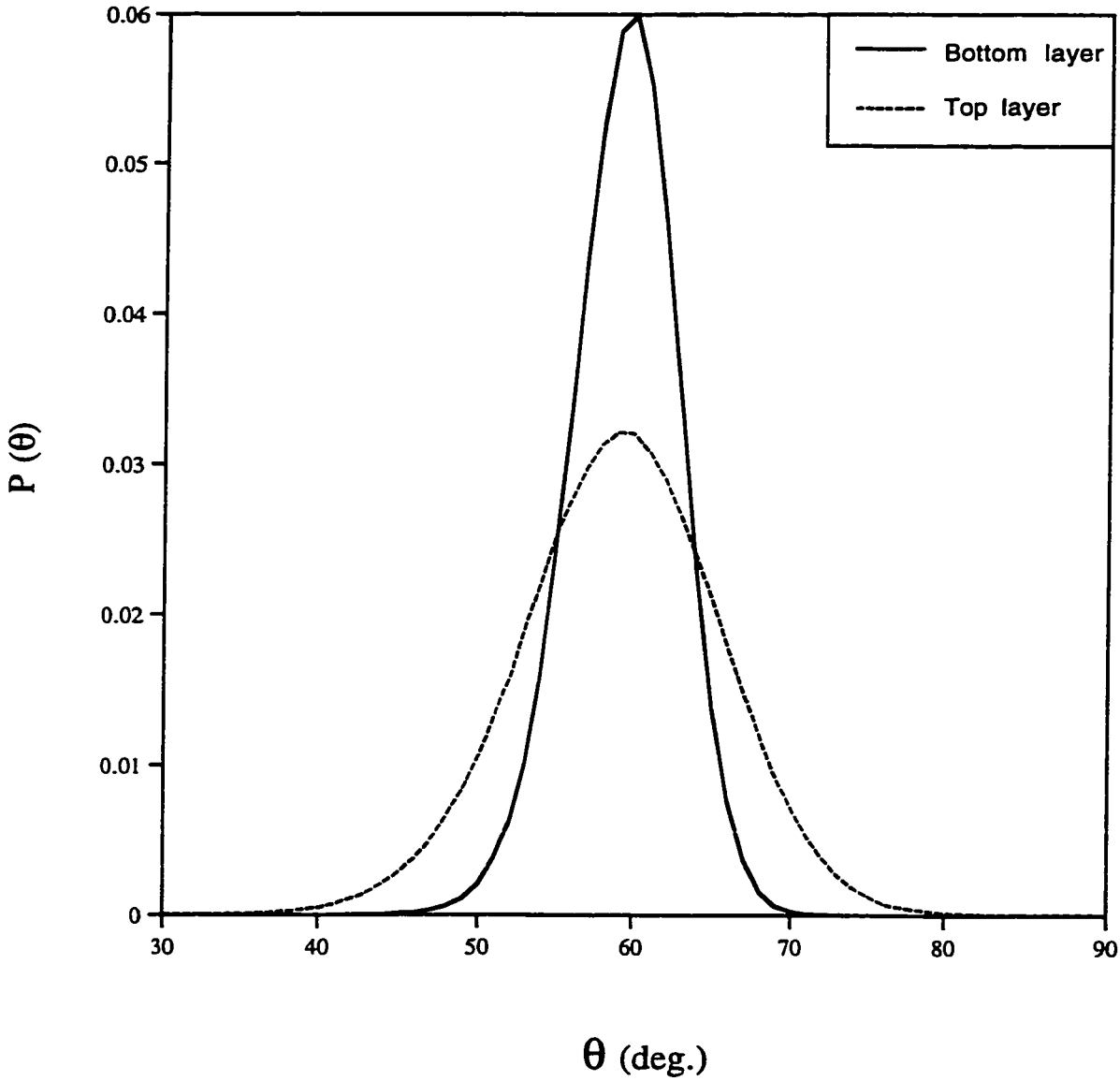

Figure 4.2.3 Theta distribution of a bilayer system at 55K {Top: $p(2\times1)$; Bottom: $p(2\times1)$}

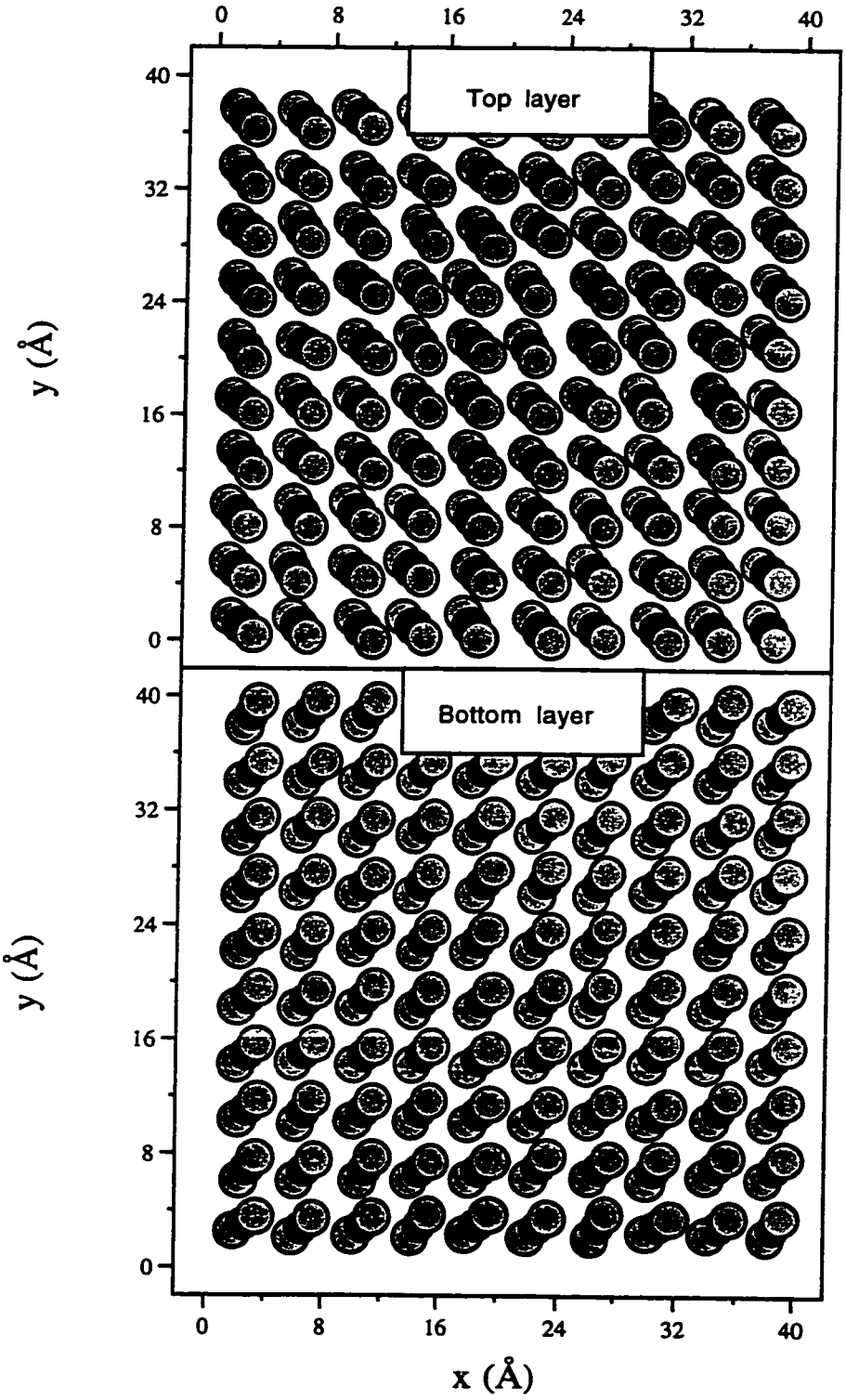

Figure 4.2.4 A bilayer {Top: $p(1\times1)$; Bottom: $p(1\times1)$} structure of CO_2/NaCl(001) at 55K

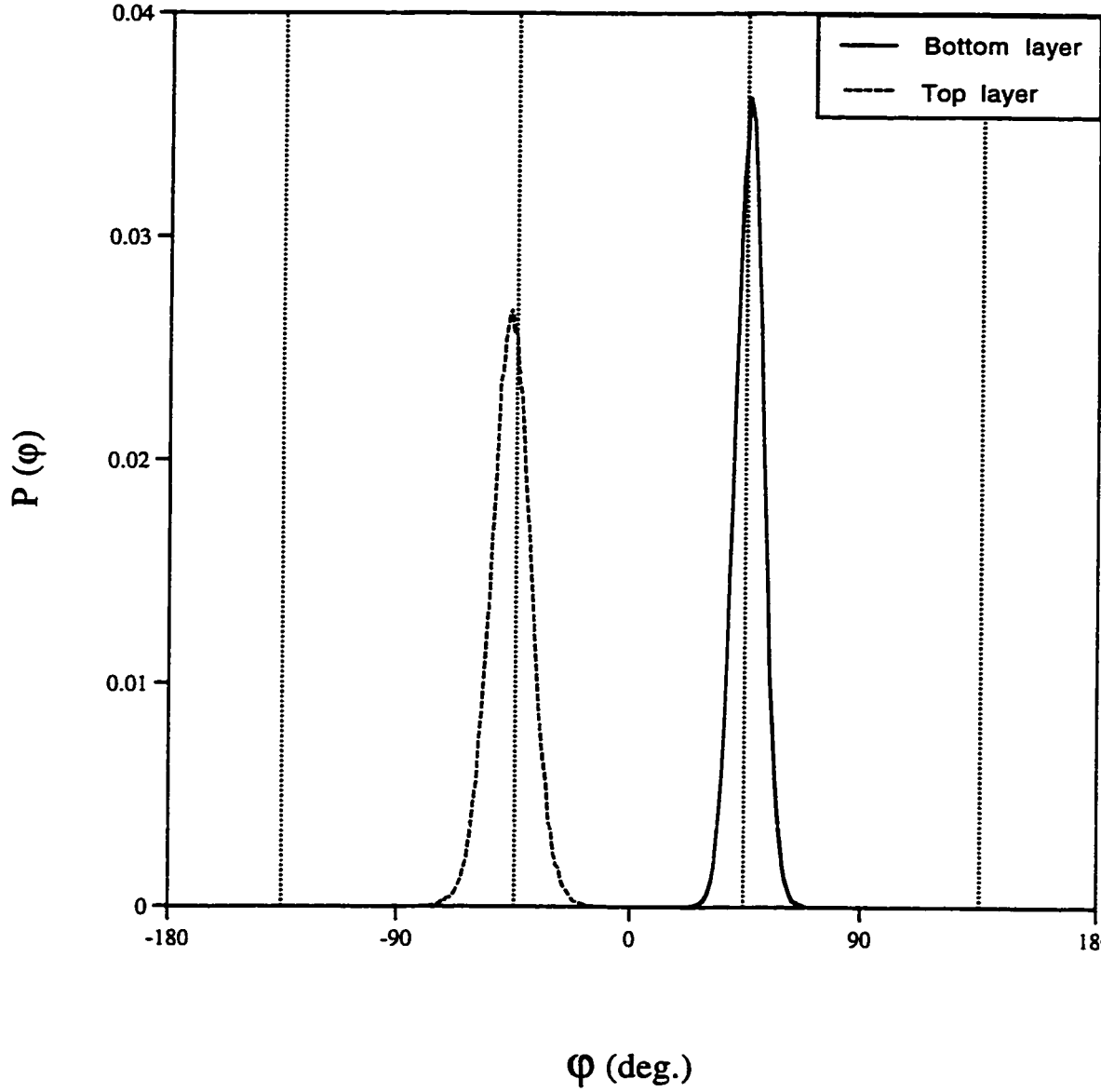

Figure 4.2.5 Phi distribution of a bilayer system at 55K {Top: $p(1\times1)$; Bottom: $p(1\times1)$}

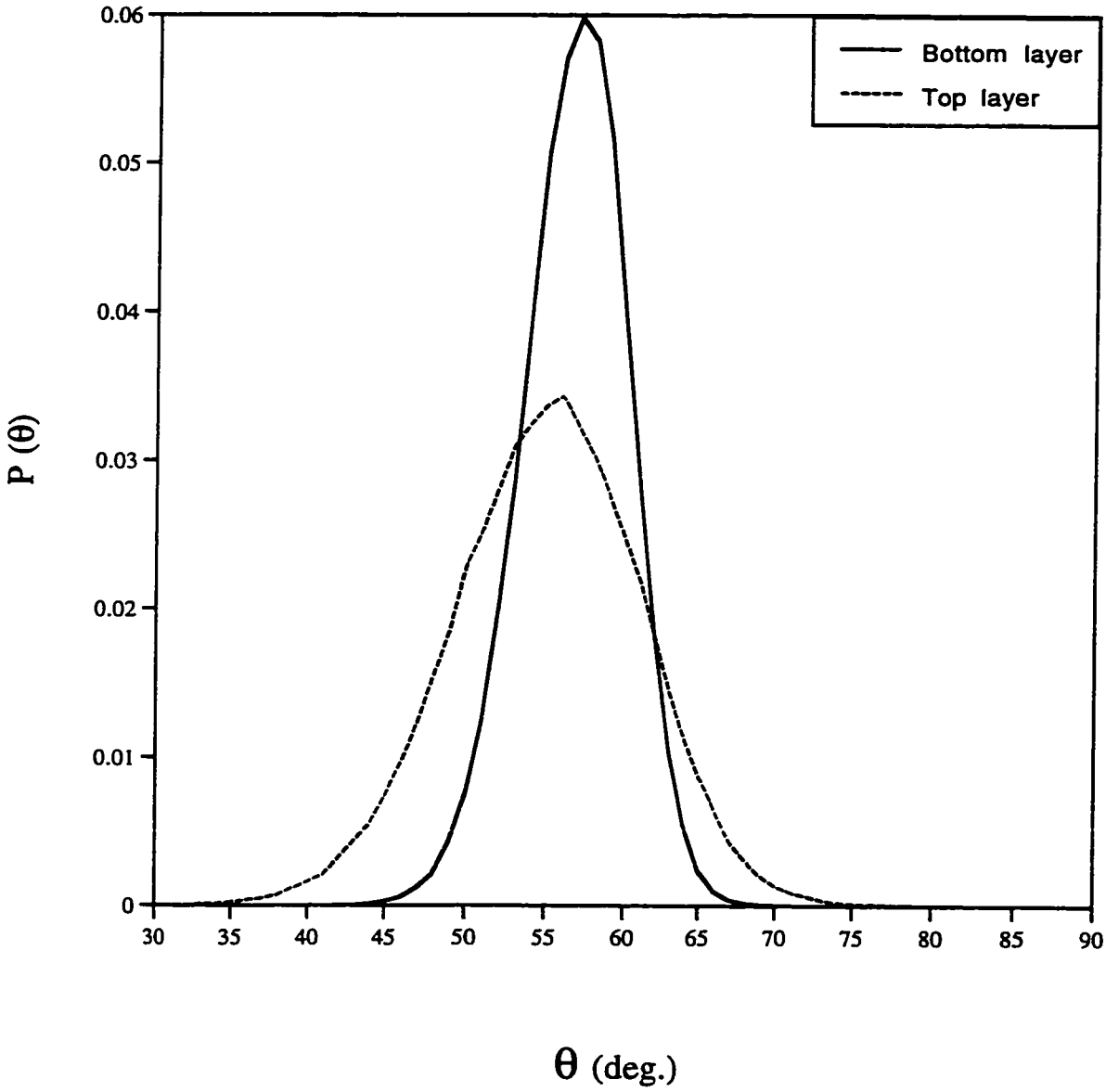

Figure 4.2.6 Theta distribution of a bilayer system at 55K {Top: $p(1\times1)$; Bottom: $p(1\times1)$}

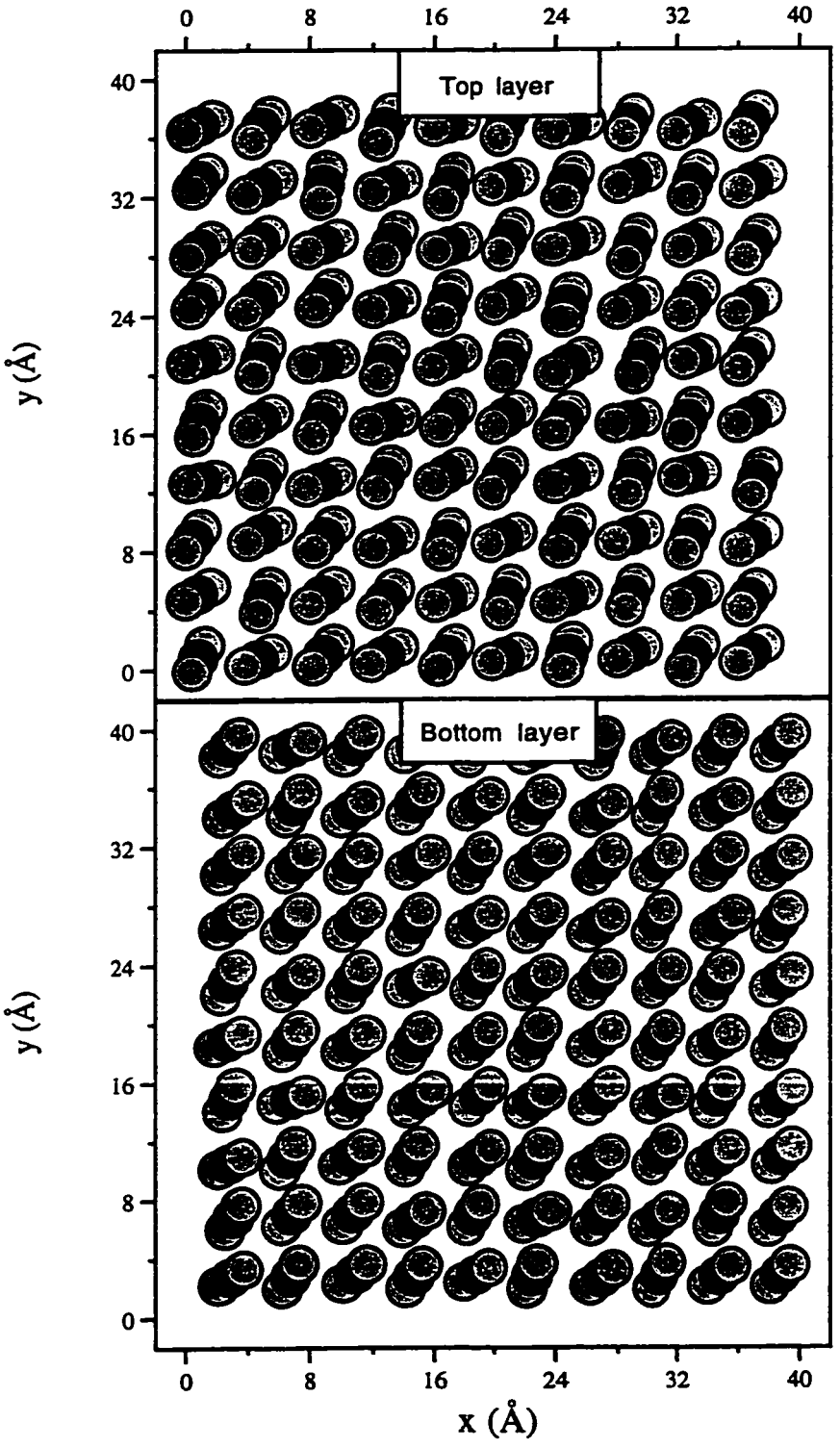

Figure 4.2.7 A bilayer {Top: $c(2\times2)$; Bottom: $c(2\times2)$} structure of CO_2/NaCl(001) at 55K

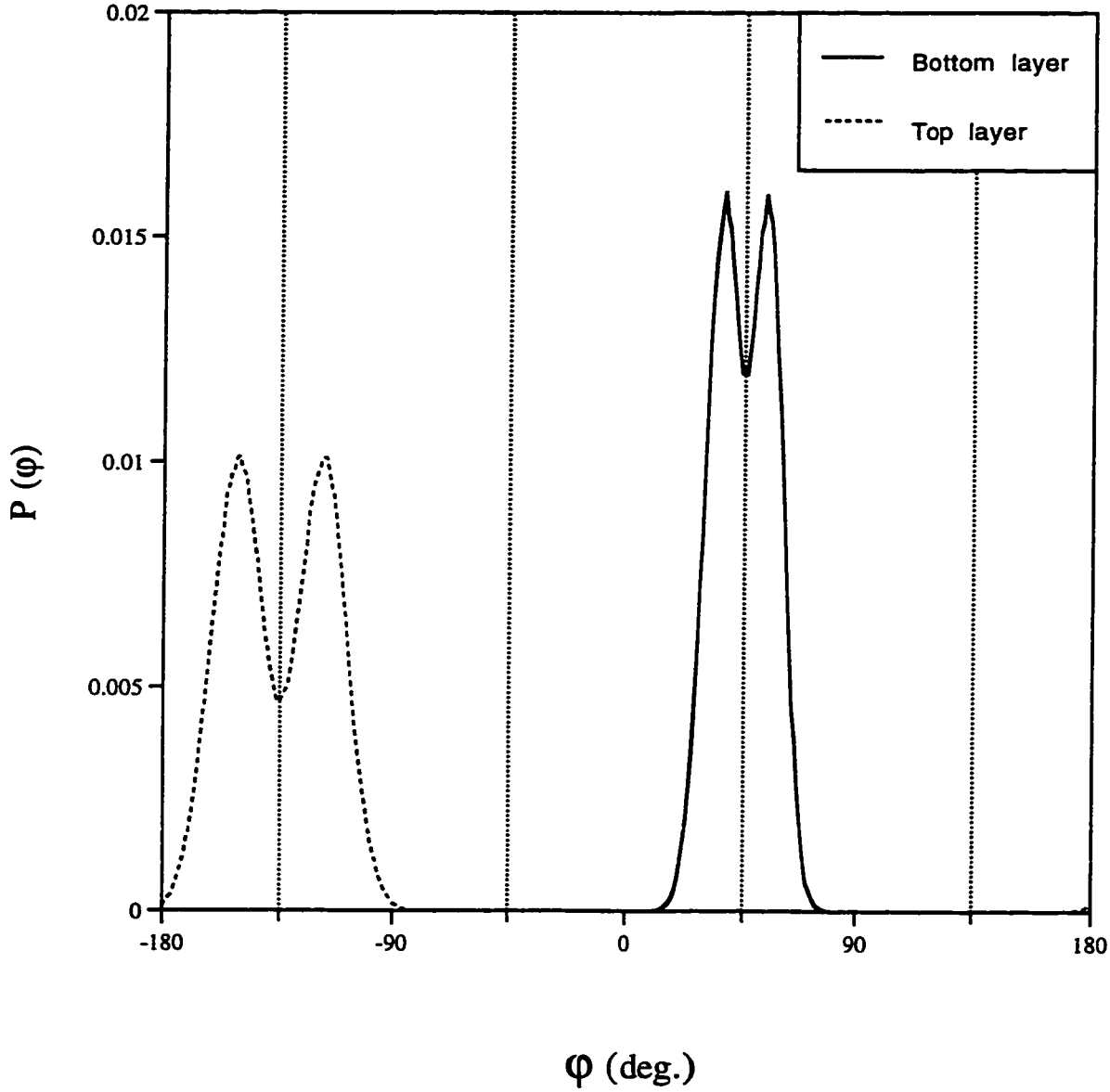

Figure 4.2.8 Phi distribution of a bilayer system at 55K {Top: $c(2\times2)$; Bottom: $c(2\times2)$}

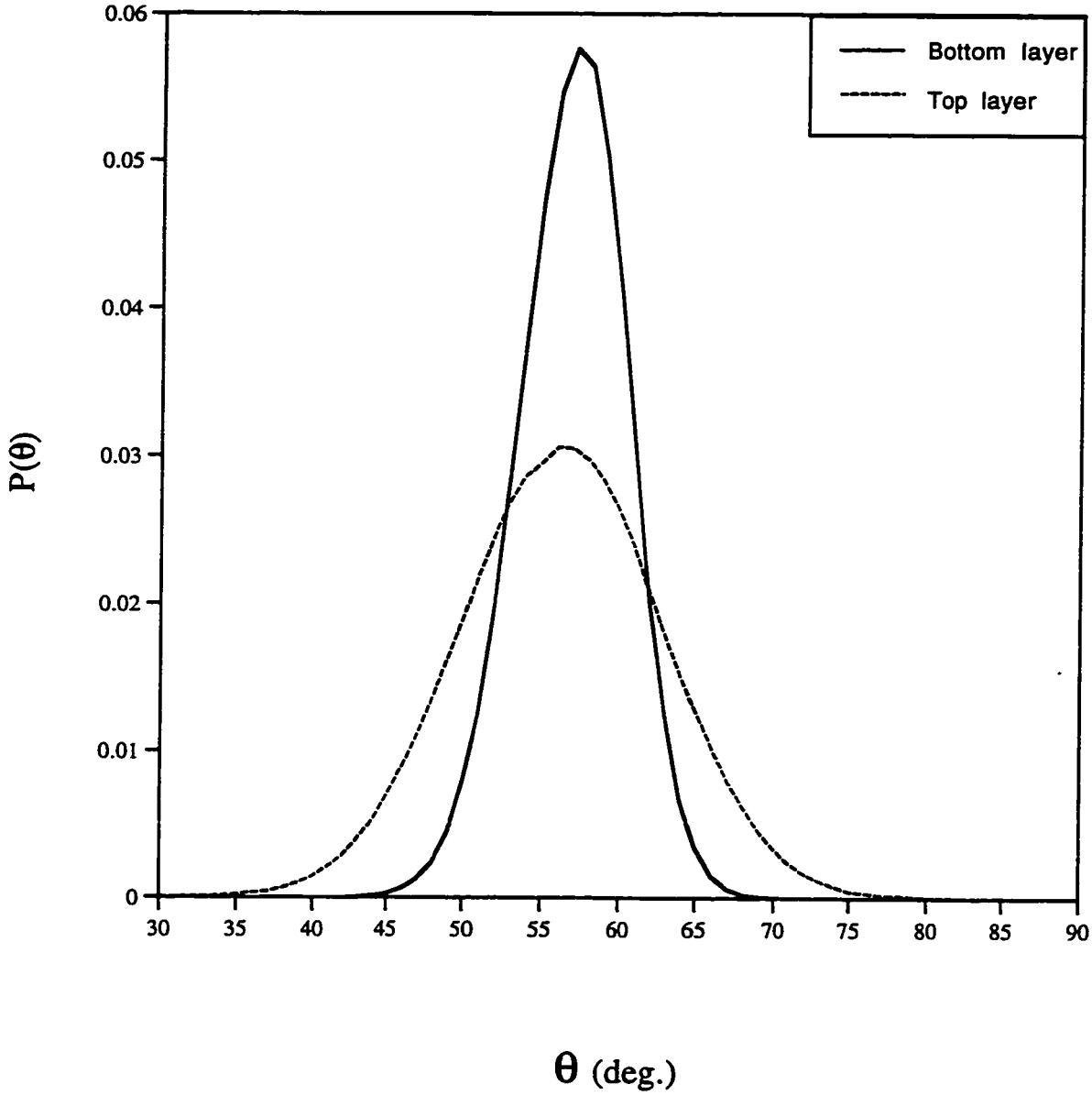

Figure 4.2.9 Theta distribution of a bilayer system at 55K {Top: $c(2\times2)$; Bottom: $c(2\times2)$}

4.3 Trilayer system

Previous work has shown that the $p(2\times1)$ trilayer system is unstable. The questions that remain are: Is a $c(2\times2)$ trilayer structure stable? And, how does it evolve to the bulk structure? Constructing a trilayer $c(2\times2)$ system just like the CO_2 crystal structure on NaCl(001) surface, we find the structure is thermally stable with the bottom layer distorting from its initial configuration (Fig.4.3.1). Moving from bottom layer to top layer, the molecular orientations come closer to the bulk crystal orientations (Fig. 4.3.2), or the separation between two azimuthal peaks gradually changes from 44° (bottom) to 84° (middle) and to 78° (top). In the meantime, the tilt angle remains the same (θ=57°) for three layers, but the peak becomes broader from bottom layer to top layer (Fig. 4.3.3).

Comparing the carbon atom average height above the surface for the $c(2\times2)$ and $p(2\times1)$ structures, we can see the $c(2\times2)$ structure is more compact than the $p(2\times1)$ structure {2.98Å/6.15Å/9.33Å for the $p(2\times1)$; 3.03Å/5.90Å/8.78Å for the $c(2\times2)$}. At T=55K, for the $p(2\times1)$ trilayer system, the structure is found to be not stable and the CO_2 molecules in the top two layers become disordered. Some of the molecules from the third layer collapse into the second layer[22]. Therefore, comparing the stability of structures and low energy, for multilayer (more than bilayer) system, the adsorbed molecules prefer the $c(2\times2)$ structure over the $p(2\times1)$ structure. These results support Toennies' group experimental results that as additional CO_2 was deposited, the resulting multilayers slowly adopted $c(2\times2)$ symmetry at the expense of the (2×1) phase leading to a range of exposures in which these two structures can coexist.

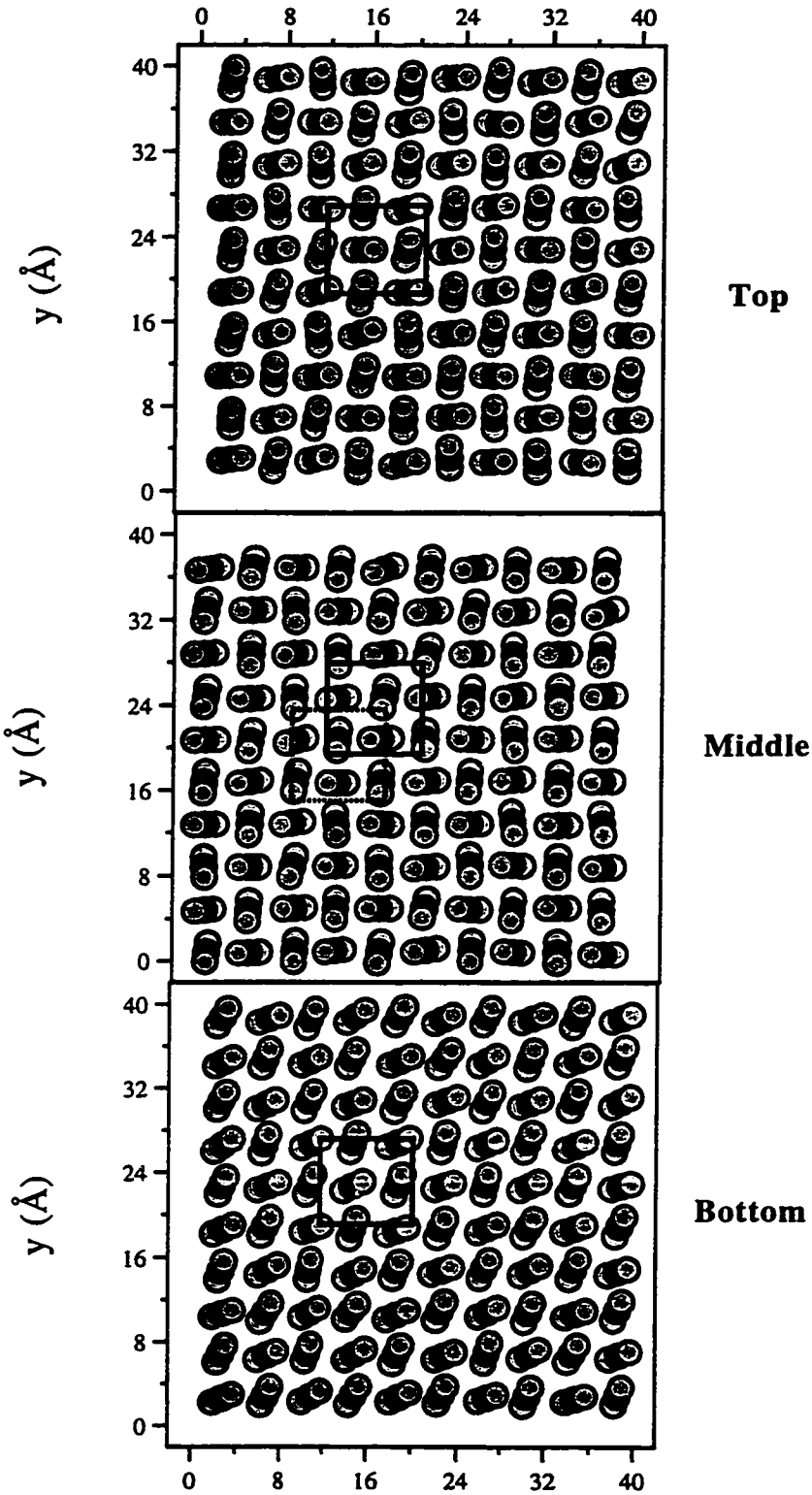

Figure 4.3.1 Top, Middle and Bottom layers of the $c(2\times2)$ trilayer structures

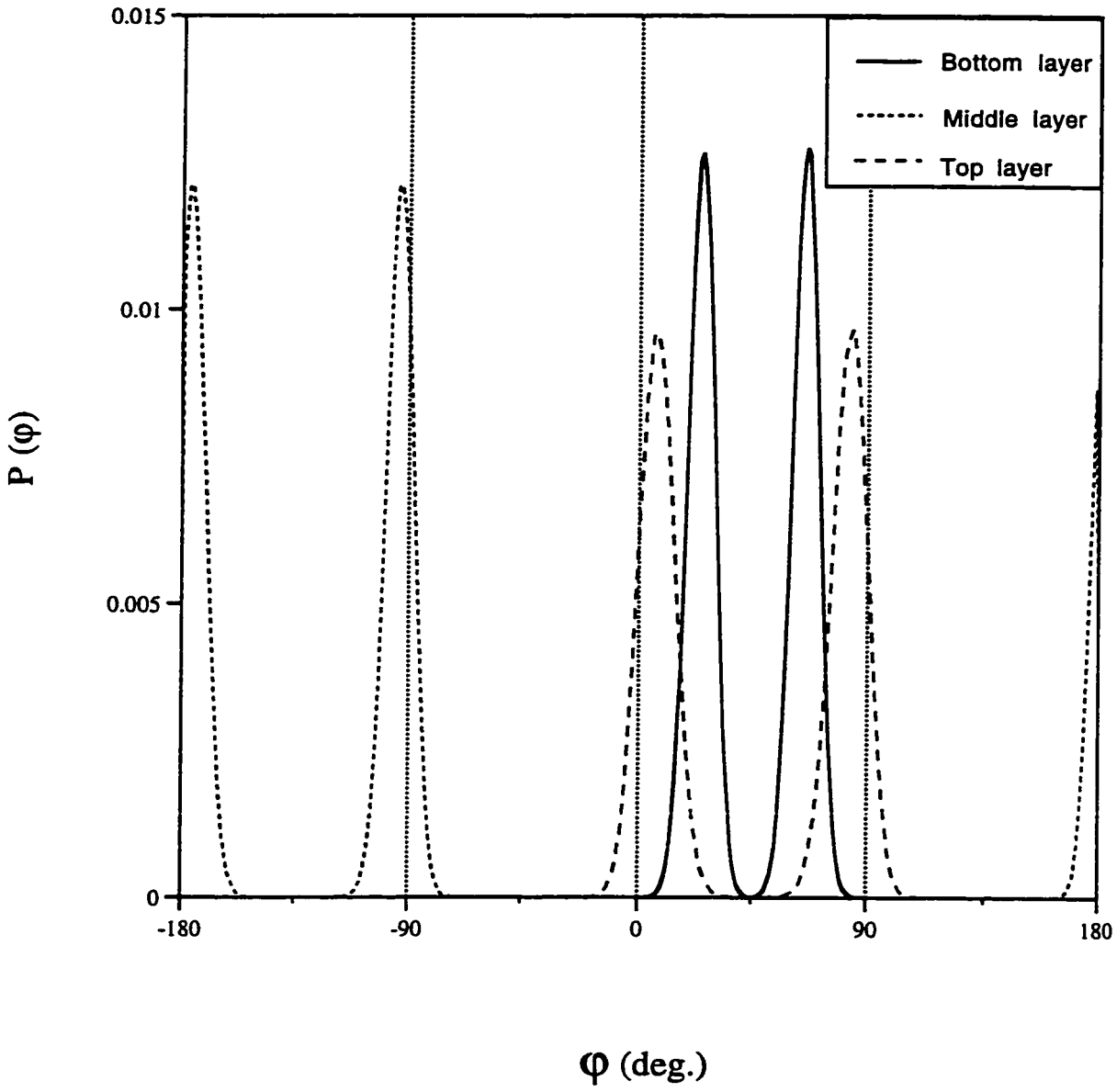

Figure 4.3.2 Phi distribution of the $c(2\times2)$ trilayer system at 55K

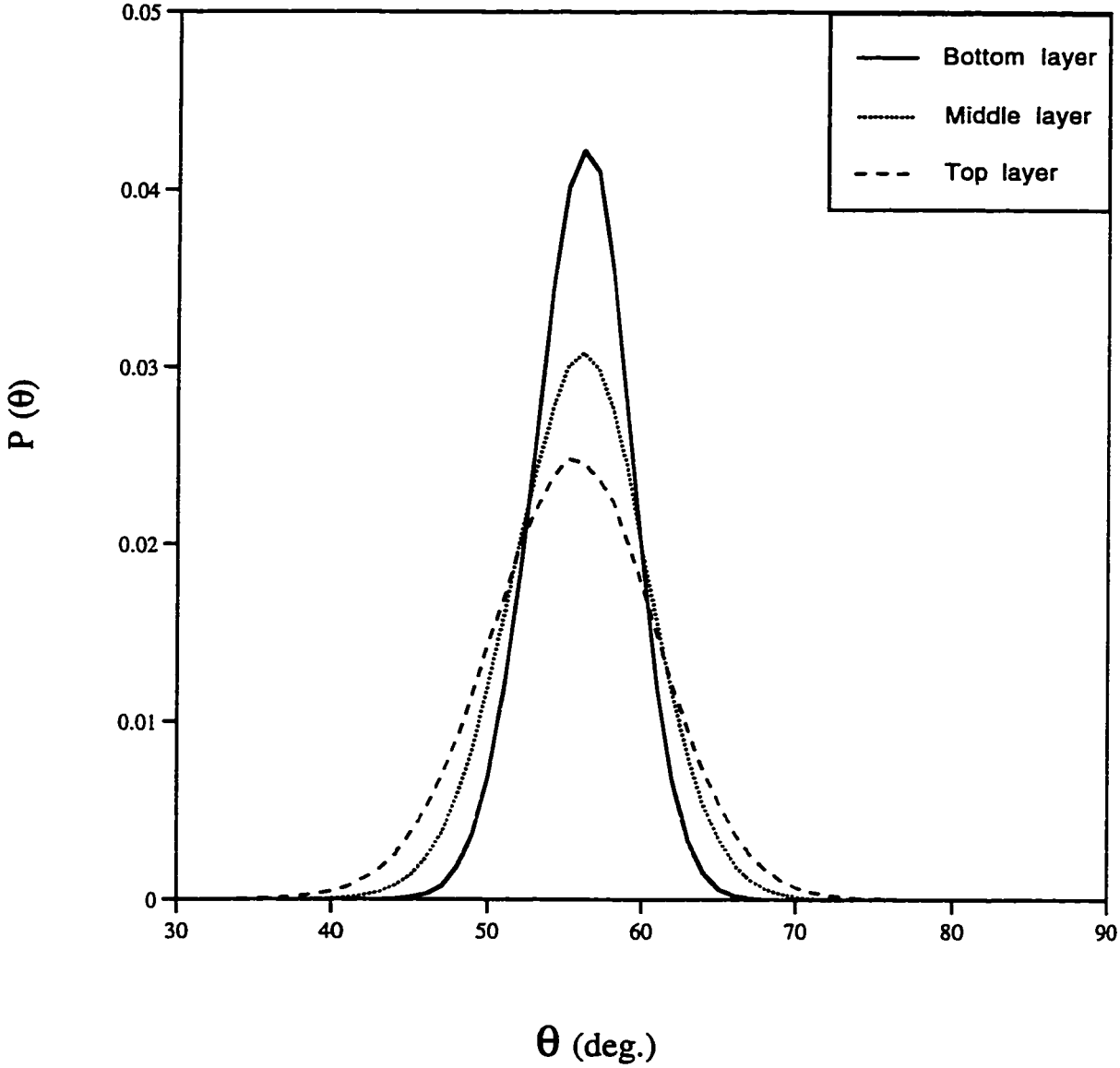

Figure 4.3.3 Theta distribution of the $c(2\times2)$ trilayer system at 55K

4.4 Nucleation and growth

4.4.1 Nucleation

Individual CO_2 molecules in the 2D gas phase lie flat on the surface and are oriented along the <110> directions whereas in the 2D solid phase $\{p(2\times1)\}$ the molecules tilt with respect to the surface and are oriented along the <100> directions. An individual molecule with the solid orientation is not at a stable point on the surface potential and will spontaneously realign to the 2D gas orientation if not stabilized. Therefore, the orientations of molecules can be used to detect different phases. We assume that an assembly of molecules are needed for the 2D solid to form. The conditions for nucleation of the 2D solid phase were examined using MC simulation.

Simulations at coverages of 5% to 25% of a monolayer were performed at same temperature where the molecules were started with random orientations and positions on the surface. The simulations were run for 100 kcycles with the first 10 kcycles discarded. We found that at T=55K, for coverages θ=5%, 8%, 10%, 12%, 14%, 15%, some of the molecules form a cluster with a small peak in the theta distribution at 58° which indicates some of the molecules have formed into the 2D solid phase. Figure 4.4.1 and 4.4.2 show the initial and final configurations for 5% and 12% coverages. Both of them form solid phase structures. For 20% coverage, all the molecules are parallel to the surface (Fig. 4.4.3). Most of the molecules are neighbors with each other, with the remaining few in an isolated state. This implies that most of molecules, which start with random

orientations and positions, aggregate together. There is a chance for some of them to form the (2×1) solid phase.

We construct a surface terrace to test if such a defect will cause for CO_2 molecules to form the (2×1) structure with the herringbone pattern on the surface. Figure 4.4.4 shows the initial configuration of 100 CO_2 molecules with random orientation and position on the NaCl defect and NaCl surface. From that configuration we run 50 kcycles with 20 kcycles discarded and got the final configuration shown in Figure 4.4.5. Although many molecules aggregate at the terrace edge, they do not form the (2×1) structure in this region. Away from the step edge a few molecules form a small cluster while the majority of molecules are parallel to the surface. The surface step is therefore not an important factor in the formation of the (2×1) structure. It is hard to form a solid cluster directly from the 2D gas phase.

Up to now, we still do not know what is the important factor for CO_2 molecules to nucleate the (2×1) solid phase structure on the NaCl(001) surface, but we notice in Figure 4.4.3 that even molecules which are parallel to the surface are likely to aggregate and form three typical kinds of structures. These structures may be considered condensed phases of molecules with the 2D gas orientation and have been tested at T=55K in both the 50% coverage and island configurations. The structures are $(\sqrt{2}\times\sqrt{2})R45°$, $(2\sqrt{2}\times\sqrt{2})R45°$ and a (2×1) gas phase structure and showing in Figure 4.4.6a, 4.4.7a and 4.4.8a respectively. We found that all of these structures are stable with all the molecules remaining flat on the surface. Islands

were formed by leaving a strip vacant ($1\sim 2d_{NaCl}$) around small clusters of these three structures (Fig. 4.4.6b, 4.4.7b, 4.4.8b). This gave more room for the CO_2 molecules to move around. All of these three small clusters are stable running 100 kcycles and discarding the first 50 kcycles. A comparison of the total energy per molecule reveals that the structures of the $(\sqrt{2}\times\sqrt{2})R45°$ and the $(2\sqrt{2}\times\sqrt{2})R45°$ have lower energies (-7.848kcal/mol and -7.821kcal/mol) than the (2×1) structure (-7.487 kcal/mol). So the possible structures of 50% submonolayer coverage are prefer the $(\sqrt{2}\times\sqrt{2})R45°$ and the $(2\sqrt{2}\times\sqrt{2})R45°$ structures.

Concentrating on these two structures, we consider what would happen if a molecule in the 3D gas phase was to adsorb onto this overlayer. We simulate this by dropping one molecule on top of such a layer. The additional molecule causes a tilt of two molecules with angle of 32°, and the CO_2 molecules to reorient their axes along the Na^+-Cl^- direction similar to the structure of the (2×1) solid phase. Figure 4.4.9a and 4.4.9b show the final configurations of structures $(\sqrt{2}\times\sqrt{2})R45°$ and $(2\sqrt{2}\times\sqrt{2})R45°$ respectively. If we drop more molecules in these systems, more of the parallel molecules will be converted to the 2D solid like structure. Therefore, it is reasonable to suppose that the $(\sqrt{2}\times\sqrt{2})R45°$ and $(2\sqrt{2}\times\sqrt{2})R45°$ (may include (2×1) gas phase) structures are precursor structures for the formation of islands with the 2D solid phase structure. After the isolated gas molecules form one of these kinds of structures, it is easy to form the solid phase (2×1) structure through the adsorption of molecules overtop of these structures.

4.4.2 Growth

In order to determine the growth fashion of adsorbed CO_2 molecule on the overlayer, we test the favored bonding sites when one molecule is putting into an adsorbed island-layer system. We consider three kinds of structures, one is $(2\times1)/(2\times1)$, one is $(2\times2)/(2\times1)$ and another is $(2\times2)/(2\times2)$ (where we use the nomenclature: island/monolayer). The system we considered consists of 150 molecules: 100 molecules form the adsorbed monolayer with either the (2×1) or (2×2) structure where another 50 molecules formed into a cluster overtop of the monolayer with the (2×1) or (2×2) structure. We put one CO_2 molecule in three position: on the top of island, at the edge of island and on the top of the monolayer respectively, and run 10 kcycles with the first 2 kcycles discarded at temperature 55K. We found that the adsorption energy of the 151st molecule is lowest (i.e. is most strongly attracted) when it adsorbs at the island edge for all these three cases. Then it is next lowest on the top of monolayer, and the highest when on the top of island (Table 4.4.1). This result shows that the adsorbed CO_2 molecules are likely to grow layer by layer with the Frank-van der Merwe mode in all of these three kinds of structures. For three layers or more, previous work[22] found that the (2×1) structure is not stable and in some regions the (2×1) structure converts to a $c(2\times2)$ structure. In that case, the growth fashion might then be of the Stranski-Krastanov type because multilayer islands on top of the bilayer will nucleate at the regions which have adopted the energetically favoured $c(2\times2)$ (bulk-like) crystalline structure. At this time, the mechanism of how the (2×1) structure converts to the $c(2\times2)$ structure is still unsolved.

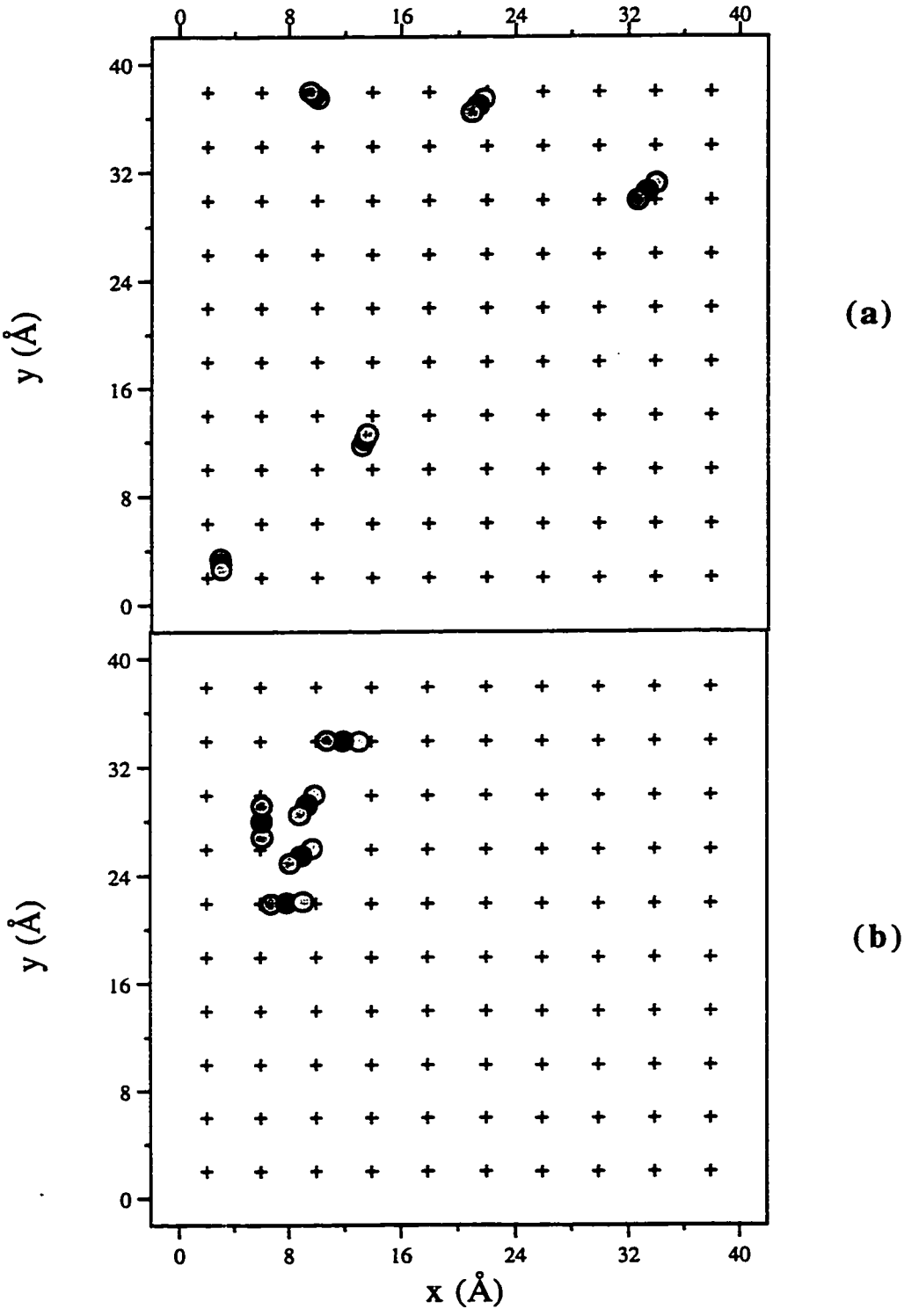

Figure 4.4.1 The initial (a) and final (b) configurations at 5% coverage of CO_2 molecules on the NaCl(001) surface at 55K

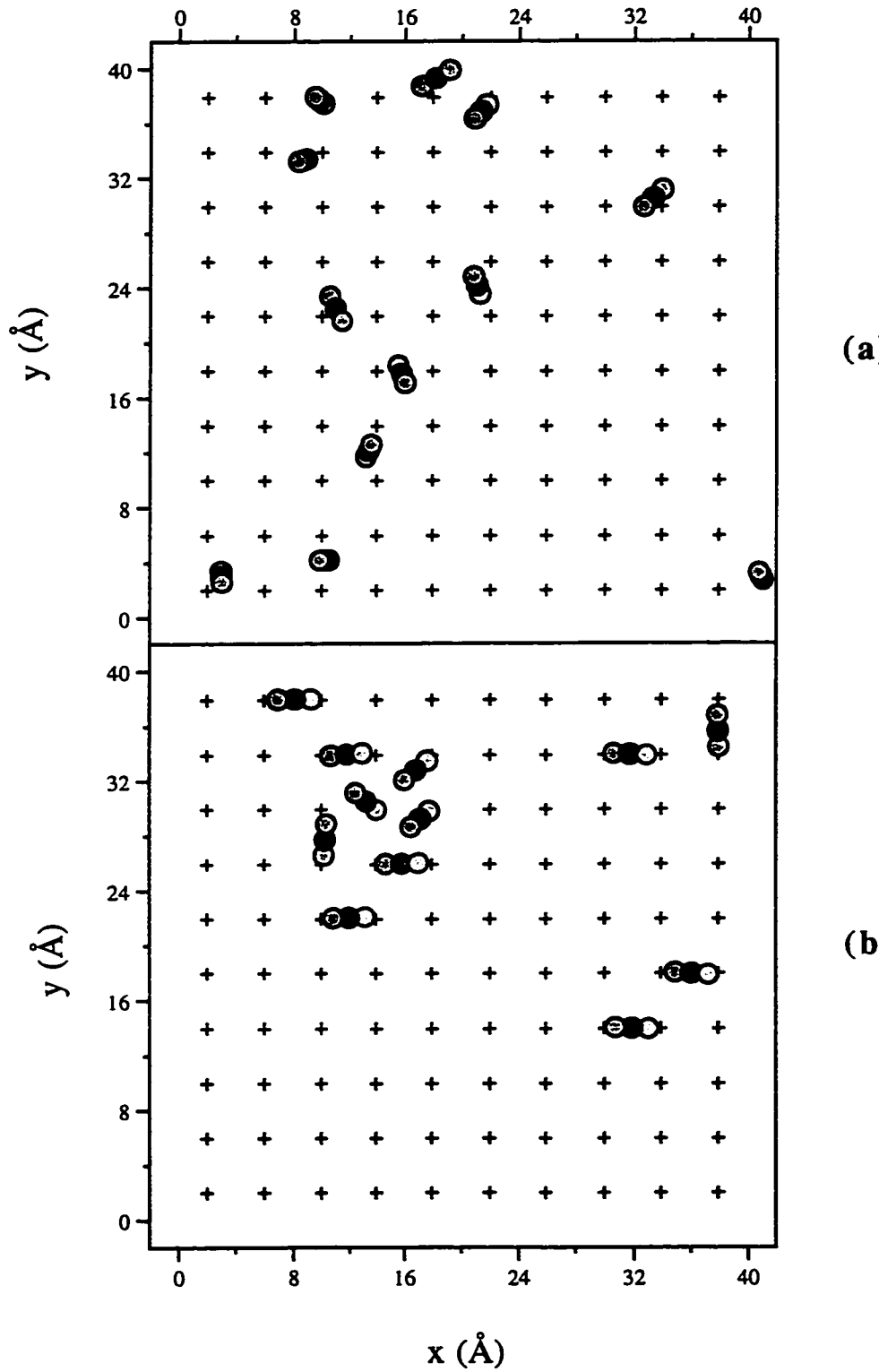

Figure 4.4.2 The initial (a) and final (b) configurations at 12% coverage of CO_2 molecules on the NaCl(001) surface at 55K

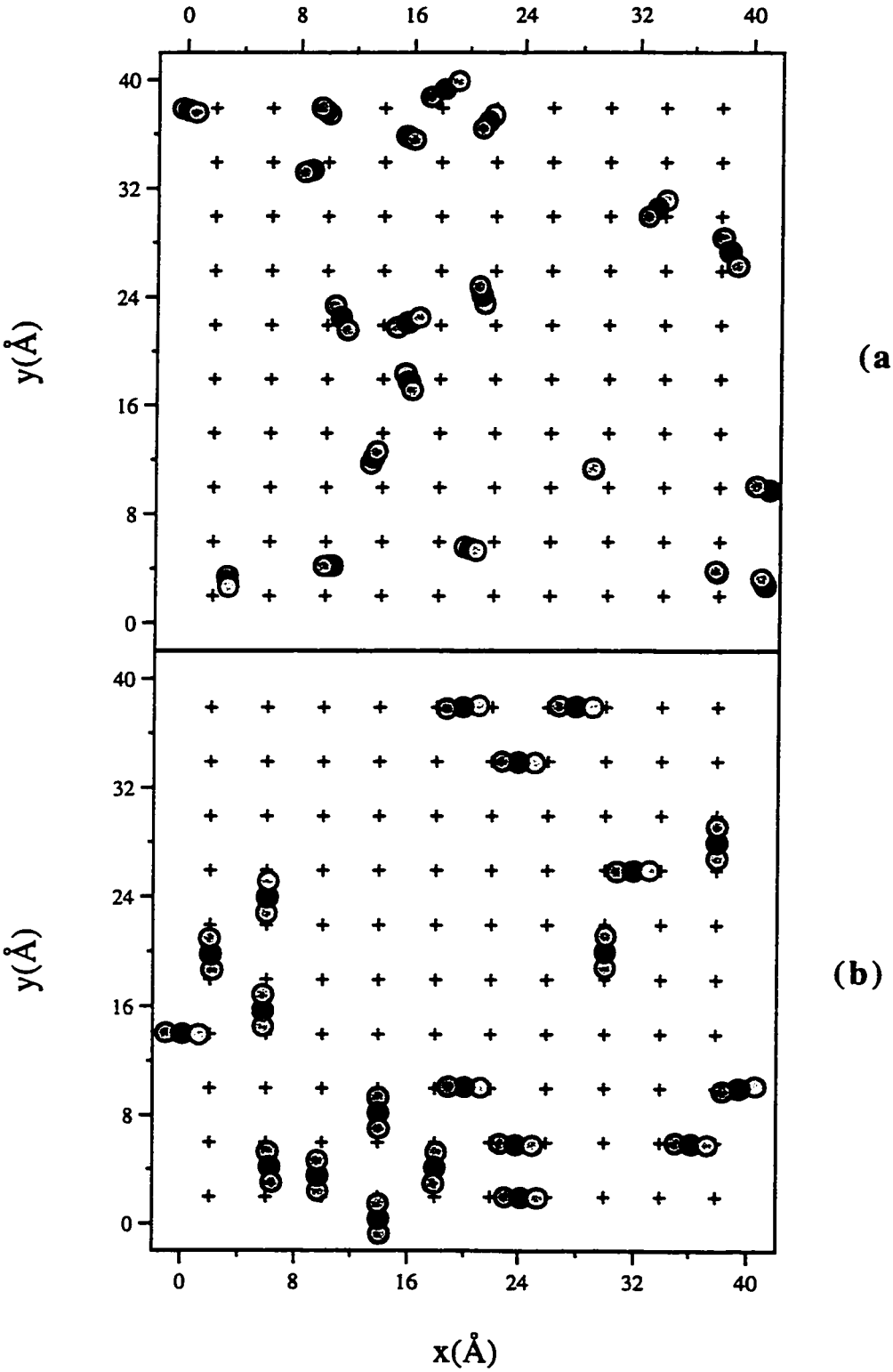

Figure 4.4.3 The initial (a) and final (b) configurations at 20% coverage of CO_2 molecules on the NaCl(001) surface at 55K

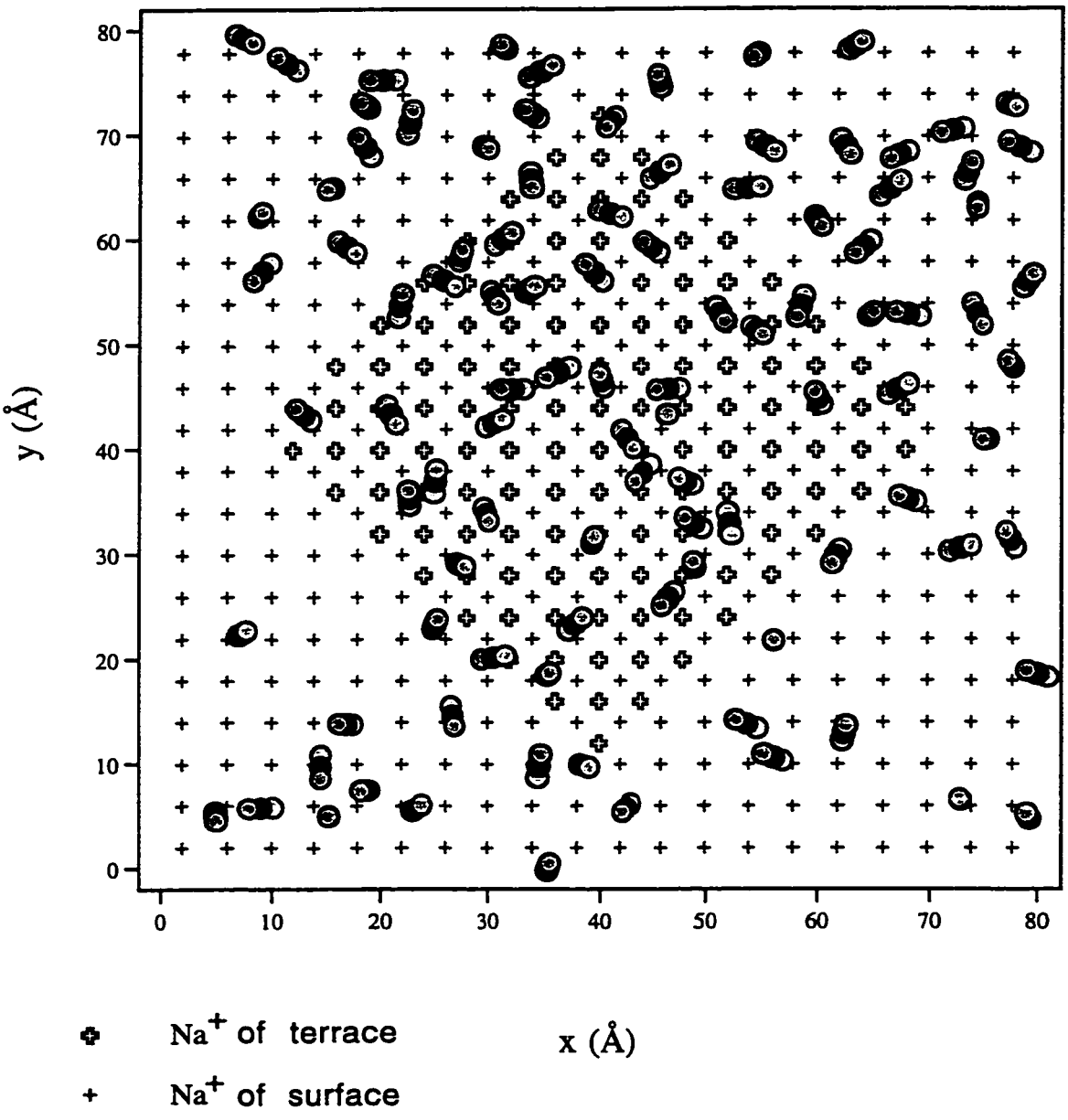

Figure 4.4.4 The initial configuration of CO_2 molecules on a NaCl(001) surface with a step defect

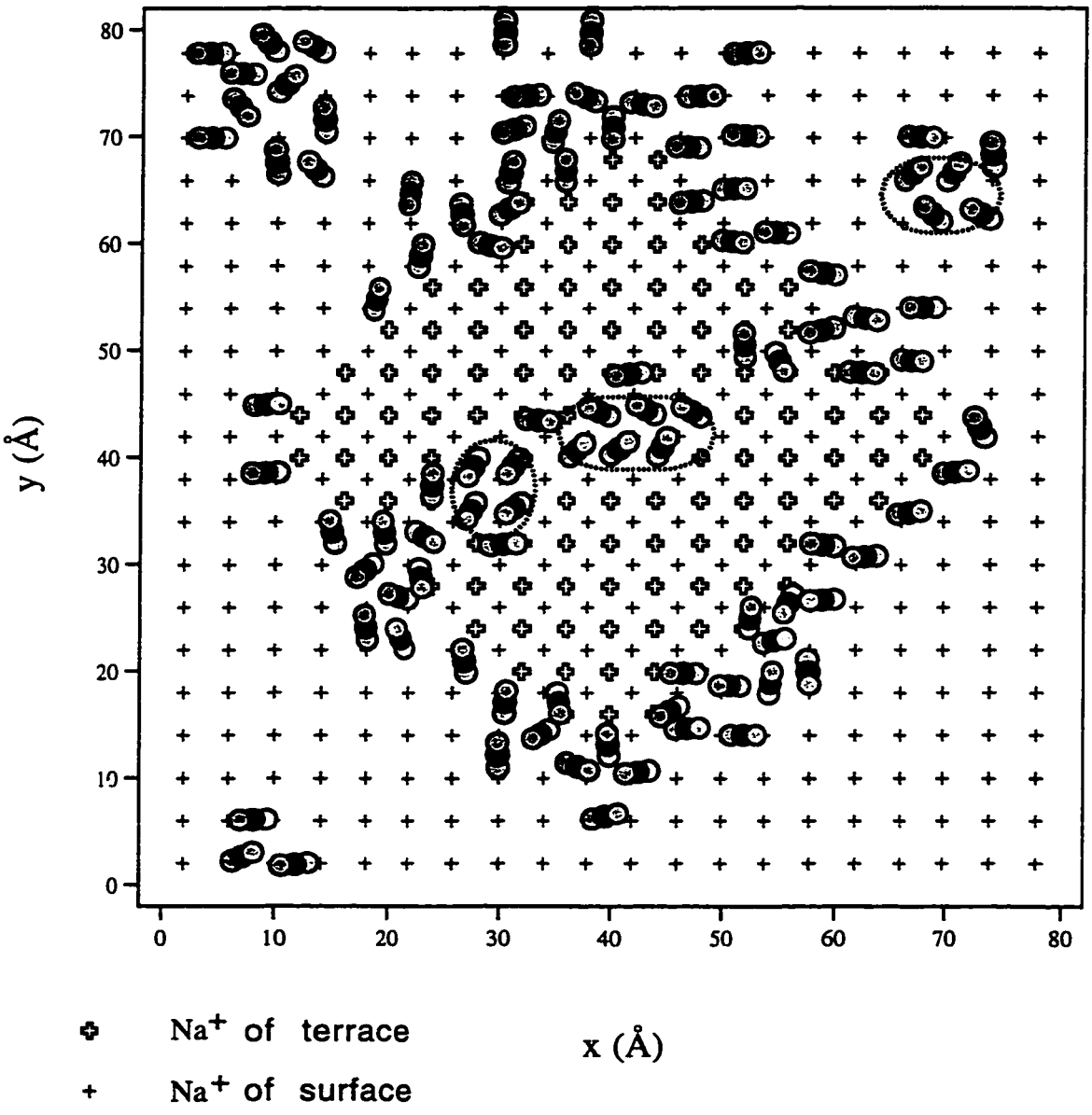

Figure 4.4.5 The final configuration of CO_2 molecules on a NaCl(001) surface with a step defect at T=55K

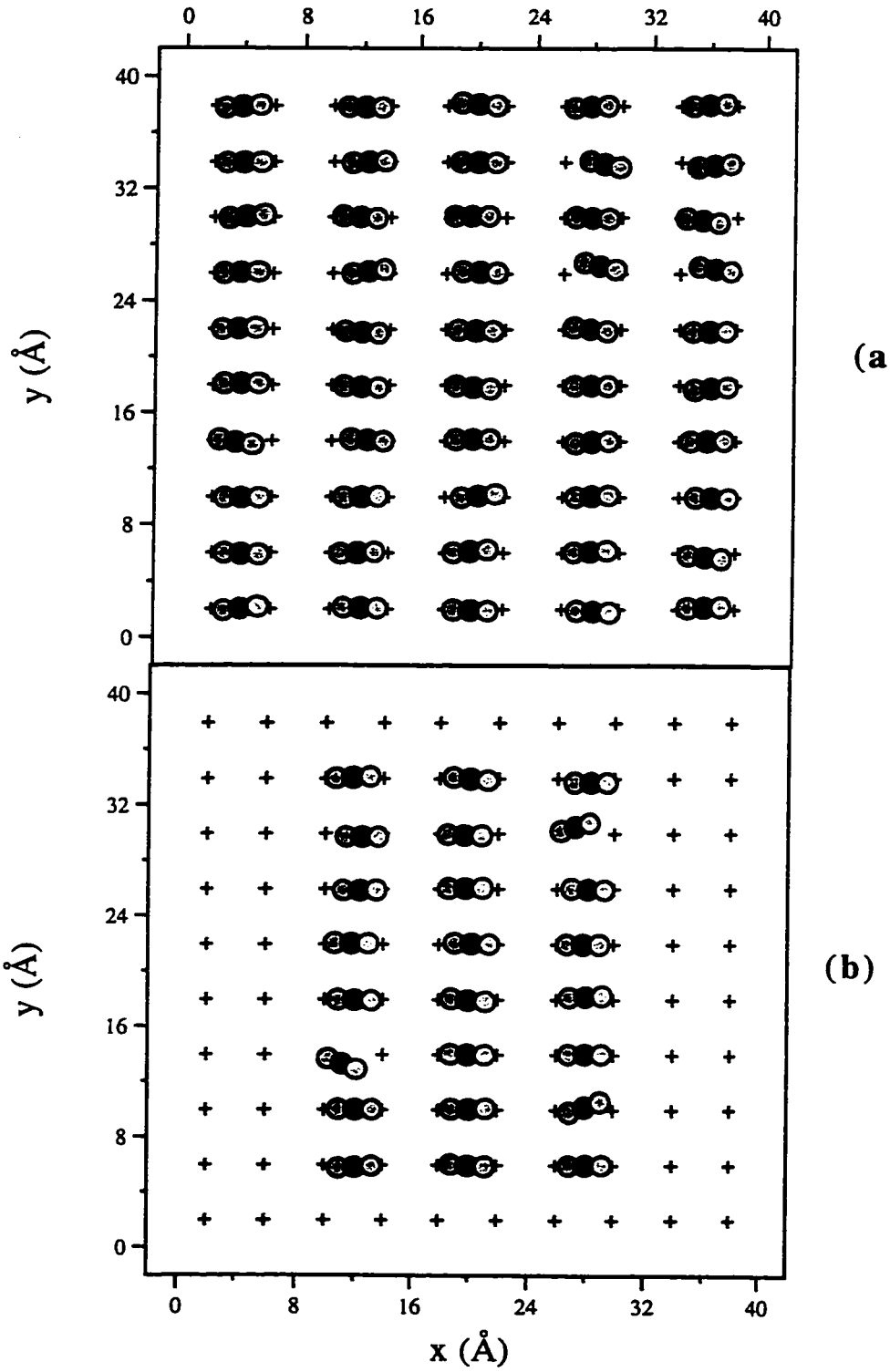

Figure 4.4.6 2D gas phase (2×1) structure of CO_2/NaCl(001) system at 55K (a) fully covered (0.5ML); (b) with a stripe space around cluster.

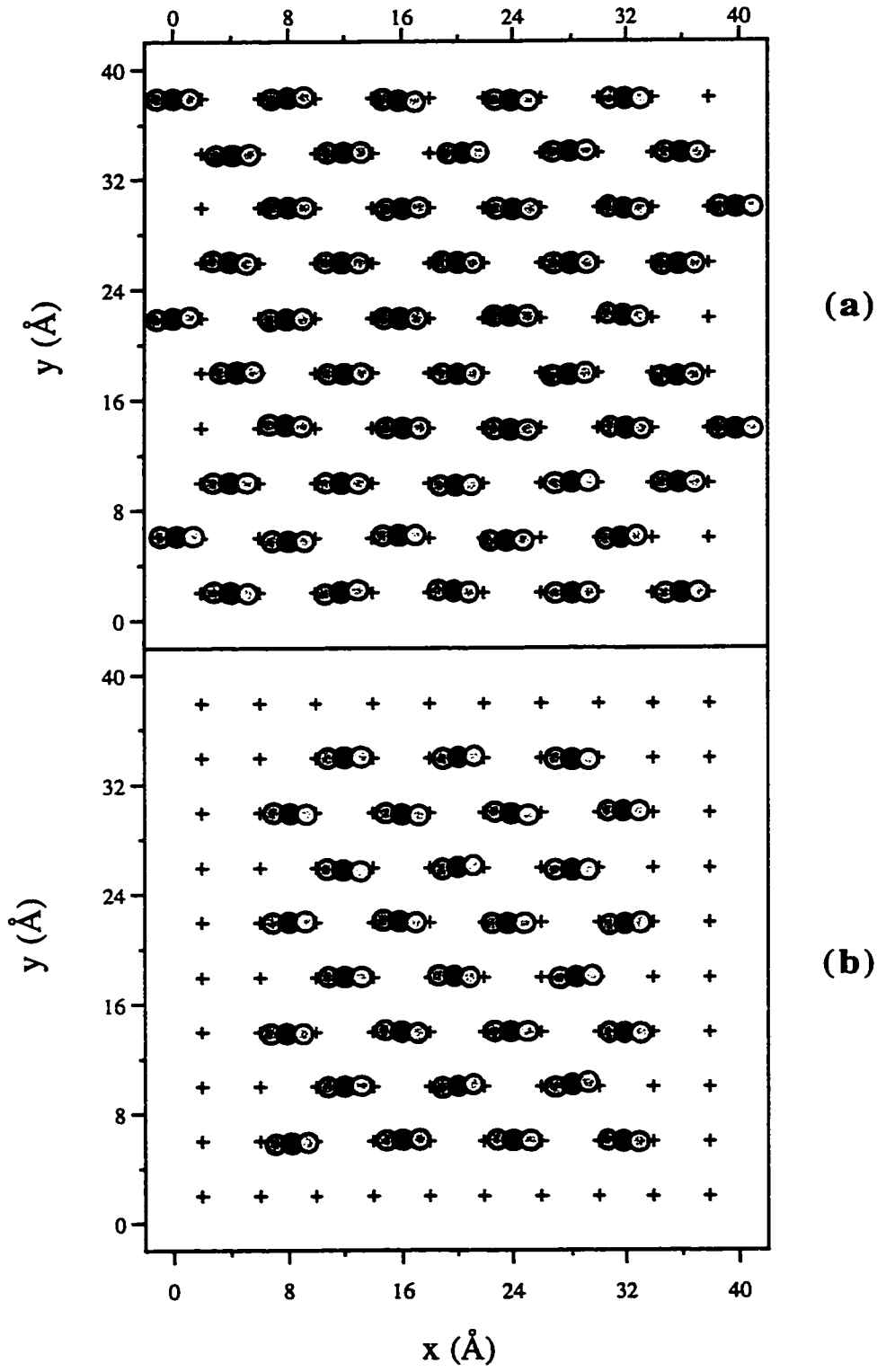

Figure 4.4.7 2D gas phase $(\sqrt{2}\times\sqrt{2})R45°$ structure of CO_2/NaCl(001) system at 55K (a) fully covered (0.5ML); (b) with a stripe space around cluster

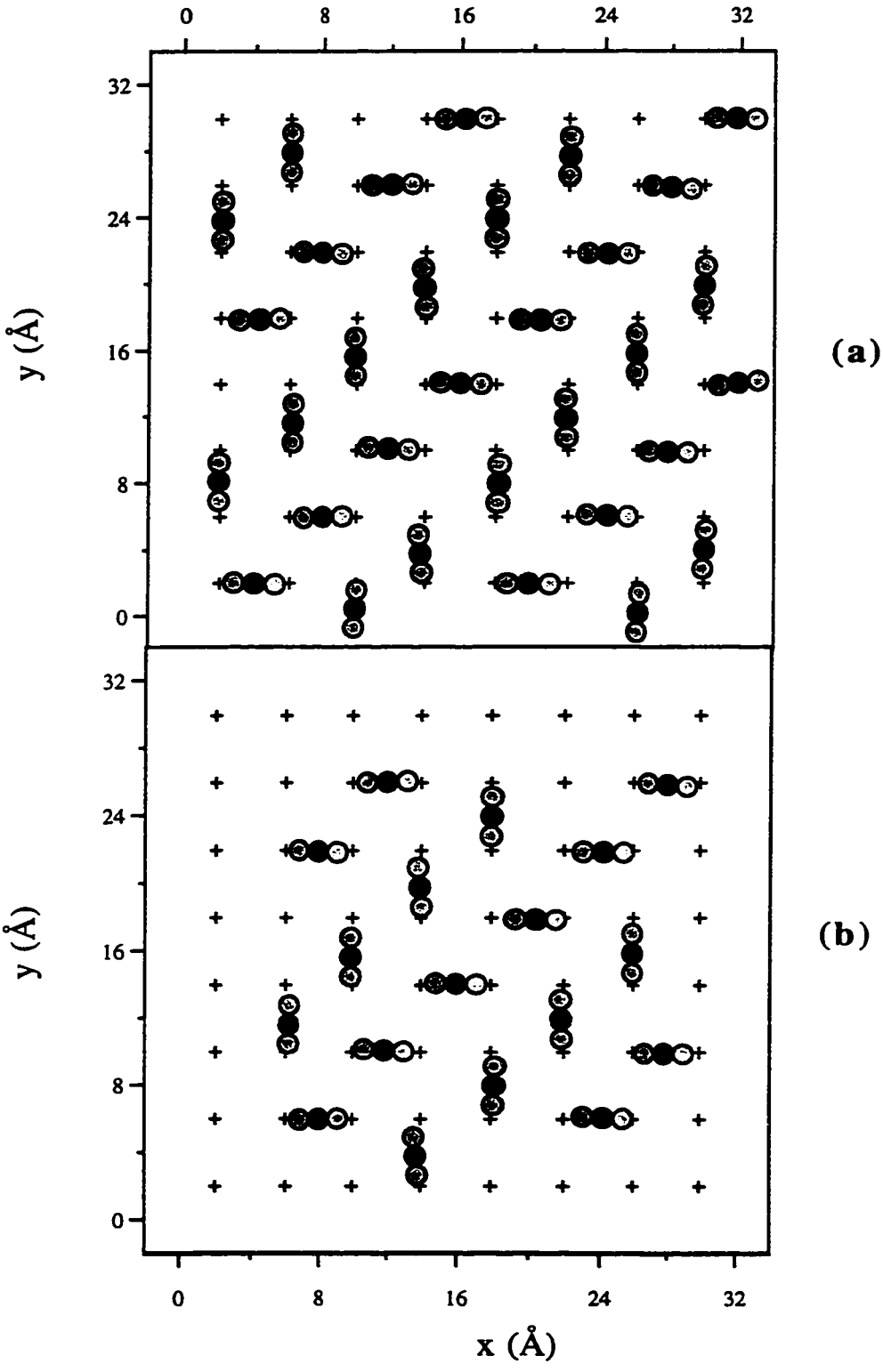

Figure 4.4.8 2D gas phase $(2\sqrt{2} \times \sqrt{2})R45°$ structure of CO_2/NaCl(001) system at 55K (a) fully covered (0.5ML); (b) with a stripe space around cluster

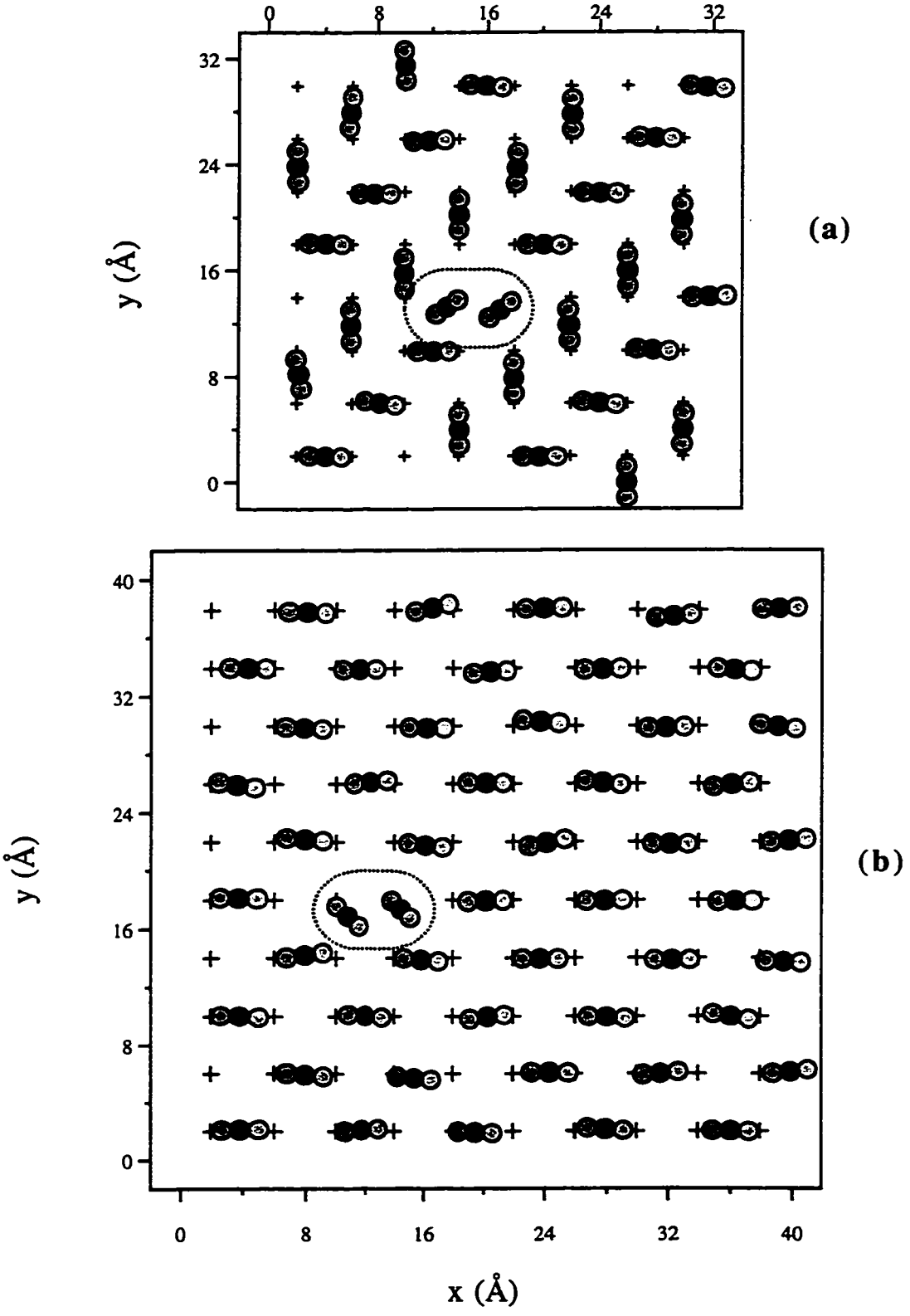

Figure 4.4.9 The (50%+1) coverages of the (a)$(2\sqrt{2}\times\sqrt{2})R45°$ and (b) $(\sqrt{2}\times\sqrt{2})R45°$ 2D gas phase structures of CO_2/NaCl(001) at 55K

Table 4.4.1 Energy for Molecules at Different Sites in Different Structures (55K)

E_{150} (kcal/mol) ($\Delta E=E_{151}-E_{150}$) (island / monolayer)	E_{150+1} (kcal/mol) (Adding molecule is at different sites)		
	at the island edge	on the top of monolayer	on the top of island
(2×1)/(2×1) -1084.93	-1090.85	-1089.10	-1089.00
ΔE	-5.92	-4.17	-4.07
(2×2)/(2×1) -1088.71	-1093.12	-1092.85	-1092.59
ΔE	-4.41	-4.14	-3.88
(2×2)/(2×2) -1098.21	-1102.72	-1102.18	-1101.60
ΔE	-4.51	-3.97	-3.39

4.5 2D gas and solid phase coexistence curve

The dynamic equilibrium between a 2D gas and a 2D solid in the adsorbed phase can be described by the two-dimensional van der Waals equation. Bauer's group has done a lot of work on the Au/W(001) system and have been able to determine the 2D condensed phase and 2D gaseous phase coexistence lines[30]. They found that these lines have the form predicted by the reduced van der Waals equation for a mobile adsorbate[31]. Using the same idea, the behavior of CO_2 molecules adsorbed on the NaCl(001) surface at low coverage also can be described by the two-dimensional van der Waals equation[32]

$$\Pi = \frac{k_B T}{\beta}\left(\frac{\Theta}{1-\Theta} - \frac{\alpha\Theta^2}{k_B T \beta}\right) \tag{4.5.1}$$

where Π is the spreading pressure, β is the area occupied by each adsorbed molecule, α is the two-dimensional van der Waals constant and Θ is the coverage. From this equation we can obtain, using the condition $\frac{d\Pi}{d\Theta} = 0$, the 2D gas-solid coexistence curve equation

$$2\,\alpha\,\Theta\,(1-\Theta)^2 = k_B\,T\,\beta \tag{4.5.2}$$

From the equation and the condition $\frac{d^2\Pi}{d\Theta^2} = 0$, we get the critical coverage $\Theta = 1/3$ and critical temperature $T_c = \frac{8}{27k_B}\frac{\alpha}{\beta}$.

Considering the fact that dropping an additional molecule on either of the two stable 50% coverage structures will cause a tilt of

two molecules, it is reasonable to assume that the 50% coverages of the (2×1), $(\sqrt{2}\times\sqrt{2})R45°$ and $(2\sqrt{2}\times\sqrt{2})R45°$ 2D "gas" structures are other kinds of 2D solid phase structures. These structures correspond to 100% coverage solid phase with molecule tilted from the surface normal. Modifying the two-dimensional van der Waals equation by using a factor 2Θ instead of factor Θ, we get

$$\Pi = \frac{k_B T}{\beta}\left(\frac{2\Theta}{1-2\Theta} - \frac{\alpha(2\Theta)^2}{k_B T \beta}\right) \tag{4.5.3}$$

Using the usual criteria ($\frac{d\Pi}{d\Theta}=0$), we get the equation of two phase coexistence curve

$$T = \frac{4\alpha}{\beta k_B}\Theta(1-2\Theta)^2 \tag{4.5.4}$$

Using the condition $\frac{d^2\Pi}{d\Theta^2}=0$ and equation 4.5.4, the critical coverage Θ_c and critical temperature T_c are found to be 1/6 and $\frac{8}{27k_B}\frac{\alpha}{\beta}$ respectively. Expanding the equation near the critical coverage Θ_c, we have

$$T = \frac{16\alpha}{\beta k_B}(\Theta-\Theta_c)^3 - \frac{8\alpha}{\beta k_B}(\Theta-\Theta_c)^2 + \frac{8\alpha}{27\beta k_B} \tag{4.5.5}$$

In the 3D gas phase, the critical temperature of CO_2 is $T_c^{3D}=\frac{8}{27k_B}\frac{a}{b}=304.2\text{K}$[9]. The relation of van der Waals constants between 3D and 2D is $\frac{a}{b}=2\frac{\alpha}{\beta}$[9]. So for 2D phase, the estimated critical temperature is $T_c^{2D}=T_c^{3D}/2=152.1\text{K}$.

In order to test these results and draw the solid-gas coexistence curve, the following work was performed:

(1) For a given coverage, we arrange the CO_2 molecules in an island with a $p(2\times1)$ herringbone structure on the NaCl(001) surface at some temperature T. From this initial configuration we run 100 kcycles, throw away the first 50 kcycles and then calculate the average of tilt angle θ for the remaining 50 kcycles. The maximum of the θ distribution found near 54° (with respect to the surface normal), is due to CO_2 molecules belonging to the 2D solid phase. The maximum near 90° is due to CO_2 molecules which are parallel to the surface and hence belong to 2D gas phase. If these two peaks simultaneously appear in the θ distribution, it means that the 2D solid and gas phases coexist (see Fig. 4.5.1). We monitor the area of the peak of the solid phase (near 54°) to judge whether the two phases can coexist. At each temperature, we calculate the area under the peak corresponding to the solid phase. Since the θ distributions are normalized to unity, this area is numerically equal to the percentage of the CO_2 adsorbate which is in the 2D solid phase. Figure 4.5.1 shows the θ distribution at coverage $\Theta=2\%$ at temperatures T=30K, 73K, and 75K. As the temperature increasing, the 54° peak decreases and the 90° peak increases.

(2) We change the temperature and repeat the above steps, then we draw a curve of the area under the solid phase peak as function of temperature T. From the curve we can estimate the first

order transition temperature T_o where the solid phase disappears and only the gas phase remains (see Fig.4.5.2).

(3) We chose several coverages (2%, 5%, 7.5%, 10%, 12.5% and 15%) and repeated the above step and found the corresponding T_o. Figure 4.5.2 shows the relation between temperature T and the percentage $P(\Theta)$ of the adsorbate in the 2D solid phase at different coverages. From this picture, we know the transition temperature T_o for various coverages (see Table 4.5.1).

Using this set of data we can draw the gas-solid coexistence curve (Fig. 4.5.3) and get a quadratic equation between temperature T(K) and coverage Θ as follows.

$$T = - 3302.7\Theta^2 + 1070.1\Theta + 54.6 \qquad (4.5.6)$$

The maximum in this equation occurs at Θ_c =0.162 where T_c=142.9K. This point on the coexistence curve correspond to the critical point. The value of 0.162 is the critical coverage and 142.9K is the critical temperature as determined by the simulations. If we reorganize this equation around the critical point, we get

$$T = - 3302.7(\Theta - 0.162)^2 + 142.9 \qquad (4.5.7)$$

Experiment[4] shows that when the coverage is equal to 0.04% of a monolayer, the coexistence temperature T is found to be 45K. From the equation above, we get the value of 54.6K for this coverage.

This equation is similar to the theoretical equation (4.5.5) if we ignore the cubic term. It is reasonable to do this because we expand the equation near the critical coverage Θ_c , so that higher orders of the $(\Theta-\Theta_c)$ term can be ignored and the quadratic equation can be used near the critical coverage. However we do not expect this equation to hold close to the critical point. The quadratic nature of the equation is typical of a mean field theory[33][34] which predicts that $\Theta-\Theta_c \sim |T-T_c|^{1/2}$ as the critical point is approached. It is well established that close to the critical point the value of the critical exponent changes from the mean field value of 1/2. In the case of a mobile atomic adsorbate the critical behavior falls into the same universality class as the 2D Ising model thus yielding a critical exponent of 1/8[33][34].

Comparing our simulation results with calculated values, the critical coverage is very close to the theoretical value $\Theta=1/6=0.167$ and the critical temperature is near the previously estimated value $T_c=151.2$K. Therefore, we can say that the 2D van der Waals equation and two-dimensional phase coexistence curve we got can well describe the behavior of CO_2 molecules on the NaCl(001) surface in the low coverage (near and below the critical coverageΘ_c) regions.

Table 4.5.1 Transition temperature T_0 and coverages Θ

Θ(%)	2.0	5.0	7.5	10.0	12.5	15.0
T_0(K)	75	103	116	129	133	143

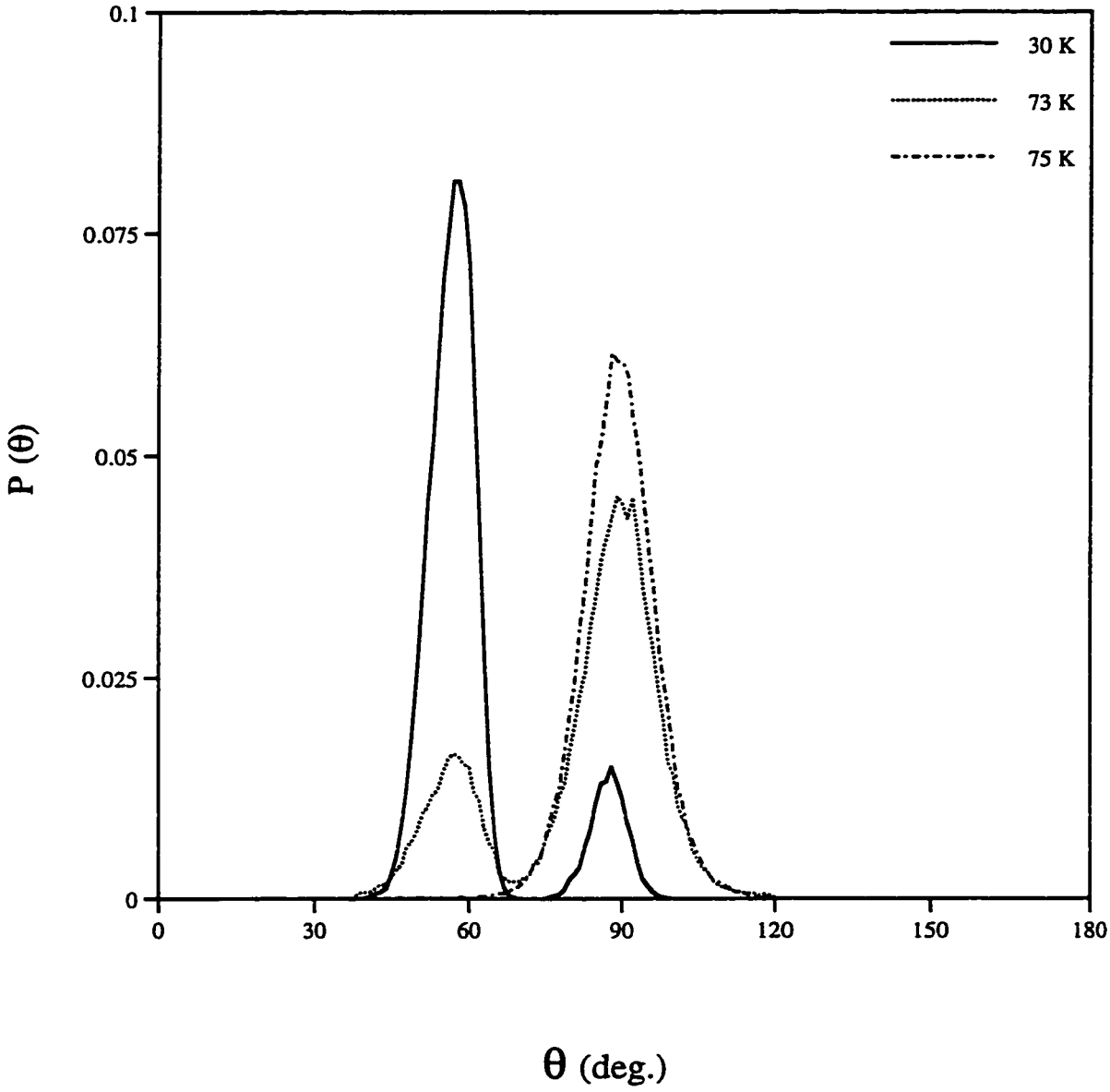

Figure 4.5.1 Theta distribution at coverage Θ = 2 % (T=30K, 73K, 75K)

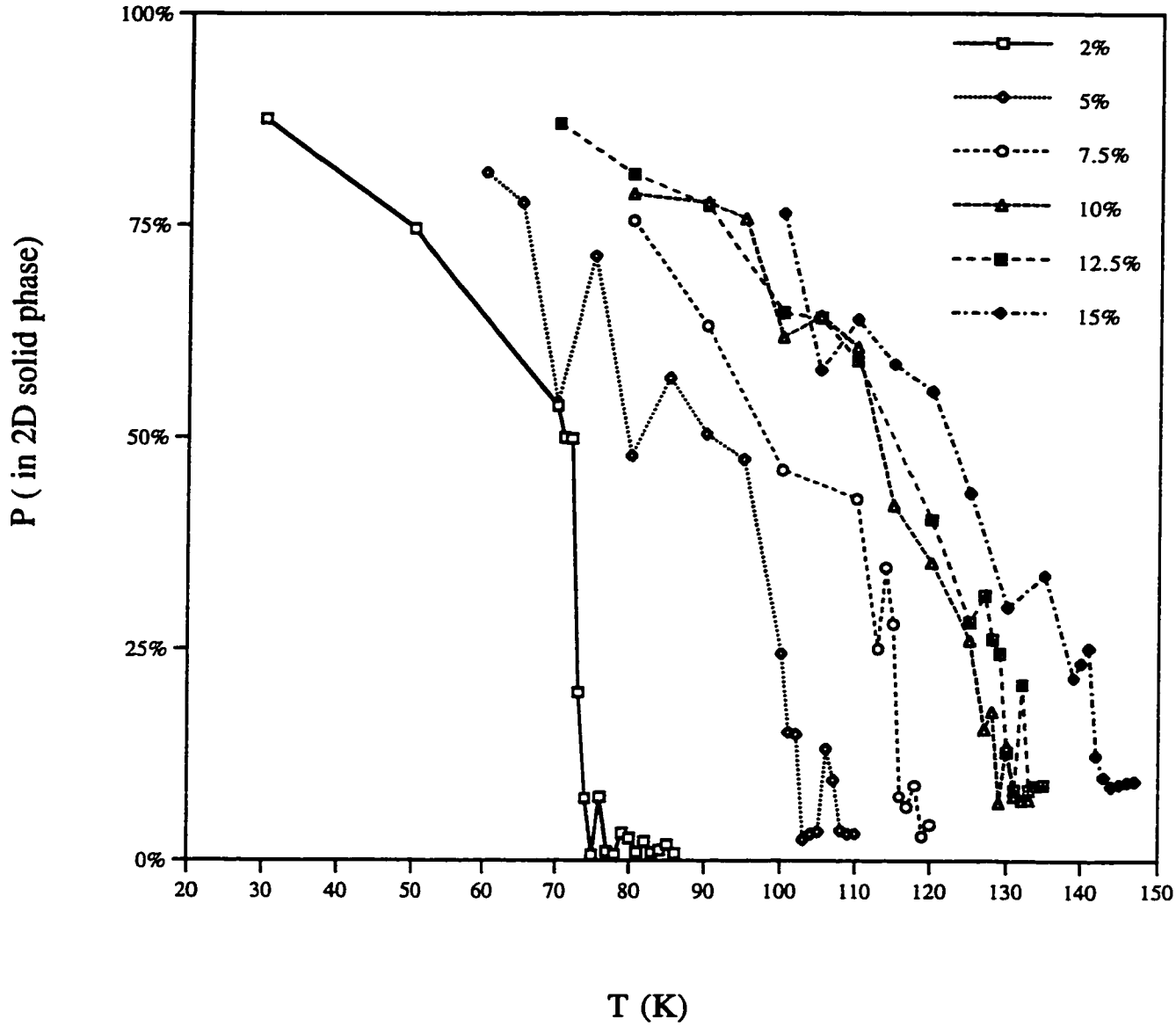

Figure 4.5.2 The percentage P of adsorbate in the solid phase as a function of temperature T at coverages Θ=2%, 5%, 7.5%, 10%, 12.5% and 15%

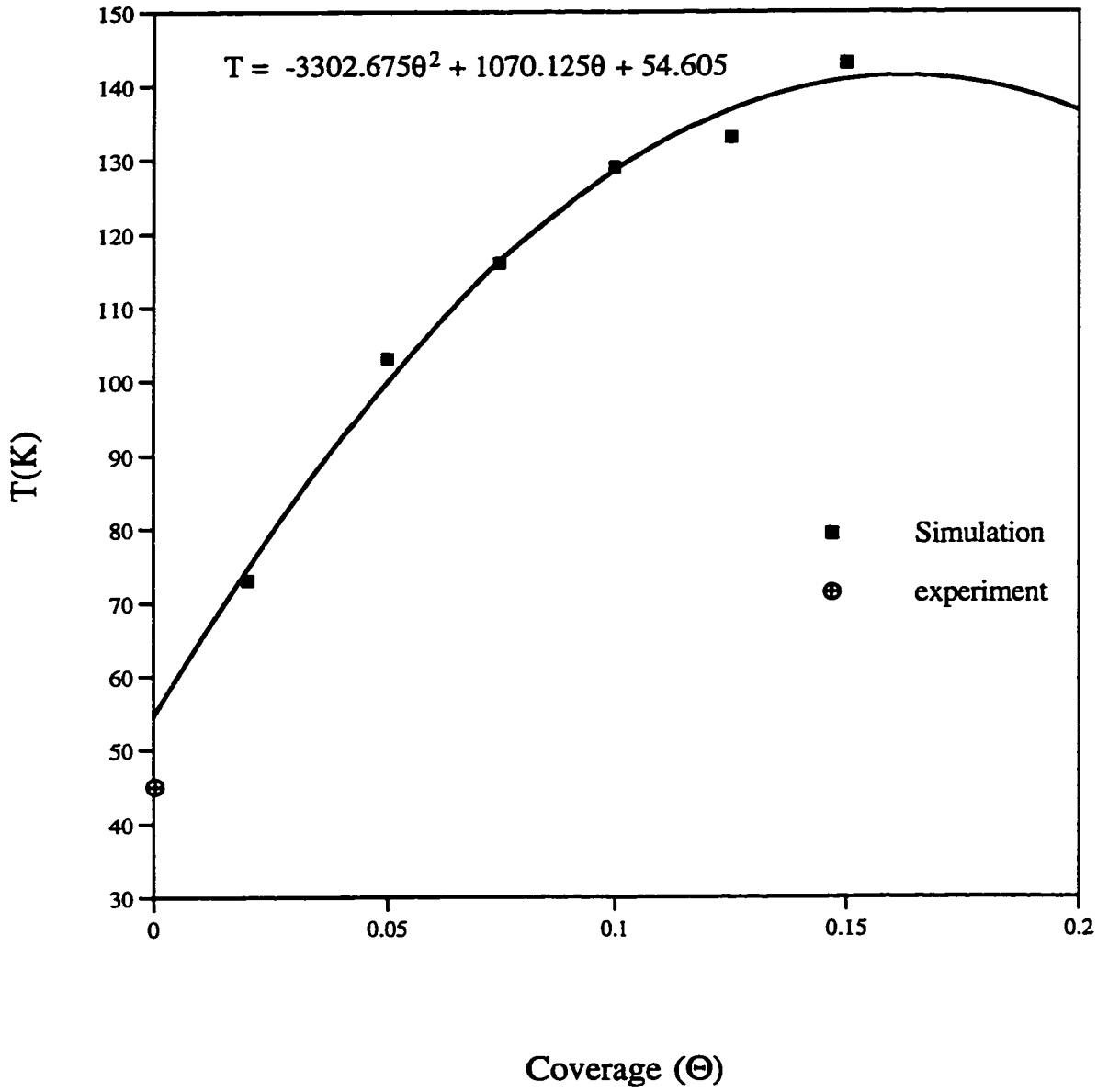

Figure 4.5.3 Coexistence curve between 2D gas phase and 2D solid phase of CO_2 on NaCl(001).

5.0 Simulation Study on CH_3Br/LiF(001) System:

5.1 Introduction

Photodissociation of small adsorbed molecules on clean single-crystal surfaces has been a topic of great interest in recent years[35][36]. The general goal of these studies is to better understand fundamental photochemical processes occurring at surfaces, which have far reaching implications in many surface phenomena. In many of these studies, knowledge of the orientation of the molecules on the surface is of primary importance in interpreting the experimental results.

For photochemical processes, a uv laser is used to promote the adsorbed molecule to its repulsive excited state(s) which leads to the dissociation of the adsorbate. Alkali halide crystals, such as LiF, are desirable substrates for photodissociation studies because of their chemical and structural stability and their high transparency to uv light. Because of these properties, photo-induced thermal desorption of the adsorbate from a LiF surface and adsorbate/substrate reactions can be largely ruled out. Furthermore, owing to the small value of the heat of adsorption (typically 0.2-0.4eV) compared with the electronic energies of the adsorbate molecules (HBr, CH_3Br, H_2S, OCS, etc...), the electronic structure and conformation of the adsorbate is only slightly perturbed in the presence of the solid surface and is assumed to remain unchanged. Because of these advantageous features many people have chosen the CH_3Br (or HBr, CH_3I

etc..,)/LiF(001) system to investigate the dynamics of uv photo-induced fragmentation of small molecules on surfaces[37][38].

J. C. Polanyi's group used infra-red spectroscopy (IR) to study a series of submonolayer, monolayer and multilayers of CH_3X (X=F, Cl, Br, I) on the surface of alkali halide (LiF, NaCl) single crystals. In particular, at monolayer coverage and less, the CH_3Br molecules tilt on average by 63±9° from the surface normal; for multilayer coverage the tilt angle is 36±5°[39]. The adsorption energy is found to be coverage dependent such that E_{ad}=0.38eV for low coverage (exposure of 0.006L; absolute coverage not known), and 0.27eV for high coverage (0.2L)[40]. More recent measurements show that the adsorption energy is 0.30eV for monolayer coverage and 0.28eV for multilayers[39].

G. Scoles' group has used low energy helium diffraction (LEHD) to determine the structure of overlayers of CH_3Br physisorbed on LiF(001) surface at T=35K. They found that for high coverages (around one monolayer), the adsorbed structure has a rectangular surface mesh with dimensions 4.52Å×6.71Å. This structure is incommensurate with the substrate unit mesh (2.85Å×2.85Å). They postulated that there are two antiferroelectrically ordered molecules per surface unit cell with the CH_3Br molecular axes nearly parallel to the surface normal[41].

These experiments have stimulated theoretical work on the structure and photodynamic of this system. H. Guo's group used

classical molecular dynamics[42] and Monte Carlo methods[43] to study the photodissociation dynamics and orientation of CH_3Br adsorbed on a LiF(001) surface. They used a pairwise additive atom-atom model approximated by Lennard-Jones potentials for the calculation of the adsorbate-adsorbate and adsorbate-substrate van der Waals interactions, and a point dipole (located at the center of the C-Br bond) model to calculate the electrostatic contribution. Polarization effects are included. They found that for an isolated molecule, the preferred orientation is perpendicular to the surface normal and the molecule-substrate interaction energy is -1.66 kcal/mol (-0.086eV), which primarily comes from the Lennard-Jones contribution. The electrostatic energy only accounts for about -0.32 kcal/mol (-0.014eV) of the binding energy. For coverages close to a monolayer, they found that the system has the lowest energy when the molecular axes of the adsorbates are parallel to the surface normal with alternating methyl-up and methyl-down configuration. The total energy is -5.44 kcal/mol (-0.236eV). These result are roughly close to experimental results (-0.3eV) at monolayer coverage but do not describe the low coverage heat of adsorption. They only qualitatively got the orientation of adsorbed CH_3Br molecules on the LiF(001) surface and did not mention the tilt angle of the adsorbed molecules.

R. R. Lucchese's group used stochastic classical trajectory calculations to simulate the photodissociation of a single CH_3Br molecule adsorbed on several LiF surfaces. They modeled CH_3Br as a diatomic molecule with CH_3 represented as a single unified atom. They used a modified Lennard-Jones potential to calculate the

dispersion and repulsion forces, and a point charge model (qH=0.323e, qBr=-0.138e and qC=-0.185e) to get the Coulomb forces between the gas molecule and the surface ions. They found that for a smooth surface the peak of the CH_3 photodissociation distribution occurs at ~68° implying that a CH_3Br molecule sits on the LiF surface at 68° from the surface normal. The molecule was bound to the surface with -6.21 kcal/mol (-0.27eV)[44].

Based on above work, we can see that for low coverage, Polanyi's group and Lucchese's group are in agreement and found that a CH_3Br molecule has a tilt angle around 65°, but Guo's group found the molecules are parallel to the surface ($\theta \sim 90°$) and have a considerably similar binding energy. For high coverages, both Guo's group and Scoles' group found that the CH_3Br molecules are perpendicular to the surface with alternating methyl-up and methyl-down orientations. In order to solve the difference between these groups about the CH_3Br molecular orientation at low coverage, and to find a reasonable structure of CH_3Br molecules at high coverage, we have set up a model using Lennard-Jones potential for molecule-molecule interaction, Tang-Toennies potential for molecule-ion interaction and a "5 point charge - 1 point dipole" model to simulate the electrostatic potential, and have performed a Metropolis Monte Carlo simulation of the submonolayer and monolayer structures of this system.

5.2 Model of CH_3Br/LiF(001)

Just like the CO_2/NaCl(001) system, the total potential of the CH_3Br/LiF(001) system separates into two parts: the intermolecular potential and the adsorbate-LiF surface potential. The surface potential is usually very weak (physisorption), and no chemical bonds are formed. The adsorption energy is estimated to be 0.28~0.30eV[39][40][45]per CH_3Br molecule at a monolayer coverage. Therefore, it is reasonable to assume that the LiF surface is basically unperturbed by the adsorbate. All these potential energies are developed in a manner similar to those in the CO_2/NaCl(001) system. The various atom-atom and atom-ion potentials assume the two body approximation with the repulsion and dispersion interactions described by either a Lennard-Jones 6-12 potential or Tang-Toennies potential and the electrostatic interactions handled through distributed multipoles (point charges and dipoles).

Using the same analysis as for CO_2/NaCl, we can write the repulsion and dispersion terms of interaction between two CH_3Br molecules as following:

$$V_{DR}^{gg} = \sum_{i=1}^{5}\sum_{j=1} V_{atom}^{gg}(X_i^n - X_j^{n'}) \qquad (5.2.1)$$

where X_i^n and $X_j^{n'}$ are the spatial coordinates of the Br atom (i, j=1), C atom (i, j=2), and three H atoms (i, j=3,4,5) on the **n**th and **n**'th molecules respectively. The term V_{atom}^{gg} is the van der Waals

interaction between two atoms on different molecules and we assume that it has the Lennard-Jones form as follows:

$$V_{atom}^{gg} = 4\,(\varepsilon_i * \varepsilon_j)^{1/2}\ \{\ [\frac{(\sigma_i+\sigma_j)}{2r_{ij}^{nn'}}]^{12} - [\frac{(\sigma_i+\sigma_j)}{2r_{ij}^{nn'}}]^{6}\ \} \qquad (5.2.2)$$

where $r_{ij}^{nn'} = |X_i^n - X_j^{n'}|$ and the ε_i and σ_i are the well depth and collision diameter of the ith atom. The values for the Br atom, the C atom and the H atoms are listed in Table 5.2.1

To calculate the Coulomb interaction, we set up a "5 charge - 1 dipole" model of the CH_3Br molecule (Fig. 5.2.1), which has partial charges on each of the Br atom, C atom and three H atoms, as well as a point dipole on the C atom. The bonds length Br=C and C=H have values of 1.939Å, 1.113Å respectively and the bond angle ∠ H-C-H has a value of 111.3°[46]. The experimental value of the molecular dipole moment $\vec{\mu}_C$ is 1.81D[47] and the quadrupole moment is Θ_{aa}=3.55D-Å[48]. Using these values and the assumption of a partial charge of 0.1e on each of the H atoms, the point charges on the other atoms and the dipole on the carbon atom can be calculated. These values are listed in Table 5.2.2.

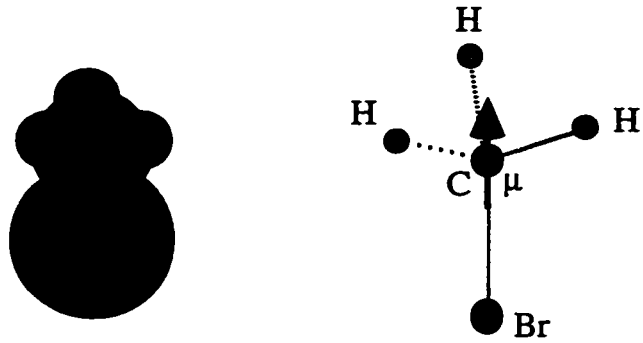

Figure 5.2.1 "5 charge - 1 dipole" model of the CH_3Br molecule

The method of calculating the electrostatic potential energy between two CH_3Br molecules, as well as the van der Waals and electrostatic terms of the surface potential between the CH_3Br molecules and the LiF(001) surface is the same as those for the CO_2/NaCl(001) system. The parameters we need are listed in Table 5.2.2 and 5.2.3.

Table 5.2.1 Lennard-Jones potential parameters for CH_3Br

(from ref.[19])

	Br - Br	C - C	H - H
ε (K)	257.2	26.30	13.40
σ (Å)	3.538	2.824	2.735

Table 5.2.2 Calculated Tang-Toennies gas-atom plus surface-ion potential parameters

(from ref. [19])

Interaction	α (Å^{-1})	A (K)	C_6 (K Å^6)	C_8 (K Å^8)
H-Li^+	4.50	2.193×10^6	1.451×10^6	2.275×10^6
H-F^-	3.28	2.054×10^6	3.000×10^7	3.950×10^7
Br-Li^+	4.63	2.750×10^7	1.900×10^7	2.980×10^7
Br-F^-	3.35	8.437×10^6	4.310×10^8	5.679×10^8
C-Li^+*	5.36	3.573×10^7	5.945×10^3	5.901×10^3
C-F^-*	3.72	1.368×10^7	2.201×10^3	3.283×10^3

* The values are for F (in HF) on LiF are used.

Table 5.2.3 Point charges point dipoles on CH_3Br molecule

	Br	C	H
point charge (e)	-0.0921	-0.2079	0.1000
point dipole (D)	0.0000	1.7960	0.0000
molecular dipole (D)	1.810		
molecular quadrupole (D-Å)	3.550		

5.3 Simulation results for $CH_3Br/LiF(001)$

We adopt the Metropolis Monte Carlo method to study the equilibrium properties of the $CH_3Br/LiF(001)$ system. For simplicity, the substrate is not allowed to move, and the CH_3Br molecule is considered to be rigid. So the movement of a molecule can be thought just include three parts: first is the translation of the center of mass, second is the reorientation of the molecular axis and the third is rotation around the molecular axis. The coordinate system used to describe the position of the CH_3Br molecules on the LiF(001) surface is the same as that in the $CO_2/NaCl$ system shown in Fig. 2.2.1 except that Li^+ and F^- replace Na^+ and Cl^-, respectively. For the orientation of the CH_3Br molecules with respect to the LiF(001) surface, we define a new spin angle ψ around the molecular axis (Fig. 5.3.1), otherwise things are similar with what we do in $CO_2/NaCl$ system.

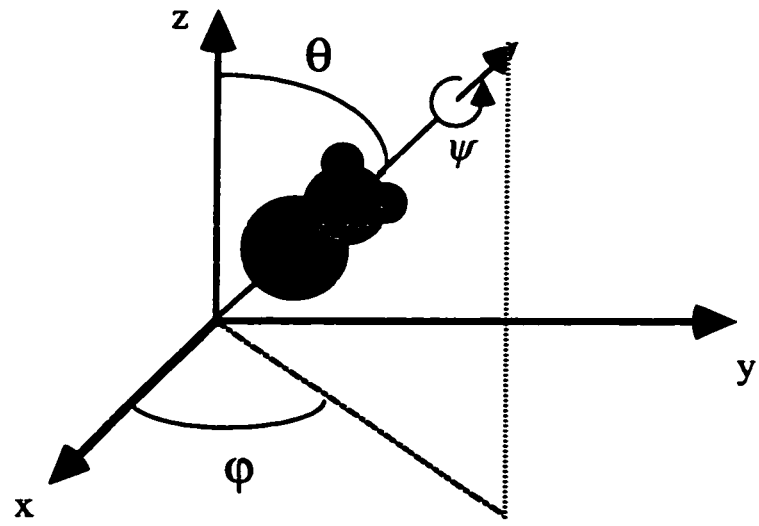

Figure 5.3.1 Angular coordinate system with respect to the xyz coordinate system

5.3.1 Submonolayer

We put a single CH_3Br molecule on the LiF(001) surface and ran it for 40 kcycles at T=50K. We found that the molecule tilts with respect to the surface normal at an average angle of 54° (Fig. 5.3.2). The result is different from Guo's group, who found that the C=Br bond is parallel to the surface, but similar to Polanyi's and Lucchese's groups results which found tilt angles around 60°. The molecule-surface interaction energy is -3.00 kcal/mol (-0.12eV), which primarily comes from the van der Waals contribution, -2.76 kcal/mol. The electrostatic energy is about -0.24 kcal/mol, which is 25% less to Guo's result of -0.32 kcal/mol. This result is less than the estimated experimental values of 0.27eV or more and is probably due to the neglect of the induction energy contribution of the surface potential.

Low coverages were simulated by putting ten CH_3Br molecules with random positions and orientations on the LiF(001) surface (The LiF surface area was chosen to be 57Å×57Å) (Fig. 5.3.3) and running it for 100 kcycles at T=50K. We found these molecules formed several dimers (Fig. 5.3.4) and the average tilt angle is near 60°. The total energy per molecule is -3.76 kcal/mol. The major contribution still comes from the van der Waals portion (-2.71kcal/mol) of the molecule-surface part (-2.93kcal/mol). The molecule-molecule interaction is small (-0.70kcal/mol) but attractive, making it favorable for molecules to form dimers.

5.3.2 Monolayer

For a monolayer with an initial configuration arranged in a (2×1) herringbone structure, the final structure was found to be stable with little disorder at T=50K. The disorder comes from the molecules' thermal vibration at their equilibrium positions. The average tilt angle is 39.2° and the binding energy is -5.41kcal/mol.

If we place a 8×8 size island with herringbone structure on the area of 10×10 surface (Fig. 5.3.5) and leave a small empty space around the island, we found after running 40 kcycles, that the structure adjusts to form a slightly disordered structure with major parts that retain the herringbone structure (Fig. 5.3.6). The reason we doing this is that the molecules have enough space to mobile and has possibility to form reasonable structure. Considering the energy, the total energy is -5.06 kcal/mol, the molecule-molecule interaction (-2.56 kcal/mol) is little than the interaction of the molecule-surface (-2.65 kcal/mol). There are two peaks on the tilt angle distribution, one at 62° and another at 34° (Fig. 5.3.7). The central portion of the island still has the 2×1 herringbone structure while the outer regions have relaxed and adopted the orientation of an individual molecules (~ 60°).

Antiferroelectrically ordered structures were also tested. A monolayer of molecules covering the whole surface with the antiferroelectrical structure, the structure is stable and is similar to the structure shown in Fig. 5.3.8. If a small space is made (8×8 island on a 10×10 surface) for the molecules to move around, then after

running 40 kcycles, a new structure evolves (Fig. 5.3.9) with a unit cell 7.28Å×7.84Å. There are four CH_3Br molecules in this unit cell with two methyl-up and two methyl-down and the unit cell is rotated by 45° with respect to the surface mesh. This structure is not commensurate with the surface unit mesh (2.85×2.85Å). Our simulation result is different from Scoles' proposed structure in which the real space structure of CH_3Br/LiF(001) has two antiferroelectrically ordered molecules per unit mesh with parameters 4.52×6.71Å. Considering the energy, the binding energy is -5.18kcal/mol (-0.224eV). The molecule-molecule interaction (-3.16 kcal/mol) is greater than the interaction of the molecule-surface (-1.85 kcal/mol) and it forces the molecules to straighten up on the surface with a tilt angle near 10° and 170°, as is shown in Figure 5.3.10. In this figure, a small peak near 63° is also found. It shows that the outer regions have relaxed and adopted the same orientation as a single molecules (~60°). Our result on binding energy is little different from the experimental result, E_{bind}=-6.90 kcal/mol (0.30eV), but similar to Guo's results. Guo found at monolayer coverage, the total energy is -5.44 kcal/mol (0.236eV) and the molecule-surface interaction energies are -1.13 kcal/mol (0.049eV) and -0.057 kcal/mol (-0.0025eV) for the Lennard-Jones and the electrostatic contributions, respectively.

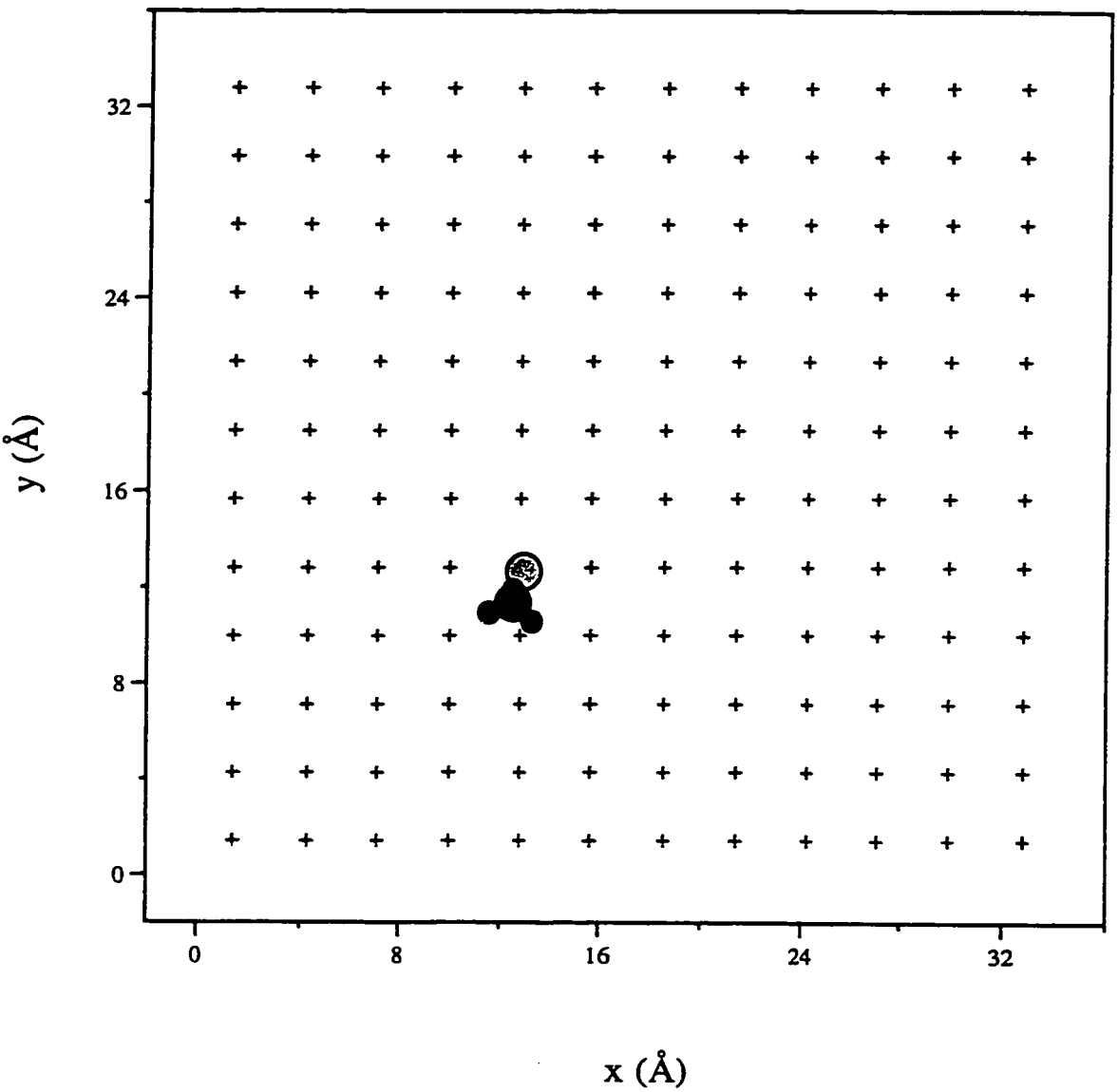

Fig. 5.3.2 Final configuration of one CH_3Br molecule on a LiF(001) surface at T=50K.

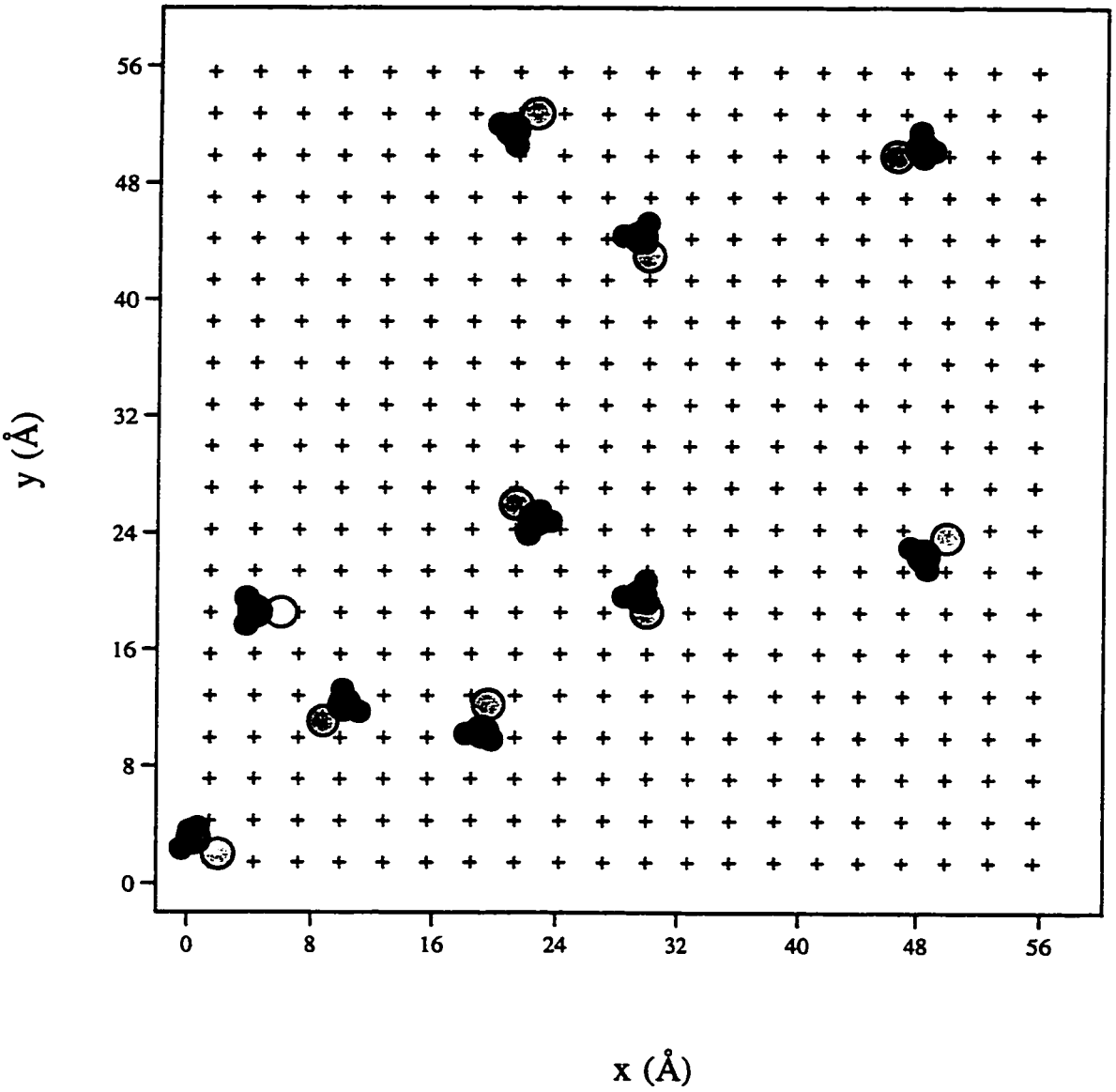

Fig. 5.3.3 Initial configuration of ten CH_3Br molecules on a LiF(001) surface at T=50K.

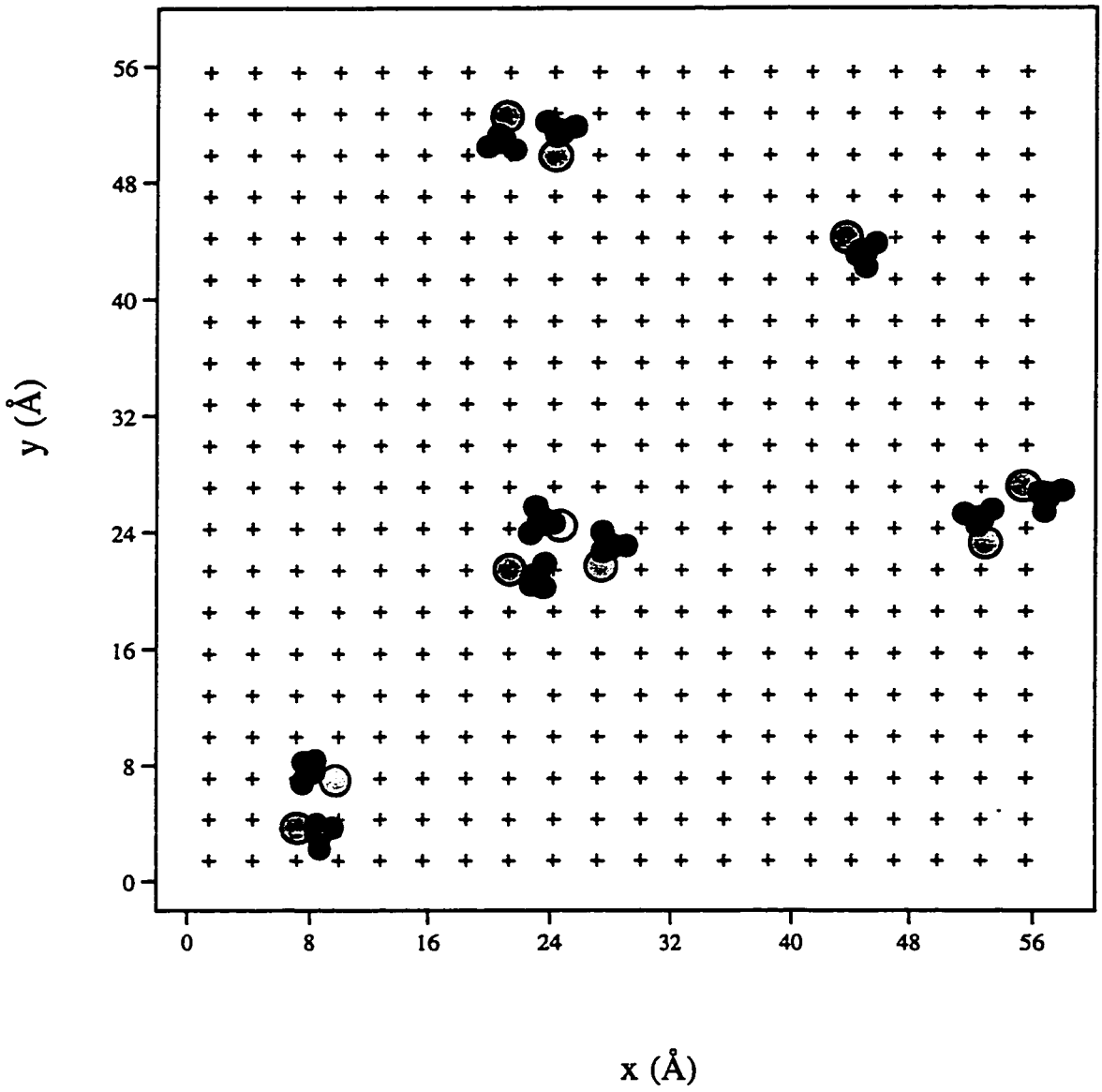

Fig. 5.3.4 Final configuration of ten CH_3Br molecules on a LiF(001) surface at T=50K.

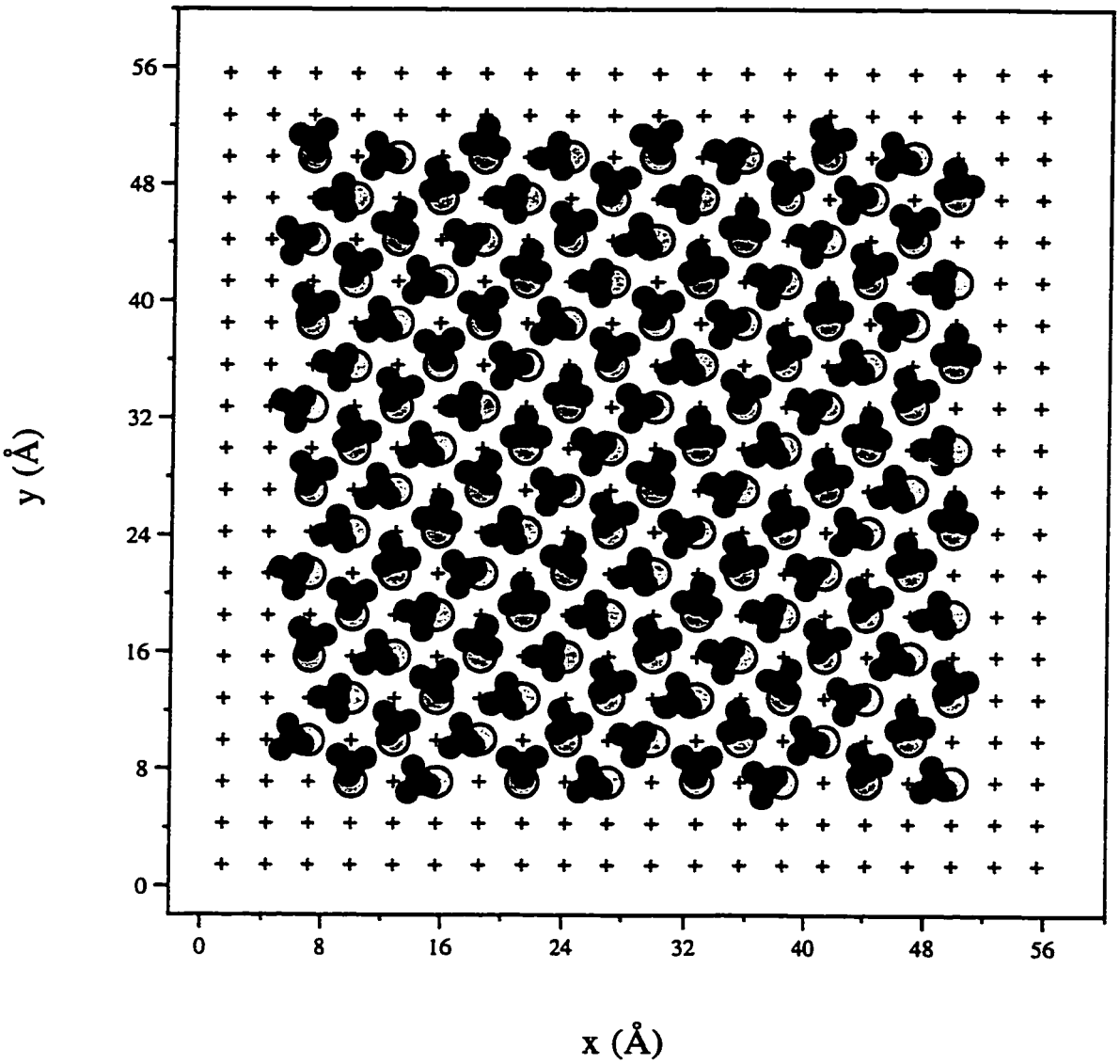

Fig. 5.3.5 Initial configuration of a (2×1) island on a LiF(001) surface at T=50K.

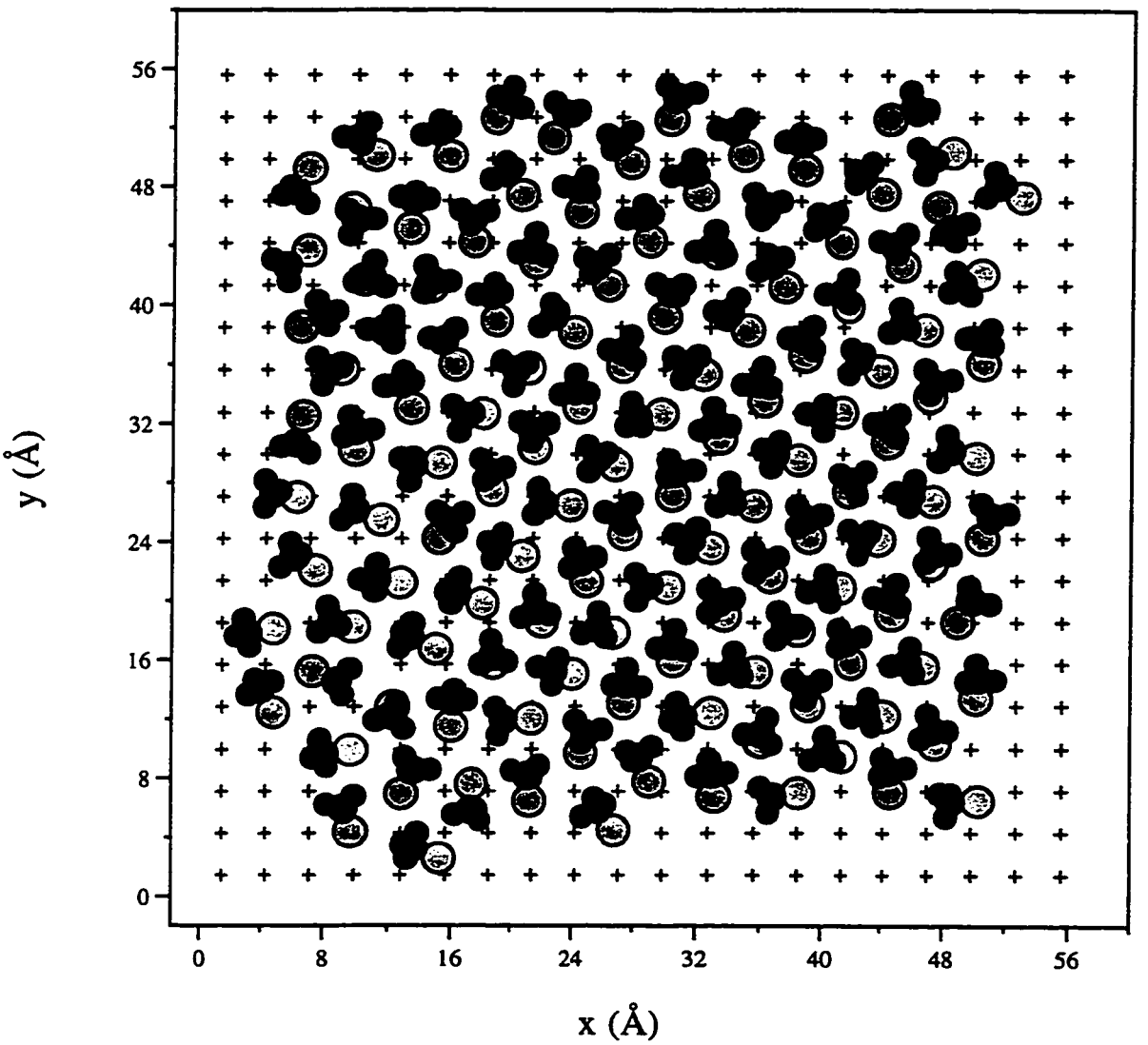

Fig. 5.3.6 Final configuration of a (2×1) island on a LiF(001) surface at T=50K.

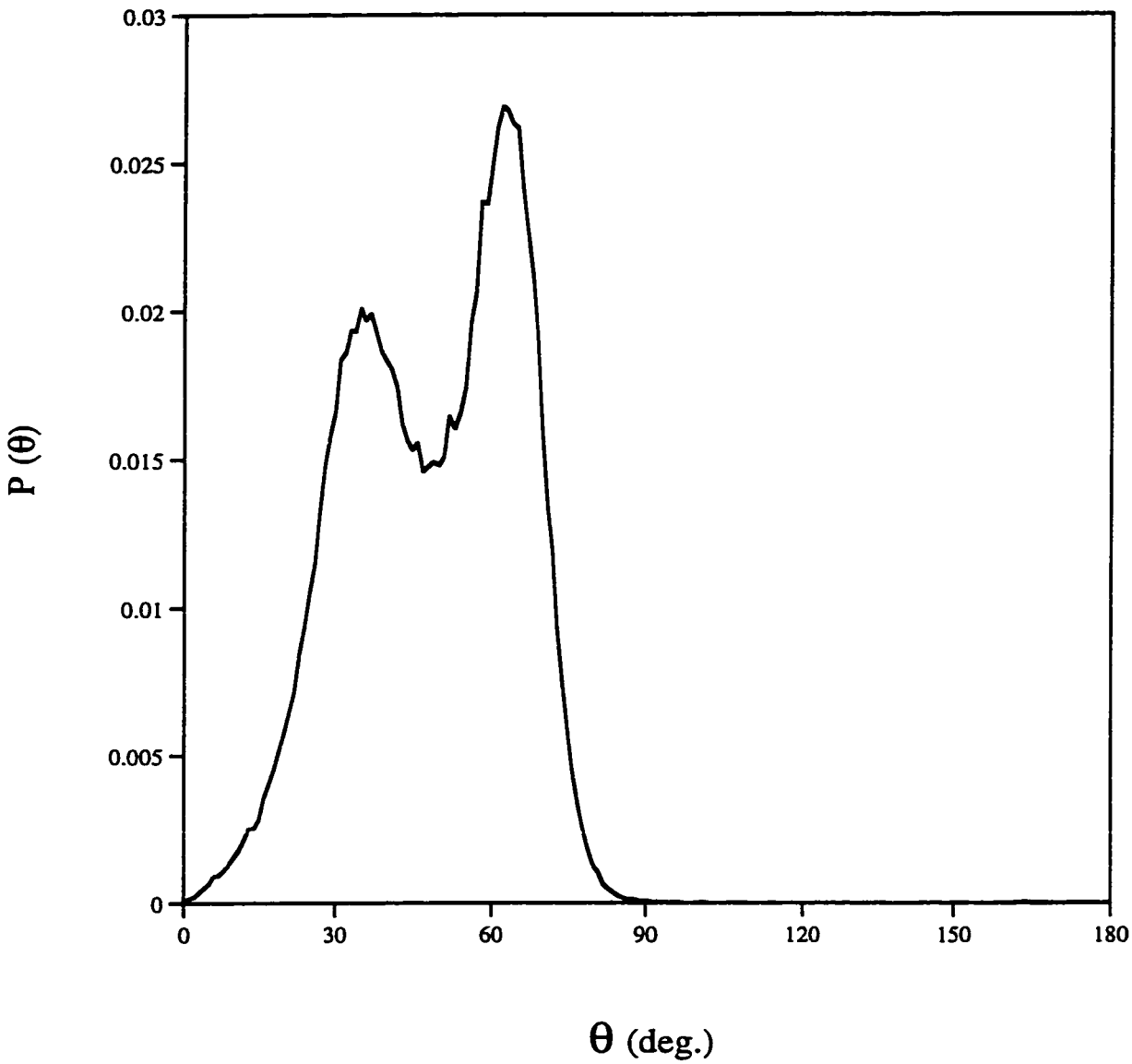

Fig. 5.3.7 Theta distribution of a (2×1) island on a LiF(001) surface at T=50K.

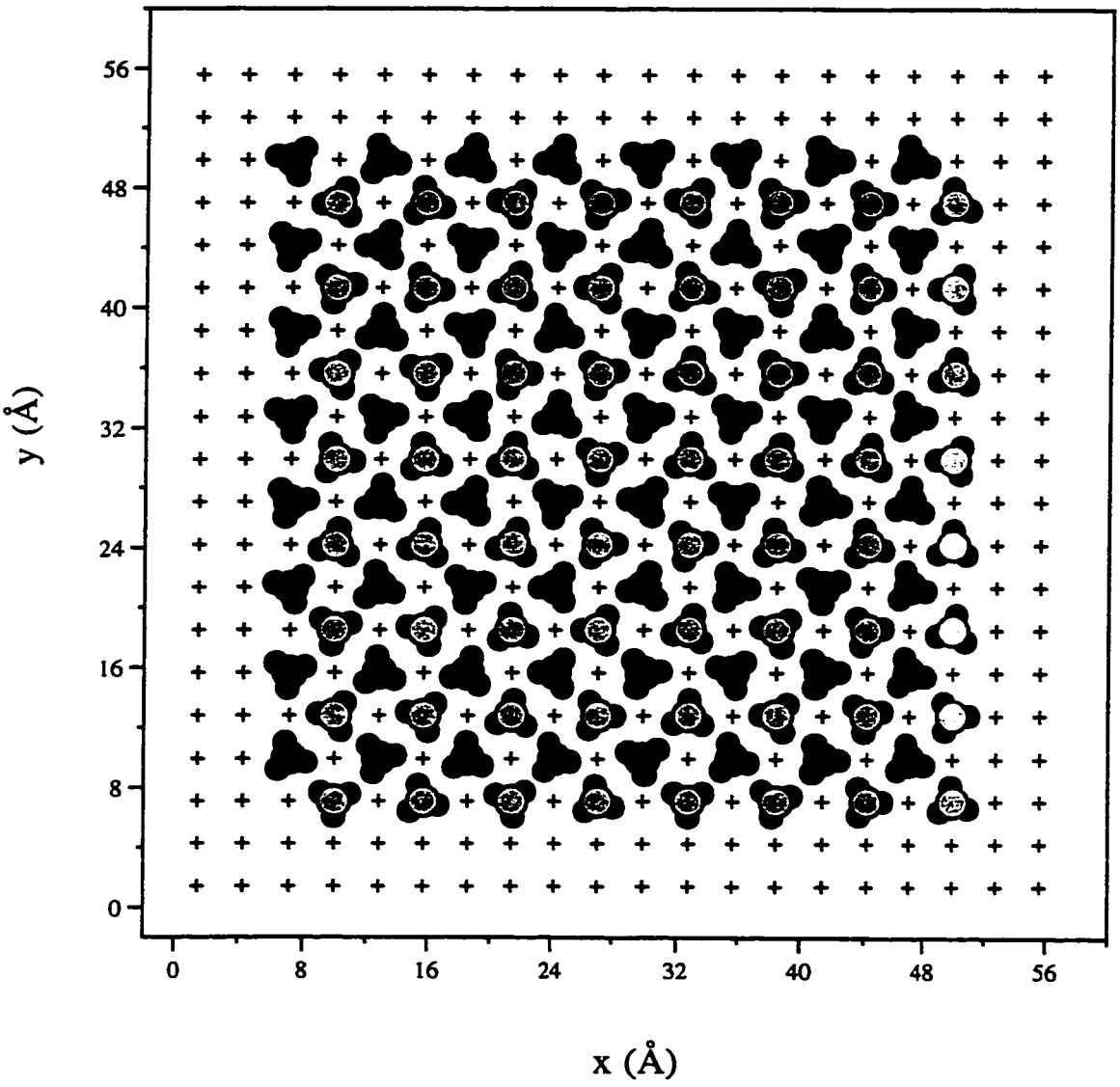

Fig. 5.3.8 Initial configuration of an island (size:8×8) with an antiferroelectrically ordered structure on a LiF(001) surface at T=50K.

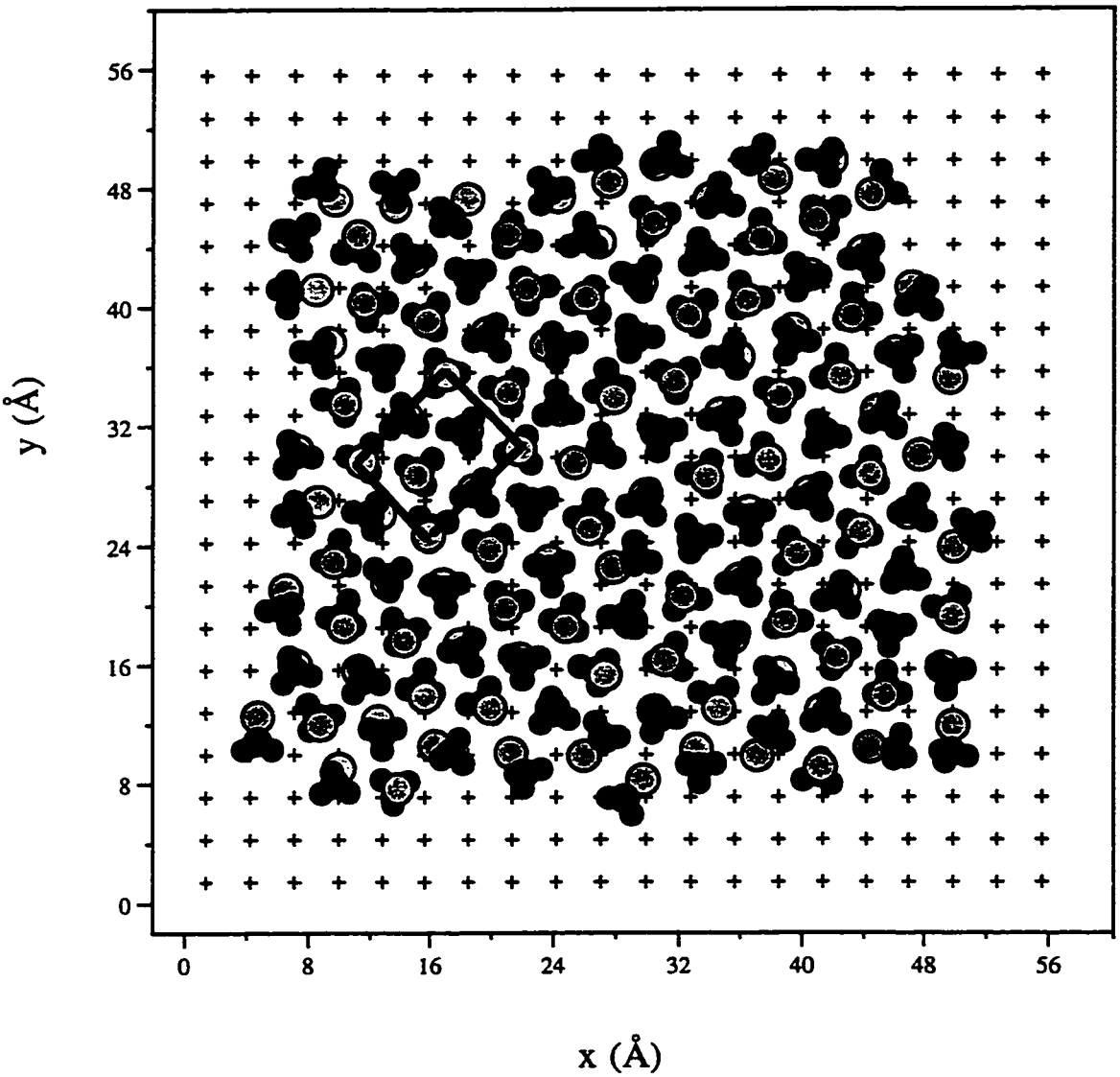

Fig. 5.3.9 Final configuration of an island (size:8×8) with an antiferroelectrically ordered structure on a LiF(001) surface at T=50K.

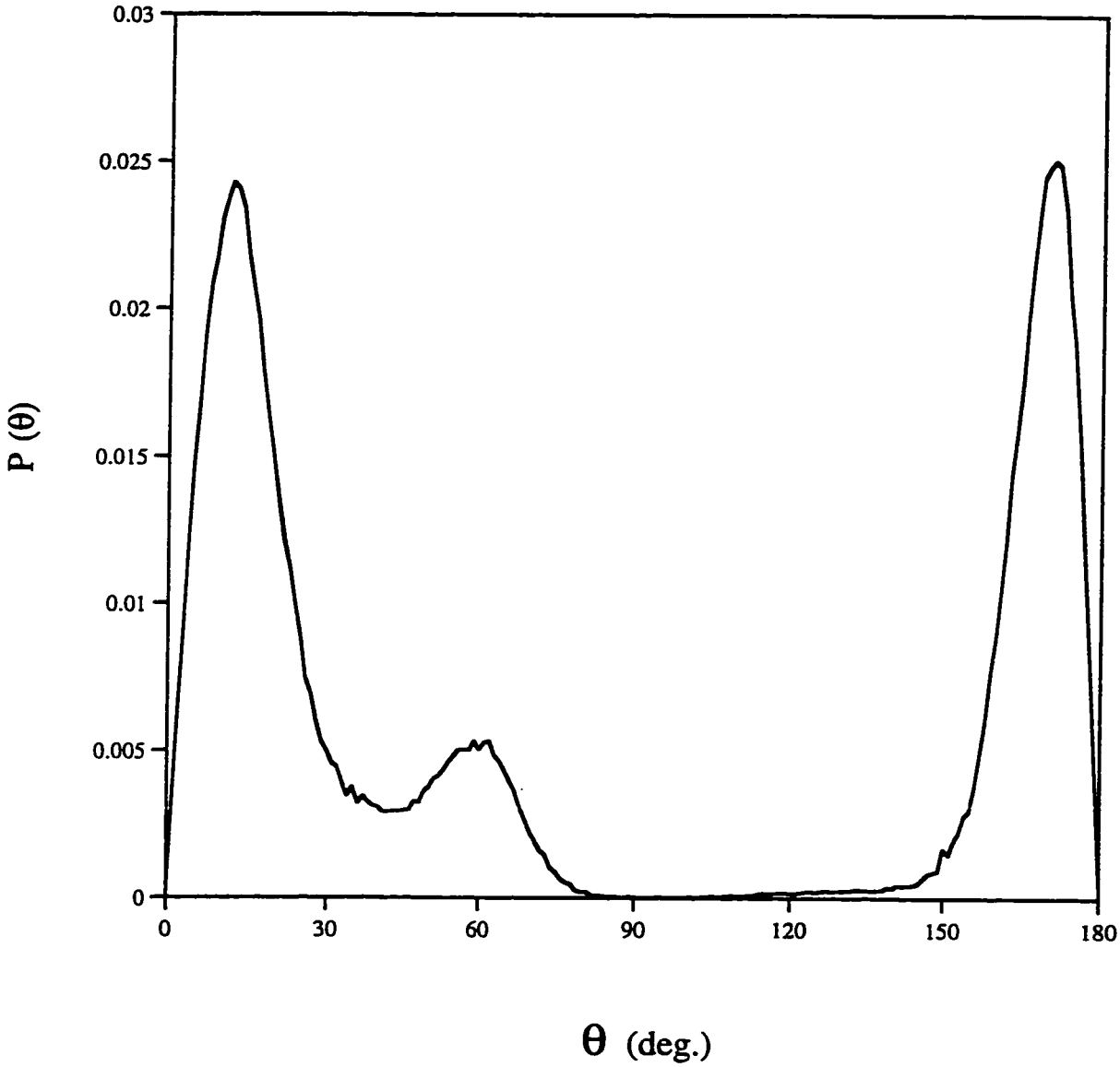

Fig. 5.3.10 Theta distribution of an island (size:8×8) with an antiferroelectrically ordered structure on a LiF(001) surface at T=50K.

6.0 Conclusions

For the CO_2/NaCl(001) system, a Metropolis Monte Carlo method was used to calculate the average potential energy, azimuthal angle φ and tilt angle θ and to examine the most energetically favorable structures for monolayer and multilayers of CO_2 molecules adsorbed on the (001) surface of NaCl. The mechanism of nucleation and growth of islands of the 2D "solid" and 2D gas-solid phase coexistence was also studied. The following conclusions can be made from the above studies.

a) For a monolayer two kinds of stable structures, a (2×1) and a (1×1), are found. The $p(2\times1)$ structure has been confirmed by the experimental results but the (1×1) structure with lower energy has not been found by the experiments. In the bilayer system three kinds of stable structures are found, which are the (2×1), the (1×1) and the $c(2\times2)$ bilayer structures. The potential energy of the $c(2\times2)$ is slightly more favorable than the (2×1) and the (1×1) bilayer structures. Owing to the (1×1) structure might not arise in experiments (because of steric considerations during the formation of the 2D solid phase), bilayers should adopt either a (2×1) or a $c(2\times2)$ structure with the $c(2\times2)$ structure energetically favoured. In the trilayer system, the trilayers adopt a $c(2\times2)$ owing to the instability of the (2×1) structure which will convert to a $c(2\times2)$ structure with time. The result is consistent with experimental findings.

b) At low coverages the CO_2 molecules aggregate together but it is hard for the (2×1) structure of the 2D solid phase to form directly. The presence of a surface step is not an important factor in the formation of the (2×1) herringbone structure, although it does have an appreciable binding energy. In order to explain the formation of the 2D solid phase, it is reasonable to assume that aggregated 2D gas phases with the $(\sqrt{2}\times\sqrt{2})R45°$ and $(2\sqrt{2}\times\sqrt{2})R45°$ structures are other kinds of low density 2D "solid" phases. After the isolated gas molecules form one of these kinds of structures, it is easy to form the solid phase (2×1) herringbone structure by the adsorption of another molecule on top of the low density islands.

c) In studies of the mechanism of the growth of CO_2 molecules, the result suggests that the multilayer growth is most likely the Stranski-Krastanov type whereby multilayer islands on top of the monolayer adopt a bulk-like crystalline structure $\{c(2\times2)\}$.

d) To describe the behavior of CO_2 molecules adsorbed on NaCl(001), the 2D gas and solid phase coexistence curve (Θ vs. T) was determined by simulations at submonolayer coverage. It was found that the modified two-dimensional van der Waals equation of state described the gas-solid coexistence curve. The critical coverage Θ_c and temperature T_c are found to be 0.162 and 142.9K respectively. These results are very close to the theoretical value Θ=1/6 and T_c=151.2K for the van der Waals model. Therefore, the modified van der Waals equation and two-dimensional phase coexistence curve can well describe the behavior of CO_2 molecules on

the NaCl(001) surface in the low coverage (near critical Θ_c and below) regions.

For CH_3Br/LiF(001) system the favored structures and energies at submonolayer and monolayer coverages are examined using the same methods as for the CO_2/NaCl(001) system. For low coverages the CH_3Br molecules are tilted by 60° from the surface normal. A stable (2×1) structure with herringbone pattern for a monolayer was found with a tilt angle of 39.2°. This structure is compatible with the Polanyi group's work. Another stable monolayer structure was also found. In this case the molecule-molecule interaction is much stronger than the interaction of the molecule-surface to force the molecules straight up on the surface to form an antiferroelectrically ordered structure with a unit 7.28Å×7.84Å. This structure is not commensurate with the surface unit mesh (2.85×2.85Å). Our results partially reconciles the Polanyi and Scoles' experimental results.

7.0 References

[1] A. Lakhlifi and C. Girardet, Surface Science, **241**,400-415 (1991).

[2] J. Heidberg, E. Kampshoff, R. Kühnemuth and O. Schönekäs, J. Electron Spectrosc. Relat. Phenom. **64/65,** 803-812 (1993).

[3] G. Lange, D. Schmicker, J. P. Toennies, R. Vollmer, and H. Weiss, J. Chem. Phys. **103**, 2308-2319 (1995).

[4] J. Heidberg, E. Kampshoff, R. Kühnemuth and O. Schönekäs, Surface Science, **272,** 306-312 (1992).

[5] A. Glachant, J. P. Coulomb and J. P. Biberian, Surface Science, **59**, 619 (1976).

[6] A. Terlain and Y. Larher, Surface Science, **125**, 304 (1983).

[7] L. I. Osipow, *Surface Chemistry*, Reinhold Publishing Corporation, New York, (1962).

[8] H. C. Chang, H. H. Richardson and G. E. Ewing, J. Chem. Phys. **89**, 7561-7568 (1988).

[9] P. W. Atkins, *Physical Chemistry*, W. H. Freeman and Company, (1990).

[10] G. A. Somorjai, *Surface Chemistry and Catalysis*, A Wiley-Interscience Publication, John Wiley & Sons, Inc. (1994).

[11] O. G. Mouritsen, *Computer Studies of Phase Transitions and Critical Phenomena*, Springer-Verlag, Berlin Heidelberg (1984).

[12] J. Heidberg, E. Kampshoff, O. Schönekäs, H. Stein and H. Weiss, first presented at the "Joint Israel-Lower Saxony Conference on Frontiers in Biology, Chemistry and Physics", Braunschweig, F. R. Germany (1988).

[13] J. Heidberg, E. Kampshoff, R. Kühnemuth and O. Schönekäs, G. Lange, D. Schmicker, J. P. Toennies, R. Vollmer and H. Weiss, J. Electron Spectrosc. Relat. Phenom. **64/65,** 341-350 (1993).

[14] Y. Kozirovski and M. Folman, Trans. Faraday Soc. **62**,1431 (1966).

[15] O. Berg and G. E. Ewing, Surface Science, **220,** 207-229 (1989).

[16] J. Heidberg, E. Kampshoff, R. Kühnemuth and O. Schönekäs, Surface Science, **251/252,** 314-320 (1991).

[17] G. Y. Liu, G. N. Robinson, G. Scoles, Surface Science, **262,** 409-421 (1992).

[18] W. A. Steele, *The Interaction of Gases with Solid Surface*, Pergamon, Oxford, (1974).

[19] V. J. Barclay, D. B. Jack, J. C. Polanyi, and Y. Zeiri, J. Chem. Phys. **97**, 9458-9467 (1992).

[20] J. C. Polanyi and R. J. Williams, J. Chem. Phys. **94**, 978-996 (1991).

[21] J. Heidberg, E. Kampshoff, O. Schönekäs, H. Stein and H. Weiss, submitted to Ber Bunsenges. Phys. Chem. (1990).

[22] M. A. Saberi, M.Sc. Thesis, Concordia University (1996).

[23] István Náray-Szabó, *Inorganic Crystal Chemistry*, Akadémiai Kiadó. Budapest (1969).

[24] A. D. Buckingham and R. L. Disch, Pro. R. Soc. A. **273,** 27 (1963).

[25] C. S. Murthy, S. F. O'Shea and I. R. McDonald Molecular Physics, **50**, 531-541 (1983).

[26] M. Rigby, E. B. Smith, W. A. Wakeham and G. C. Maitland, *The Forces Betweem Molecules*, Clarendon Press, Oxford (1986).

[27] J. E. Lennard-Jones and B. M. Dent,
Trans. Faraday Soc. **24**, 92 (1928).

[28] K. T. Tang and J. P. Toennies,
J. Chem. Phys. **80**, 3726-3741 (1984).

[29] M. P. Allen and D. J. Tildesley, *Computer Simulation of Liquids*,
Oxford Science Publications (1987).

[30] J. Kolaczkiewicz and E. Bauer,
Physical Review Letters, **53**, Number 5, 485-488 (1984)

[31] J. Kolaczkiewicz and E. Bauer,
Surface Science, **151**, 333-350 (1985).

[32] S. Ross, *On Physical Adsorption*, John Wiley & Sons, Inc. (1964).

[33] N. Goldenfeld, *Lectures on Phase Transitions and the Renormalization Group*, Frontiers in Physics,
Addison-Weley Publishing Company (1992).

[34] J. M. Yeomans, *Statistical Mechanics of Phase Transitions*,
Clarendon Press, Oxford (1992).

[35] J. C. Polanyi and H. Rieley, *Photochemistry in the Adsorbed State*, in Dynamics of Gas-Surface Interactions, edited by C. T. Rettner and M. N. R. Ashfold, The Royal Society of Chemistry, Cambridge, (1991).

[36] X. L. Zhou, X. Y. Zhu and J. M. White,
Surf. Sci. Rep. **13**, 77 (1991).

[37] E. B. D. Bourdon, J. P. Cowin, I. Harrison, J. C. Polanyi, J. Segner, C. D. Stanners and P. A. Young,
J. Phys. Chem. **88**, 6100-6103 (1984).

[38] S. A. Costello, B. Roop, Z. M. Liu and J. M. White,
J. Phys. Chem. **92**, 1019-1020 (1988).

[39] Private conversation.

[40] I. Harrison, J. C. Polanyi, and P. A. Young,
J. Chem. Phys. **89**, 1475-1523 (1988).

[41] G. N. Robinson, N. Camillone III, P. A. Rowntree, G. Y. Liu,
J. Wang, and G. Scoles, J. Chem. Phys. **96**, 9212-9220 (1992).

[42] Z. H. Huang and H. Guo, J. Chem. Phys. **97**, 2110-2118 (1992).

[43] Z. H. Huang and H. Guo, J. Chem. Phys. **98**, 7412-7419 (1993).

[44] J. M. Waston, I. Noorbatcha, and R. R. Lucchese,
J. Chem. Phys. **96**, 7771-7787 (1992).

[45] F. L. Tabares, E. P. Marsh, G. A. Bach, and J. P. Cowin,
J. Chem. Phys. **86**, 738 -744 (1987).

[46] S. L. Miller, L. C. Aamodt, G. Dousmanis, C. H. Townes
and J. Kraitchman, J. Chem. Phys. **20**, 1112-1114 (1952).

[47] C. W. N. Cumper, Tetrahedron **25**, 3131 (1969).

[48] D. L. Vanderhart and W. H. Flygare, Mol. Phys. **18**, 77-93 (1970).

TEST TARGET (QA-3)

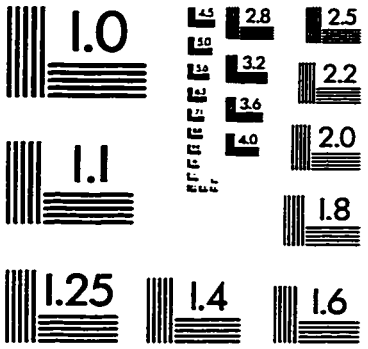

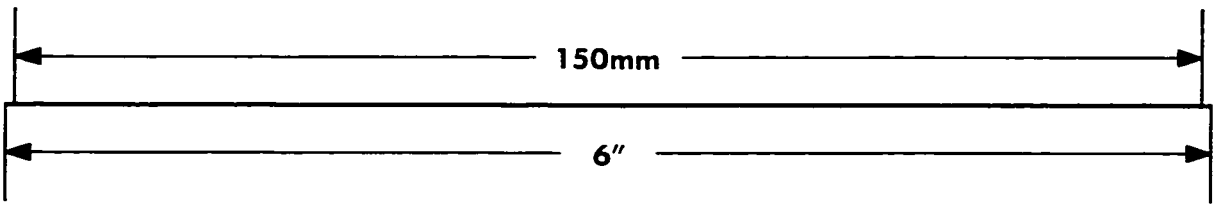

APPLIED IMAGE, Inc
1653 East Main Street
Rochester, NY 14609 USA
Phone: 716/482-0300
Fax: 716/288-5989